University of Zurich UZH

Photogrammetric Analysis of Surge-type Movement on a Small Alpine Glacier

GEO 511 Master's Thesis

Author
Riet Armon Könz
14-721-039

Supervised by
Dr. Martin Lüthi

Faculty representative
Prof. Dr. Andreas Vieli

21.09.2021
Department of Geography, University of Zurich

Photogrammetric Analysis of Surge-type

Movement on a Small Alpine Glacier

Author

Riet Armon Könz, 14-721-039
rietarmon.koenz@uzh.ch

Supervisor

Dr. Martin Lüthi
martin.luethi@geo.uzh.ch

Faculty Member

Prof. Dr. Andreas Vieli
andreas.vieli@geo.uzh.ch

University of Zurich UZH

Summary

Glacial instabilities have the potential to cause major disasters if they develop into an ice avalanche or are at the beginning of a process chain such as glacier lake outburst floods (GLOFs) or landslides. Reliable forecasting is a critical step in minimizing the risk of such events. Therefore, understanding the stability of glaciers is an essential but still challenging field. To understand the processes that influences glacier stability, this study focuses on a small alpine glacier, Ärlen Glacier, which showed interesting sliding instabilities over several years (2014 - 2020). Given the flat slope and small size of the glacier, such mass movements are actually unexpected. The main objective of this study is to quantify and understand the temporal and spatial patterns of mass movements at Ärlen Glacier and to analyse the significance of the event in the context of glacier-related natural hazards.

After unusual crevasse patterns were observed in the northern part of Ärlen Glacier, the glacier was closely monitored from August to October 2020. For this purpose, a time-lapse camera was installed and images of the area were taken during several helicopter flights. The time-lapse camera images were used to calculate surface flow velocity with time-lapse photogrammetry using pointcatcher software developed by James, How, and Wynn (2016). Images from the helicopter survey flight were used to create DHMs with SfM using Agisoft PhotoScan. SWISSIMAGE and open-source satellite imagery were also used to examine the long-term development of the glacier. The results were then compared to meteorological data from the nearest weather station. For this purpose, weather data was extrapolated to the height of the Ärlen Glacier. In addition, a PDDM was calculated to estimate the presence of meltwater.

The first sliding instabilities of Ärlen Glacier were detected in 2014, after the glacier had melted back over a terrain step in 2013. During 2020 the glacier slipped with velocities of up to 5 m/d over a total distance of ca. 60 m. The instable ice volume is estimated at 338,000 m^3 during 2020 and up to 1 million m^3 during previous events. This shows the major impact of climate change on glacier-related sliding instabilities caused by glacier retreat. However, several factors must interact to trigger a sliding event, as evidenced by quiet years such as 2016, when the glacier was above the terrain step but did not advance. We found that a hard and smooth bedrock combined with a period of increased basal motion is critical to collapse an entire part of the glacier. This mechanism shows many similarities with glacial avalanches observed at Allalin Glacier and, more generally, with glacial avalanches at temperate ramps. Therefore, hard-bedded glaciers that melt back over terrain steps need to be monitored more closely in the future, even if they appear flat and small like the Ärlen Glacier. This is especially critical when such glaciers are in a situation where they could affect infrastructures or trigger a process chain.

Acknowledgments

Table of Contents

List of Figures

List of Tables

1. Introduction

1.1 Motivation

Observations of the northern part of the Ärlen Glacier started because unusual crevasse patterns have been observed in the last years. To study the development of the glacier, a time-lapse camera was installed and pictures of the area were taken during helicopter survey flights. Then, during August and September of 2020 the glacier started unusual dynamics. First, the terminus collapsed in an ice avalanche. Subsequently, a rapid surge-type movement of the whole lower part of the glacier ensued, with maximal velocities of up to 4 meters per day. After first assuming that this was a singular event, further research including satellite imagery revealed that the glacier was in an unstable state since 2013 with further advances during 2014 and 2017/18 and more quiescent years with a melting terminus in between. For the small size (0,4 km^2) and flat slope (18,5° average instable area) of the glacier such mass movements are quite unexpected.

As Glaister (1951) accented after watching a major slide at Glacier Du Tour, glacier slides on this scale must necessarily be rare occurrences. Which makes it interesting to look for meteorological explanations for such events. Another event researched in detail by Röthlisberger (1997) and Faillettaz, Funk and Sornette (2012) is the catastrophic event at Allalin Glacier which claimed 88 lives in 1965, and its following instabilities. After researching large-scale glacier detachments Kääb *et al.* (2021) found that climate change not only accelerates glacier retreat, but also introduces a previously unobserved but catastrophic mechanism of glacier destruction. Recent large-scale glacier detachments have been observed around the world (Jacquemart *et al.*, 2020). Including Kolka Glacier 2002 (Haeberli *et al.*, 2004 and Evans *et al.*, 2009), the double 2016 detachments of the Aru Glaciers in Tibet 2016 (Kääb *et al.*, 2018), Leñas Glacier in the Argentinian Andes 2007 (Falaschi *et al.*, 2019), and repeated ice detachments from an unnamed glacier in central China (Paul, 2019).

Faillettaz, Funk and Vincent (2015) studied glacier instabilities in the Swiss Alps and concluded, that climate warming is likely to affect the stability of some glaciers in the near future. So, the events at Ärlen Glacier were not completely unexpected. The importance of understanding such events is noted by Huggel *et al.* (2004) with the reasoning, that glacier hazard caused severe damage in populated mountain regions such as the Swiss Alps. And that the assessment of such hazards must consider basic glaciological, and hydraulic principles together with experiences gained from previous events. Which reasons the question about the mechanisms and triggers of the instabilities at Ärlen Glacier. Fortunately, the glacier slide did not affect any infrastructure. But it shows how important it is to understand such processes in terms of natural hazards. In particular, due to the rapid changing characteristics of glaciers under the influence of climate change (Stoffel and Huggel, 2012).

1.2 Study Approach, Aim and Research Questions

The main research goal of this thesis is to quantify temporal and spatial pattern of the mass movements at Ärlen Glacier. Interesting factors are the evolution of flow speed and the timing of the surge-like advances. In addition to the precise analysis of the 2020 event with DHM generation from SfM and time-lapse photogrammetry, aerial photographs and satellite imagery are used to reconstruct the timeline of events and past of the glacier. The different glacier sliding instabilities during several years allow a detailed analysis for triggers of such glacier sliding instabilities. Which, complemented with a detailed analysis of the 2020 event, gives a rare opportunity to analyze such an event on different time scales ranging from years to hours. The approach is to reach a better understanding of such events considering basic glaciological and hydraulic principles. The results are then compared with experience from previous events, in particular the very similar case of the Allalin Glacier. This helps to assess the significance of such glacier disruptions in terms of natural hazards. In summary, the following research questions and sub-questions are addressed:

- **What were the main triggers for this mass movement?**
    - **How great was the influence of melt water for this process?**
    - **What is the influence of the polished sloping bedrock as a sliding interface?**
    - **How large was the geometric displacement for this rapid sliding event?**
    - **How important is the control of terminus stabilization?**
- **How does the speed and movement of this process compare to other glacier observations?**
- **What is the significance of this event for glacier related natural hazards in the Alps?**

The study is structured in logical order, similar to the workflow. The following chapter contains a brief summary of what is known about glacier ice dynamics and similar events in the Swiss Alps. In chapter 3 the data used for this study is presented and chapter 4 describes the applied methods in detail. Chapter 5 presents all results obtained from the analysis of the data. Then, chapter 6 contains the interpretation of the results, which are then compared to findings from other studies in related fields. Eventually, chapter 7 concludes the main findings by answering the research questions above. Furthermore, suggestions for improvement of the results as well as for additional topic-related research are presented.

2. Background

This chapter provides an overview of the study area. It then summarizes the current state of scientific knowledge on the flow dynamics of glaciers with emphasis on flow instabilities, including a closer look at a case with many similarities to Ärlen Glacier, the Allalin Glacier.

2.1 Study Site

The Ärlen Glacier is a small alpine glacier situated between 2540 and 3070 m.a.s.l. with a length of 0,8 km and an area of about 0,4 km^2. This study area is situated in the Swiss Alps, Canton of Bern, near the Grimsel Pass. More precisely from Handegg the Ärlen creek fallows the equal named valley till it branches. One leads trough the "Rinderthal" to the Ärlenglacier. Which is situated between the "Graugrat" and the "Ärlengrätli". The Glacier is now separated into a southern and a northern part which are both called "Ärlengletscher" due to their joined past. In this study the focus is on the northern part of the glacier (figure 1) which we refer to as simply Ärlen Glacier.
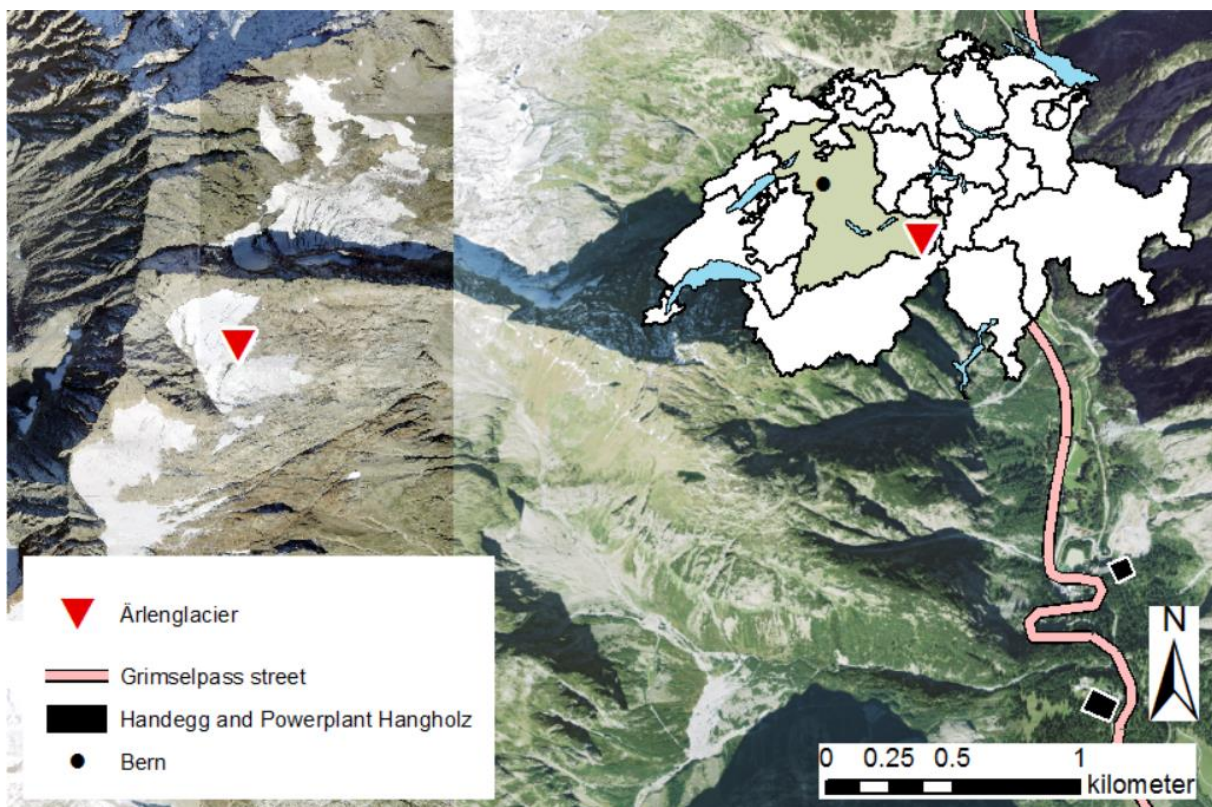
Figure 1: Location of Ärlen Glacier with Swissimage from 2018 for glacier and surrounding and Swissimage 2015 for the rest. Including the Grimselpass street and the two infrastructures (Handegg and Powerplant of Hangholz) situated beneath the Ärlenglacier. The insert map shows an overview of the location in Switzerland.

Beyond the glacier lays one of Switzerland most important and touristic pass streets (figure 1) the Grimselpass. Which connects the Bernese Upland with the Valais. One popular attraction is the Gelmerbahn which leads from Handegg to the Gelmersee. The area is also an important water energy producer for Switzerland which provides around 7% of swiss power every day (BKW, 2018).

The pass street leads through a wild bleak landscape with impressive granite walls and artificial lakes. The geology at Ärlen Glacier consist of Granite, Granodiorite and Quartz-diorite for the upper part of Ärlen Glacier and Gneiss and Mica Shist ("Glimmerschiefer") at the lower part of the glacier. The glacier is situated on a slab of hard bedrock which is polished from the glaciological past and is really slippery. A description from the field was: hard to walk on even at stunningly flat areas surrounding the glacier.

2.2 Dynamics of Glaciers

Glaciers slide because the accumulated excess of ice mass in the upper parts of the glacier must be balanced by the outflow of ice to the ablation area, where the loss of ice by melting or calving is replaced by the inflow of ice. Theoretically this discharge happens to maintain a steady-state glacier profile which is the balance flux (Jiskoot, 2011). The attendant velocity, called balance velocity, is controlled by the mass balance conditions and the glaciers geometry (Clarke, 1987). Glacier flow is a delayed cause of the quantity of accumulation received, and the individual response time depends on glacier type and size. Which leads to time lagged velocity fluctuations and corresponding advance and retreat rates (Jóhannesson, Raymond and Waddington, 1989).

The flow rates depend of the various stresses acting on the glacier, the way the ice can deform, and weather and how the glacier can slide along its bed. Gravitational driving stress is defined by the gravitational acceleration, the average density of glacier ice, the ice thickness and surface slope of the glacier. As a reaction to the driving stress, glaciers can move with three independent ice flow processes: internal deformation, basal sliding and soft bed deformation (Jiskoot, 2011). According to Davies (2021) this gravitational driving stress and the ability of ice to deform control the glacier's velocity. Which is an important parameter to understand glaciers behaviour and their dynamic response to a changing climate. In our case the soft bed deformation can be neglected due to the hard Granite bed properties at Ärlen Glacier.

2.2.1 Internal Deformation

Ice is affected by shear stress which is dependent from the pressure of the overlying ice and the slope of the surface. This shear stress has an effect on single ice crystals and also on a body of several crystals. As a polycrystalline and anisotropic body, glacier ice has a complex reaction to pressure and shear stress (Hagg, 2020).

The flow of a glacier can be described with a force-balance equation. In which the gravitational driving stress is balanced by resistive stresses (Jiskoot, 2011). This relation of stress and strain of glacier ice can best be described with Glen's power flow law, whereupon the deformation raises exponentially with increasing pressure (Glen, 1958). In glaciers, the relationship between strain rate ($\dot{\varepsilon}$) and effective shear stress (τ) is given by:

$$\dot{\varepsilon} = A\tau^n$$

Where A is a constant related to temperature and n is an exponent with a mean value of approximately 3 (Glen, 1958; Allaby, 2008 and Jiskoot, 2011). As a consequence, glacier ice gets more fluid with increasing pressure and increasing temperature (Hagg, 2020).

2.2.2 Basal Sliding

Basal sliding can only occur with a film of water between the ice-bed interface. Therefore, it can only happen at glaciers with temperate or warm ice. It happens because ice melts under pressure. This reduces the number of contact points and the friction between the two surfaces. This can ease decoupling and enhance fast ice flow and even allows the ice to slightly float if water pressure becomes high enough. If the glacier bed is rough, with a lot of bumps and obstacles, a process called regelation can occur. This process increases melting and ice flow and leads to enhanced strain melting at the upside. The following effect is that water overpasses the rock feature in a liquid state and refreezes at the backside due to a decrease of pressure. The sliding velocity is controlled by basal shear stress and the effective pressure, which results in the difference between ice overlay pressure and water pressure (Jiskoot, 2011 and Hagg, 2020).

Processes of basal sliding have a seasonality with their maximum at particularly high appearance of melt water, obliquely during summer especially during heat waves. The supraglacial accruing melt water finds its way partially below the glacier and raises the basal water pressure. Especially through high pressures in subglacial cavities the roughness of the bed gets smaller which alleviates the gliding process (Hagg, 2020).

2.2.3 Glacier Crevasses

Glacier ice is a polycrystalline viscoplastic material in the stress regime which is normally found in glaciers, with a plasticity after Glen's flow law depending on temperature and pressure. When a large amount of pressure is applied rapidly, glacier ice can break. Which results in glacier crevasses (Jiskoot, 2011 and Hagg, 2020). The pressure and consequently the plasticity increases with depth. From a certain depth ice is deforming so fast, that crevasses can no longer develop. Consequently, there is a maximal depth for crevasses which depends on the temperature. In the mid-latitudes this values lies at ca. 30 m (Hagg, 2020).

Depending on their formation different crevasses can occur. Crevasses are usually classified by their orientation in regard to the long axis of the glacier. The three main types are: transverse, marginal, and longitudinal crevasses. Transverse crevasses form before the terrain gets steep, as example in front of an icefall. Crevasses at the edge of the glacier occur due to different flow velocities of the ice in the middle and at the edge. They are arranged skewed to the glaciers edge. Longitudinal crevasses are rare and occur when the glacier diverges due to the topography and break up parallel to the direction of flow. Bergschrund crevasses form where the ice pulls away from the wall of the valley. Usually, some ice is left on the rock wall. Bergschrunds can get much deeper than 45 m (Freers, 1997; Colgan *et al.*, 2016 and Hagg, 2020). Seracs are needle like towers, of individual blocks of ice on a glaciers surface. They can be found within ice falls or on the lower edge of hanging glaciers. Commonly they are formed by intersecting crevasses where the glacier is periodically broken as it passes a steep slope (Konz, 2011).

2.2.4 Glacier Surges

A glacier surge is a quasi-periodic oscillation between long periods (tens or hundreds of years) of slow flow, called the quiescent phase, and shorter periods of typically 10 - 1'000 times faster flow, called surge phase or active phase. The change from slow to fast velocities is an internally triggered instability of the ice flow and reflects a sudden change within the glacier system. During the surge, the velocity increases abruptly and the faster flow can be sustained for a period of 1 - 15 years. These changes can sometimes correlate with extern factors (e.g. weather, climate and earthquakes). This is only possible if the glacier system was already close to a critical threshold. During the surge, a large volume of ice gets transported from the reservoir zone to the receiving zone (beneath), which can result in prominent advances at the glaciers tongue (kilometre scale) (Jiskoot, 2011; Paul, 2015 and Benn *et al.*, 2019).

Only about 1% of the world's glaciers have been observed to surge (Jiskoot, 2011 and Sevestre *et al.*, 2018). But the significance of surge-type glaciers extend their numbers because they raise questions about the general assumptions of glaciers dynamics (Benn et al., 2019). They can occur on land-terminating glaciers, tidewater glaciers, cirque glaciers, valley glaciers and ice streams and also on glaciers with both, temperate or polythermal regime. They show a large range of cycle length and amplitudes. And they often form a continuum with non-surge-type glaciers (Herreid and Truffer, 2015).

Analyses on global and regional scales showed that surge-type glaciers occur within clearly defined climate envelopes, and show consistent geometric characteristics despite of their thermal regime (Clarke *et al.*, 1986; Jiskoot, 2011 and Sevestre and Benn, 2015).

The analysis of Sevestre and Benn (2015) showed that surge-type glaciers occur within a well-defined climatic envelope bounded both by temperature and precipitation. Surge-type glaciers are absent above a threshold of MST = 0.001MWP+ 8.4 (MST: mean summer temperature in °C; MWP: mean winter precipitation in mm a^{-1}), and below MST = 0.0014MWP - 0.97. The clear threshold of precipitation provides the lower boundary for the optimal surge envelope with MST = 0.015MWP - 28.4. The surge-type glaciers in this zone belong to the two main superclusters. The arctic ring, extending from Alaska/Yukon to Novaya Zemlya (but excluding Arctic Canada) and High Mountain Asia, particularly the Pamirs, Karakoram and Tien Shan. Much lower concentrations of surge-type glaciers are found in the colder, drier climates of Arctic Canada (Sevestre and Benn, 2015). Additionally a soft glacier bed seems to be a necessary (but not sufficient) condition (Harrison and Post, 2003 and Truffer *et al.*, 2021).

Surges apparently happen due to a combination of the deformable properties of the subglacial sediment, in combination with changes in glacier thermal regime and feedbacks that disturb subglacial hydrology. If the gravitational force of the glacier exceeds the friction at the base certain changes happen in the subglacial system. The friction is decreased, subglacial deformation is enabled and surges occur. The surge ends when the reservoir is depleted, or a change in the hydrological system happens. Surges may also appear when meltwater becomes available suddenly at the base of the glacier. Which lubricates the bed and helps the glacier to flow faster. The appearance of surges is relatively unpredictable, and understanding of surge-type glaciers is limited (Davies, 2020).

2.2.5 Glacier Avalanches and Slides

Glacier avalanches are masses of ice that have detached from the glacier and plummet into the valley. They usually occur during summer and result from a destruction of tensile strength in the ice mass through progressive fragmentation associated with crevasse development, melting of parts of the glacier that may be frozen to the substrate, and reduction of frictional resistance at the ice-rock interface due to increased water pressures (Evans and Clague, 1994).

Historical events in the Alps are known to have involved volumes of up to a few million cubic meters, and to have reached horizontal run-out distances of up to about 6 km; with even higher values known from other mountain areas of the world. Proceeding from such historically documented extreme run-out distances, the area where potentially dangerous ice avalanches may start can be roughly defined as a first step. Factors affecting the stability of ice on steep slopes are adhesion of temperate and cold ice on bedrock, cohesion with more stable up-slope ice, shear strength with respect to lateral abutments, and support both from down-slope ice and more especially from cold ice margins frozen to bedrock if the starting zone is not (yet) at the terminus (Röthlisberger, 1981).

With respect to the glacier-bed geometry, it is appropriate to distinguish two morphological types of starting areas. The Ärlen Glacier can be classified as ramp-type geometry. Therefore, only this type is further discussed. The ramp-type (figure 2), has a starting area which is situated on a steep and uniform slope, on which the ice slides or shears. The instability affects primarily the base of the glacier. Ramp-type slab failures can release very large volumes of ice, and in such cases the critical slope for possible avalanche formation appears to increase with increasing altitude and decreasing bed temperature. The possibility for an avalanche formation also increases at edges where the starting area lies at a marked break of the slope angle. Due to strong tensile stresses the ice cracks in form of unstable seracs (Iken, 1977 and Alean, 1984).
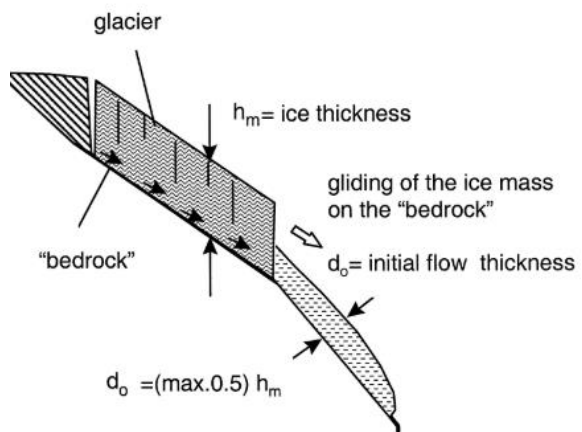
Figure 2: Ramp-type slab failure (Margreth and Funk, 1999). Morphological type which comes closest to situation at Ärlenglacier.

Major ice avalanches from temperate ramps seem to be limited to the late melt season. On cold ramps however they can occur during the whole year. According to Haeberli *et al.* (1989) the existence of a critical bedrock slope is a necessary condition for the formation of large avalanches on ramps, although it's not the only requirement. With warm ice, where a film of water between the ice and bedrock enables basal sliding, ice avalanches can occur with a slope of only 25° (Haeberli *et al.*, 1989).

Usually the slips starts between the start of summer and fall but stops at the beginning of winter, between the midst of September and midst of November (Röthlisberger, 1981). This process cannot be explained only with one factor and the main factors according to Röthlisberger (1981) are discussed in the following paragraphs.

The temporal confinement of the phase with enhanced basal motion (which will be referred to as the "active phase") to the ablation period suggests a climatic influence. The natural choice would be the influence of temperature. But the stagnation during fall is difficult to explain by cooling alone, because the ice could only cool fast enough to freeze to the rock at the front, edges and bottom of crevasses. The assumption would be that in years with early snow, the glacier would not freeze further and the slide would not stop due to the insulating properties of snow. Thus, it appears that the temperature has an indirect effect on detours via melt water. When there is no melt water available, the glacier stops.

In contrary it seems like the start of a slide is not controlled by meltwater, because the acceleration happens randomly at any time during summer or fall. However, heavy hints persist that the mass distribution determines if and when a slide happens during a particular year. Observations lead to the assumption that only if enough ice is gathered at the back of the unstable area a slip can appear. The area at the top of the unstable glacier section seems to have the function of a reservoir. On the top of this area a characteristic listric breakout niche opens during slide events. If the reservoir zone empties heavily during a strong slide, it takes longer to reach the next slide than after a short incomplete slide. Which leads to the effect, that typically after a heavy slide the glacier experiences one to two quiescent years.

2.3 Allalin Glacier

The Allalin Glacier is located in Valais, in the Swiss Alps near the head of the Valley of Saas. It has a temperate tongue (Röthlisberger, 1981) with an altitude ranging from 2200 to 2800 m.a.s.l.. The glaciers tongue advanced repeatedly and blocked the river Saaser Vispa leading to the formation and outburst of an ice dammed lake. During the centuries, the glacier was mentioned repeatedly, mainly due to floods caused during stages of glacier advance, and when it cut off the path leading to alpine meadows and pass routes leading to Italy (Faillettaz, Funk and Sornette, 2012). After the advances of 1920 the glacier retreated during three decades. From 1954 the glaciers terminus stayed unchanged for about 10 years except from a few variations (Röthlisberger, 1997).

During the 30th of August 1965, nearly 2 million m^3 of ice broke off at the terminus of Allalin Glacier. They moved down a rock slope of ca. 27° over the vertical distance of 400m and continued for a further 400 m across the flat bottom of the valley (Faillettaz, Funk and Vincent, 2015). This suddenly shortened the length of the glacier by 400m (Röthlisberger, 1997). The catastrophic event claimed 88 victims at the Mattmark construction site (Faillettaz, Funk and Vincent, 2015). During July 2000, the glacier geometric configuration reached a position similar to 1965. For safety reasons the hazard zone was closed during summer. On the 31st of July an ice volume of 1 million m^3 broke off, but did not cause any damage. Subsequently the glacier remained stable, and the terminus remained roughly at the same latitude (Röthlisberger, 1997 and Faillettaz, Funk and Sornette, 2012).
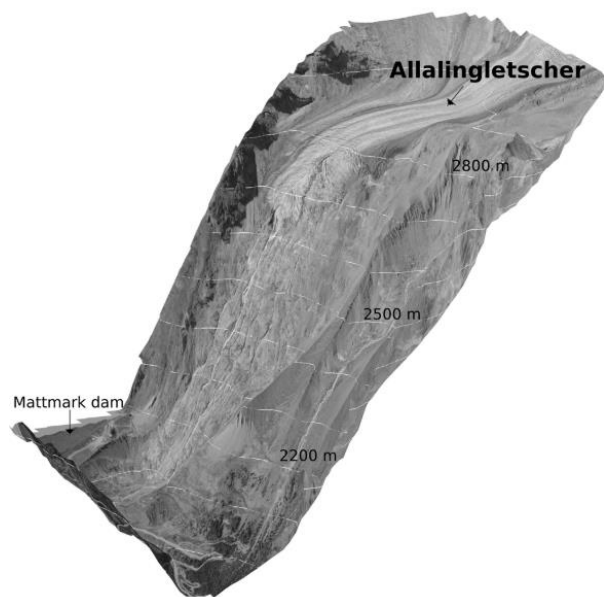
Figure 3: Detailed topographic map of Allalin Glacier from Faillettaz, Funk and Sornette (2012).

According to Röthlisberger (1981) the slides in the case of Allalin Glacier follow each other at intervals of one, two or three years, takin place on an area with a slope of 22°, beyond a steep step with seracs. Glide velocities of up to 4,5 m/d were measured, compared to typical winter velocities of 5 cm/d during calm phases. During heavy slides the moving mass separates from the bottom of the seracs zone and the bedrock emerges. Accordingly, to the stepped terrain ice debris peaks grow, which melt away during quiescent years.

The changes at the terminus show a restless pattern of advances and retreats in the range of tens of meters from year to year. They show a number of similarities with surge-type glaciers (Röthlisberger, 1997). Surface velocity measurements performed on the steep tongue after the event of 1965, revealed periods with enhanced motion for nearly every year. The active
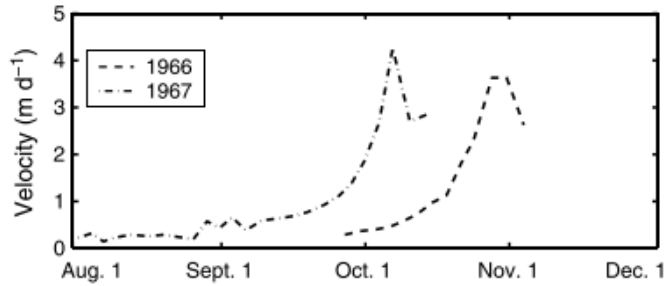
Figure 4: Surface velocities measured on the tongue of the Allalinglacier in 1966 and 1967 from Faillettaz, Funk and Vincent (2015).

phases usually start in the late summer and last for two to three weeks (figure 4). Röthlisberger (1997) pointed out a possible connection with subglacial water flow. However, with an exception of the two events in 1965 and 2000, the active phases ceased suddenly without triggering any major sliding event. This shows, that these active phases are not sufficient for the occurrence of a slide event, but are a necessary condition (Faillettaz, Funk and Vincent, 2015).

On steep temperate glacier tongues, sliding instabilities may occur. These instabilities are strongly affected by the subglacial hydrology, because infiltrated meltwater causes a lubrication of the bed and decreases the effective pressure at the bed, which decreases the basal friction. The results of a study over three cases in Switzerland by Faillettaz, Funk and Vincent (2015) showed that five different criteria have to be met for such an instability to occur:

1. A critical geometrical configuration at the glacier tongue is necessary (steep slope, no frontal abutment, and convex shape of bed topography).
2. The glacier should have gone through an active phase.
3. The subglacial drainage network has to be distributed.
4. A colder period with decreasing runoff is needed (reduces efficiency of drainage network and favours fracturation process).
5. A pulse of subglacial water flow is a probable trigger for the catastrophic break-off event.

Röthlisberger (1997) also analyzed possible criteria and causes of the glacier instability of the Allalin Glacier:

- The stepped characteristics of bedrock.
- The active phase the glacier was already experiencing during 2-3 weeks as the lowermost part detached and plummeted.
- The heavily crevassed glacier tongue.

- Possible formation of an ice arch due to the high velocities (active phase). Which collapsed after the loss of its abutment after it was showed over a terrain step below.

To achieve a major break off event the combination of two opposing phenomena is required. The glacier needs to be in an active phase with strongly enhanced basal motion and this active phase must be halted abruptly with a sudden recoupling of the glacier to its bed (Faillettaz, Funk and Vincent, 2015).

To check the plausibility of this process chain Faillettaz, Funk and Sornette (2012) researched the runoff, which is assumed to be proportional to the meltwater input, during the years 1965 and 2000 when the major break offs happened. It appears that in both years meltwater increased sharply one month before the event, resulting in an active phase. During the 6 days prior to the break off the runoff dropped from 13 to 5 m^3 s^{-1} in 2000 and from 14 to 5 m^3 s^{-1} in 1965. Then the runoff increased again for e few days before the major break off happened. This reinforces the assumption that an additional water pulse is required as a trigger for instabilities once the glacier is re-coupled to its bedrock.

The modelling study by Faillettaz, Funk and Vincent (2015) showed that this observed sequence of basal water pressure change corresponds to the process chain leading to the final breakoff. In their study they assume, that this sequence of basal water pressure that enables a catastrophic breakoff can be interpreted as follows: The stability of subglacial water channels is controlled by the balance between creep closure and melting of ice on the channel wall based on turbulent heat dissipation of the flowing water. Therefore, a persistent decline in runoff would result in progressive channel closure and a reduction in the efficiency of the drainage network. A subsequent runoff pulse would result in an increase in basal water pressure and a corresponding decrease in basal resistance. This could potentially trigger the catastrophic breakoff event.

Similar glacier instabilities are rare, but some examples (e.g., Le Tour 1949 (Glaister, 1951) and Fee Glacier 2009 (Faillettaz, Funk and Sornette, 2012)) have already been documented in detail. Faillettaz, Funk and Vincent (2015) conclude, that in a more general context climate warming will likely affect the stability of some glaciers in the near future. With the ongoing glacier retreat presently dangerous glaciers will disappear (e.g., Allalin Glacier, or Altels Glacier), but other glaciers may become unstable.

3. Data Description

3.1 Time-Lapse Camera

A time-lapse camera was installed on the south side of Ärlen Glacier to monitor and research the sliding event (figure 5). Recording began on July 31, 2020, with a time interval of 30 minutes. The observations considered in this study extend until October 25.

Survey gaps

- 07. Aug; no images
- 08. - 10. Aug; only one image per day
- 11. - 12. Aug; Only few images per day
- 15. Aug - 21. Aug; no images
- 22. Aug – 25 Aug; only few images per day
- 23. Sep; only 3 images
- 25. Sep; no images on the afternoon (whole day bad weather)
- 26. Sep; snowfall and ice on the lens
- 28. Sep; only images till noon
- 20. – 25. Oct; only one picture per day
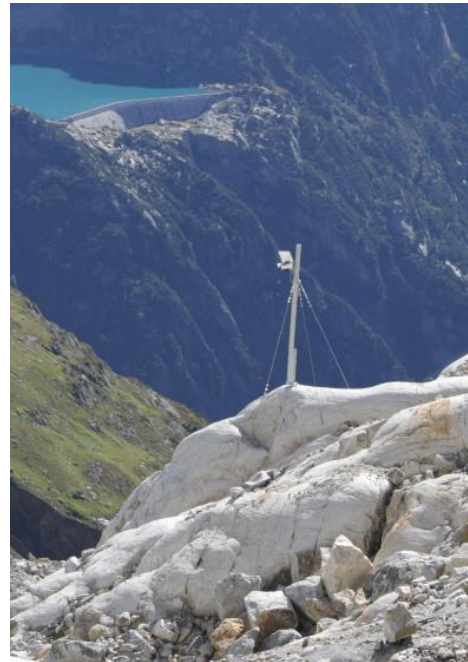
Figure 5: Time-lapse camera installed at Ärlenglacier (2020). With the dam wall of Gelmersee in the background.

3.2 Ground Control Points

During the survey on September fourth, ground control points (GCPs) were painted on rocks and boulders (figure 6). The goal was to have regular points around the entire unstable part of the glacier that would be visible from the time-lapse camera. The locations of the points were surveyed with precision GPS. The GCPs with the corresponding coordinates were later verry useful for various applications. It provides an easy way to convert data from images to distances in meters or to a coordinate system. The points were used in this work for georeferencing, SfM and time-lapse distance measurements.

Figure 6: Example of a GCP painted at rocks and stones, which are visible from the time-lapse camera.

3.3 Airborne High-Resolution Photographs

In order to document and observe the evolution at Ärlen Glacier, survey flights were conducted by helicopter (figure 7). In this study, the images of two flight surveys were used, mainly for the SfM surveys. The first flight took place on September 4 and the second on September 22, 2020.

3.4 Images from Known Ground Positions

During the survey on the 4th of September at Ärlen Glacier, images were taken from known places around the glacier. For this study, these images were mainly used for visual interpretation.

3.5 SWISSIMAGE

The orthoimage mosaic SWISSIMAGE is a compound of digital color aerial photographs. In an orthoimage the angle influences of the camera and terrain are corrected. Therefore SWISSIMAGE has consistent scale and radiometry properties over the whole area of Switzerland (Swisstopo, 2020).

Figure 7: Helicopter over heavily deformed Ärlenglacier during a survey flight (04. Sep 2020).

From 2011 the product SWISSIMAGE FCIR was launched. It consists of three channels, near infrared, red and green (Regamey, 2017). This additional information improves the visibility of some glacier structures in poor conditions. In this work it was used in 2013 because of the snow cover.

SWISSIMAGE RS contains orthoimages with even more information. The four spectral ranges visible to Leica's ADS (Airborne Digital Sensor) (near infrared, red, green and blue) were orthorectified and merged into the same file (Regamey, 2017).

The data is produced in tiles. The tiles used for this Study are: 2662_1164 / 2663_1164 / 2662_1163 / 2663_1163. The numbering represents the kilometer coordinates of the southwestern vertex of a tile.

Table 1: SWISSIMAGE Products used in this study. Including the year and date of flight, and the spatial resolution. The appertaining images can be found in the appendix, chapter IV.

Year	SWISSIMAGE Product	Resolution	Date of flight
2018	SWISSIMAGE 10 cm	10 cm	26. Sep
2017	SWISSIMAGE RS	25 cm	29. Aug
2016	SWISSIMAGE 25 cm	25-50 cm	07. Sep
2013	SWISSIMAGE 25 cm SWISSIMAGE FCIR	25-50 cm	23. Sep
2010	SWISSIMAGE 25 cm	25-50 cm	21. Sep
2004	SWISSIMAGE 50 cm	50 cm	09. Sep
2000	SWISSIMAGE 50 cm	50 cm	24. Aug
1993	SWISSIMAGE HIST	50 cm	18. Aug
1986	SWISSIMAGE HIST	50 cm	29. Sep
1980	SWISSIMAGE HIST	50 cm	26. Aug

3.6 Open-Source Satellite Imagery

For better temporal resolution, all open-source satellite imagery available for Ärlen Glacier from 2013 to 2020 was examined. Open-source satellite images are usually limited in resolution. Therefore, they were used only for front position mapping and detecting the timing of changes in frontal positions and ice avalanches.

Sentinell-2 and Landsat-8 data is freely available from Sentinel Hub (https://www.sentinel-hub.com/). World Imagery is a compilation of various high resolution satellite imagery, provided by Esri for most of the world (Esri, Maxar, Earthstar Geographics, USDA FSA, USGS, Aerogrid, IGN, IGP, and the GIS User Community).

Table 2: Open-source satellite imagery, available for interesting time period of Ärlen Glacier slide. The appertaining images can be found in the appendix, chapters V and VI. Images with no cloud cover und as less snow as possible were chosen.

Year	Satellite	Spatial Resolution	Temporal resolution	Date	Source
2020	Sentinel-2	max. 10 m	2-3 days (mid-latitudes)	19. Aug; 27. Aug; 08. Sep; 13. Sep	(European Space Agency, 2015)
2019	Sentinel-2	max. 10 m	2-3 days (mid-latitudes)	19. Sep; 27. Sep	(European Space Agency, 2015)
2018	Sentinel-2	max. 10 m	2-3 days (mid-latitudes)	09. Sep; 27. Sep; 29. Sep; 12. Oct	(European Space Agency, 2015)
2018	World Imagery	1 m or better	Compilation of different satellites worldwide.	23. Oct	(Esri, 2021)
2017	Sentinel-2	max. 10 m	2-3 days (mid-latitudes)	15. Aug; 23. Aug	(European Space Agency, 2015)
2015	Landsat-8	30 m	16 days	07. Aug; 30. Aug	(U.S. Geological Survey, 2016)
2014	Landsat-8	30 m	16 days	28. Sep	(U.S. Geological Survey, 2016)

3.7 DEMs

The digital height model DHM 25 is a dataset containing the three-dimensional form of the Earth's surface without vegetation and constructions. It was essentially derived from the height information of the National Map 1:25 000 (LK25). The model is a height matrix with a mesh size of 25 meters. Figure 8 shows the year in which the height information was taken. For this work the left upper year was considered, because it contains the update year for height contour lines on glaciers (Swisstopo, 2005). Which is 1993 in the case of Ärlen Glacier.
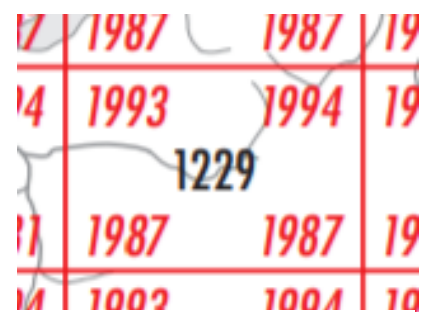
Figure 8: Perimeter of DHM25, containing Ärlenglacier. Left, upper year: Update, hight contour lines on glaciers (Swisstopo, 2005).

swissALTI[3D] is a high-resolution digital terrain model (DTM). Which shows relief features of Switzerland and Liechtenstein without vegetation and constructions. The actualization cycle is 6 years. The data is available as Raster dataset or as xyz-file. With a regular grid of 2m, 5m, and 10m. Each cell of the grid contains a height value. The grid is oriented in the Swiss coordinate system CH1903+ (Swisstopo, 2018).
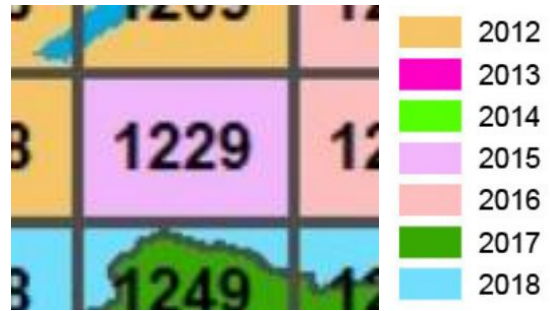
Figure 9: Perimeter of swissALTI[3D] containing Ärlenglacier (1229). Legend on the right side contains the flight year for the updates of each perimeter (Swisstopo, 2019).

The elevation data are taken from various data sources. Above 2000 m.a.s.l. point values are calculated with stereo correlation, and if necessary, specifically photogrammetrically revised. Considering the different data sources and survey methodologies the dataset has no consistent accuracy. Over 2000 m.a.s.l. the estimated accuracy is : ± 1 m - 3 m 1 σ; and 25 cm - 1 m for manual revisions (Swisstopo, 2018).

Figure 9 shows the tile number and flight year of updates for the concerning perimeter. For the area containing Ärlen Glacier the flight year is 2015. This was considered for the PDDM and volume change calculations.

3.8 Climate Data

The weather station *Grimsel Hospitz* is situated at 1988 m.a.s.l. close to the Grimselpass. It is the closest weather station to the Ärlen Glacier (7,74 km airline).

The following parameters are measured in time intervals of one hour.

- Total snow height [cm]; instantaneous value
- Air temperature 2m above ground [°C]; hourly mean
- Global radiation [W/m^2]; hourly mean
- Fresh snow height [cm]; instantaneous value
- Precipitation [mm]; hourly sum

In this study mainly the air temperature and precipitation from this weather station are used. The other measurements, such as global radiation, would be interesting for melt modelling, but the changes in comparison with the Ärlen Glacier are probably too large. In-situ measurements would be necessary, since the effects on global radiation are indeed site-dependent.

4. Methods

4.1 Glacier Front Positions and Length

To understand the evolution that led to the critical state of the Ärlen Glacier, all available imagery since 1980 was examined.

The front positions were mapped free-hand in *ArcMap*, if available according to orthoimages (SWISSIMAGE HIST, SWISSIMAGE 25, SWISSIMAGE 10 cm, SWISSIMAGE RS) (chapter 3.5) or satellite imagery (*Sentinell-2, Landsat-8,* World Imagery) (chapter 3.6).

To convert the frontal positions into numbers, the length of the glacier was measured along the centerline for each available image (figure 10). Then, the cumulative changes in length relative to 1980 were calculated. The resulting numbers are meters of melt relative to the frontal position at the centerline in 1980 (= 0 m).

Figure 10: Estimated center line for Ärlen Glacier. Drown by visual interpretation of Aerial Images and crevasse patterns. Background is the aerial image from 2016 and contour lines from swissALTI ^{3D} from 2015.

To map a reasonable center line for a glacier like the Ärlen Glacier is only possible by free hand. First, because the glacier was connected to the southern part of Ärlen Glacier till ca. 2013. Second, the melt is very heterogenous along the vertical terminus profile. In this case, some simple rules were followed as suggested by Le Bris and Paul (2013). The line should extend from the highest to lowest point and should always be in the middle of the glacier.

4.1.2 Timing of Mass Movements

To understand the mechanisms of the mass movement the timing is really important. The mass movement in 2020 was really nicely documented with the time lapse camera and the helicopter survey flights. For the other mass movements, the data consists of a few aerial or satellite images per year. To narrow down the possible time frame of the movements, the first date on which a change was detectable was noted. With this approach the events could be allocated to a time period. In some cases, with a precision of a few days and sometimes only months. For further restriction and reasoning of triggers the timing is compared with triggers described by Faillettaz, Funk and Sornette (2012).

4.2 Surface Flow Velocity with Time-Lapse Photogrammetry

Time-lapse photogrammetry has its advantages of providing results with high spatial and temporal resolution results (Ahn and Box, 2010) while being simple and inexpensive to apply (Messerli and Grinsted, 2015). Therefore, it is a powerful technique to obtain detailed information about glacier speed and its variations (Harrison *et al.*, 1992). But as Harrison *et al.*, (1992) also mentioned in their research, the conditions are often not ideal. This leads to problems when the data needs to be converted into absolute glacier velocity.

4.2.1 Pixel Tracking with Pointcatcher

There are a lot of different software applications to track pixels and calculate their velocity (How *et al.*, 2020 and Messerli and Grinsted, 2015). The one used in this research was developed by James, How and Wynn (2016) and is freely available (https://www.lancaster.ac.uk/staff/jamesm/software/pointcatcher.htm). This software was chosen for this approach because of its simplicity. The tracked pixels can be easily exported as text file for further review and editing.

The ability to manually track points was also very useful for this study. Due to the large light and surface variations (snowfall, rain), automatic tracking was not possible. Tracking points manually leads to quite a large subjective uncertainty. It is also very labor intensive. But the ability to track prominent crevasses or dirt deposits in changing light conditions provides an opportunity to understand the speed variations of such a process.

Nevertheless, some points were difficult to track even manually. The changes in the appearance of the ice during changing light conditions or precipitation events are impressive. Due to the rapid flow of the glacier, the appearance and patterns of crevasses and debris deposits change greatly as it flows downstream. This is especially true for a glacier as highly crevassed as the Ärlen Glacier during 2020.

Figure 11: Examples for good trackable points (red cross) in the Ärlen Glacier images from the time-lapse camera. The red cross is the exact point tracked by Pointcatcher. For the most accurate tracking, the edge of a trackable shape was chosen whenever possible.

Very useful were well visible edges and corners in crevasses. Dirt deposits are also very good for tracking, but disappear completely in fresh snow. The best points are dark shadows in crevasses or under ice blocks, which remain in shadow in almost all light conditions (figure 11).

To understand the temporal patterns of the ice movement, this study examines different temporal resolutions. For the daily speed variations, one picture was chosen for each day. If available between 11:30 and 13:30, for easier trackability under similar light conditions. On days without a picture around noon, the best picture of the day was chosen. For the hourly speed variations one picture every hour was utilized.

4.2.2 Conversion to Distance

Figure 12: Displacement vectors from Pointcatcher for the three observed points (Pt1 to Pt3 from left to right). The background image is from the time-lapse camera at the 26th of August just before the break off at the front.

To determine the distance traveled by the observed points over the duration of a day, the distance d in the x and y directions was evaluated for each image. The Δ was obtained by subtracting the previous pixel value. This results in two sides of a rectangular triangle. The distance was calculated using the following formula.

$$d = \sqrt{\Delta x^2 + \Delta y^2}$$

When trackable points were not visible in an image due to bad weather, fog, or lighting conditions, an average of the velocity was assumed until the point could be recovered in a subsequent image.

4.2.3 Conversion from Distance in Pixel to Meters

For the conversion of the distances measured by pixel tracking into meters, it was planned to use the GCP (figure 13). However, since the GCP on the north side of the glacier were not visible on the time-lapse camera images, another approach had to be taken. The first other idea was to look for clearly visible terrain points on the north side. But due to the low resolution, there were not enough good terrain points.

Finally, the approach chosen, was to use a georeferenced image from one of the helicopter survey flights. The GCP were clearly visible on some of those images and could be used for the georeferencing with ArcGis.

The pixel size per meter differs depending on the position on the time-lapse camera image. This is also strongly dependent on the terrain. To account for this effect, calibration of the calculation from pixels to meters is required. We choose a simple approach where the pixel size in meters decreases linearly with increasing distance from the nearest edge of the image.
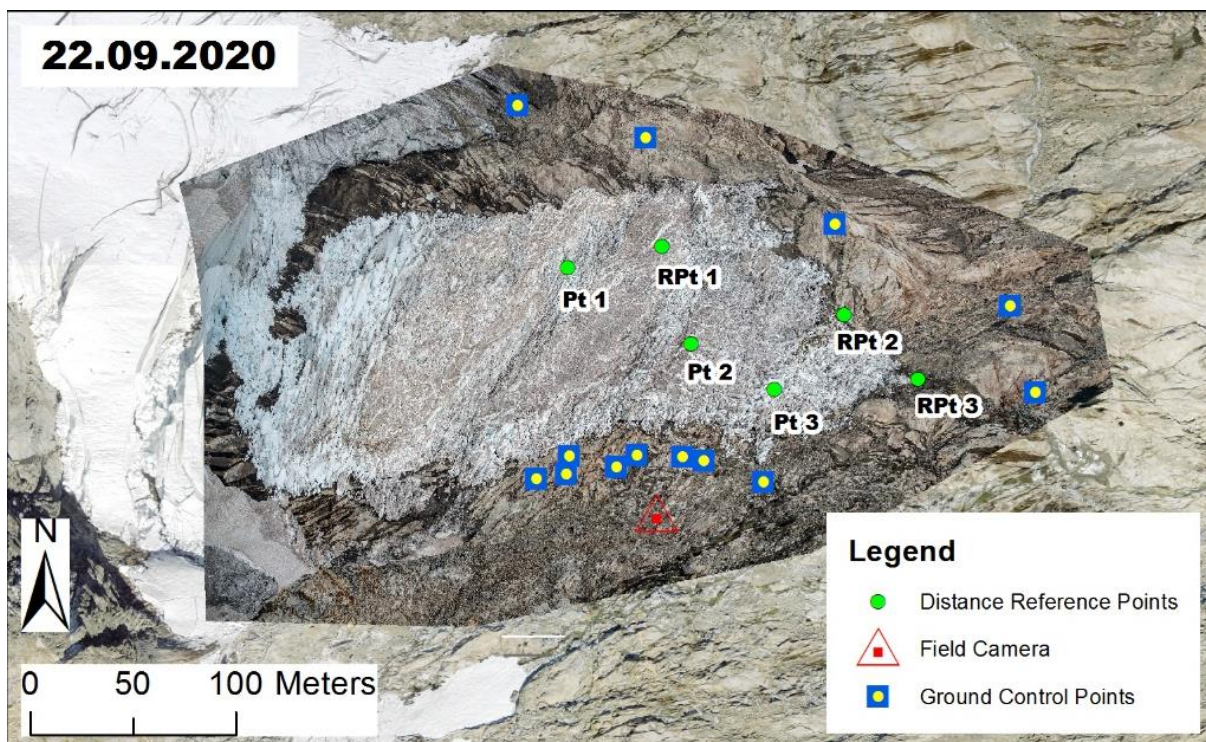
Figure 13: Helicopter survey flight image from the 22nd of September with points used for calibration (Distance reference points). Background is the Swissimage Orthophoto from 2018. Where Pt1 - 3 are the first points and RPt1 - 3 the corresponding points to which the distance was calculated. Once in pixel from Pointcatcher and once in meter with ArcGis.

To estimate the decrease in resolution, points were searched on the helicopter survey flight image from September 22 and the field camera image from the same day. The GCP (1 to 8) on the southern part of the glacier could be found on both images. In addition, 6 points were identified on both the helicopter image and the time-lapse image (figure 13). Due to the assumption of a linear decline with distance from the lowest edge of the image, the points were paired with another point with a similar y-pixel value.

Because the ground control points are on a similar distance, the distances between all found GCP was calculated. The distances in pixel and in meters were then compared, and a pixel per meter value was calculated for the distance between the used points (table A6).

Because it was assumed, that the resolution declines linearly with the distance in y direction the Δ was calculated for each point. In comparison with the conversion factor, it made some sense, but the variations were quite big. But there were clusters with nearly the same pixel per meter seizes. This clusters where grouped and the mean Δy for each cluster was calculated (table A8). For the mean Δy a linear trend line was calculated (y = - 8605,3x - 219,77) (figure A60). This trend line was then used to calculate the conversion factor for each point of the time-lapse tracking. The whole calculation of the calibration line can be found in the appendix chapter II.

Compared to the distance advance in the Semtinel-2 images, the resulting values are comprehensible. However, the uncertainty in this approach is estimated to be quite high since the topography has a substantial effect on the resolution of the image with distance.

4.3 SfM of Helicopter Aerial Images in Agisoft PhotoScan

Structure-from-motion (SfM) is a very useful tool for creating DEMs from images. As the name implies, SfM derives the structure of the measured surface from data captured by a moving sensor. The sensors are often optical or thermal cameras, and motion is usually achieved by mounting the sensor on drones, aircraft, or satellites. In this study, an approach is taken using high-resolution imagery captured during a survey flight by a helicopter. The challenges and opportunities of this approach are discussed later in the paper (chapter 6.4.4). In this way, series of overlapping images are acquired, which are finally processed in a digital SfM software (Agisoft PhotoScan in this study) to create 3D models of the surveyed area. The 3D geolocations and 3D structures of the surveyed objects are calculated according to the principles of photogrammetry, using algorithm-based identification of identical points in over-lapping images to triangulate their relative positions (Honegger, 2020).

Agisoft PhotoScan is a highly advanced image-based 3D modelling program. From a user's perspective, SfM software is largely a black box. Because the exact functionality of the underlying algorithms is not available. The program is based on the latest multi-view 3D reconstruction technology and operates with arbitrary images. It works both in controlled and uncontrolled conditions which was a huge ben-efit for the characteristics of the data for this study. The Images can be taken from any position, as long as the object to be reconstructed is visible on at least two photos (Agisoft, 2018).

Due to the poor quality of the first results, many different processing options and combinations of GCPs were used aiming for improvement. However according to Honegger (2020) the main limiting factor is the contrast and color quality of the input images. The quality of the resulting DEMs is discussed in chapter 6.4.4.

Compared to drone SfM projects the number of images taken during the helicopter survey flights is low. Which largely effects the processing time. This made it possible to process in Agisoft PhotoScan with high/-est accuracy settings with manageable time investment. The output coordinate system was set to LV03, according to that of the GCPs.

4.3.1 Ground Control Points Selection

Due to the unknown camera coordinates, GCPs are used to set the coordinate system and for photo alignment optimization. The photo alignment is done automatically by PhotoScan for most images. However, for images where the angle deviates too much, manual GCPs are required for photo alignment. According to Agisoft (2018) at least 5 GCPs are needed for manual photo alignment. The GCPs are used to specify locations within the scene. The more images used to determine marker location, the higher the accuracy of GCP placement. To define the GCP location within a scene, it should at least be placed on 2 photos (Agisoft, 2018).

Because the GCPs painted around the glacier were not yet painted for the first survey flight, additional GCPs had to be selected. These had to be inside of the stable ground (chapter 4.3.2). Points were selected which could be found both, on the helicopter images and on the SWISSIMAGE 10 cm from 2018 (figure 14). This approach needed a lot of adjustment with trial and error, to learn which additional GCPs work and which are too unprecise. Uncertainties and precision of this methods are discussed in chapter 6.4.4.
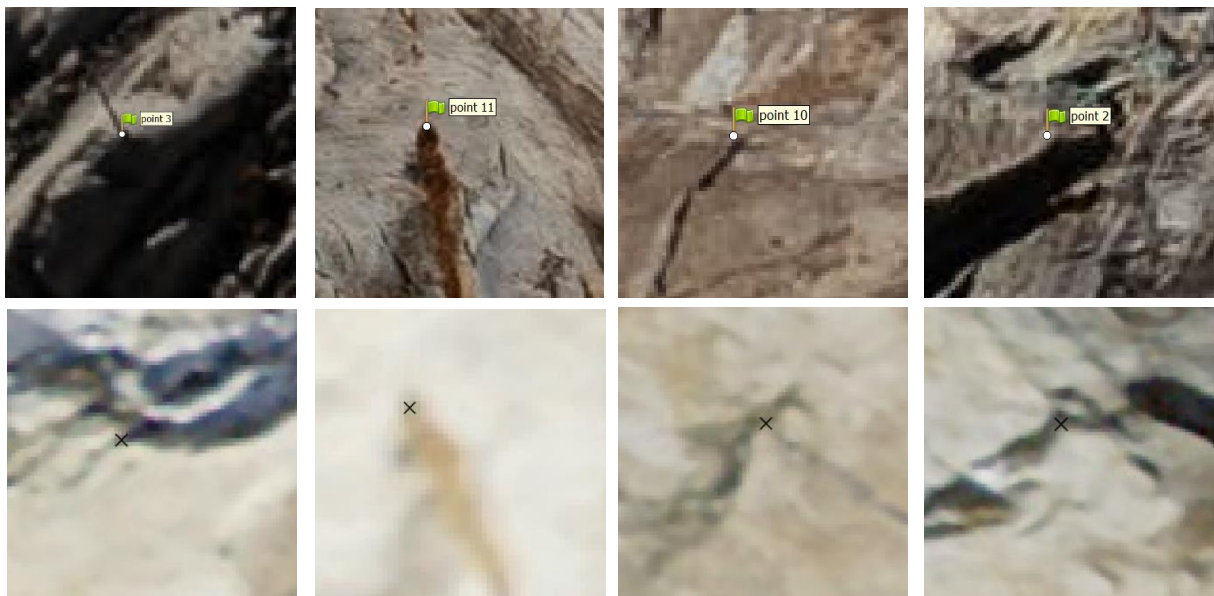
Figure 14: Examples of additional GCPs at the top found on the images from the helicopter survey flight (green flags), and their corresponding points on the Swissimage from 2018 (black crosses). The corresponding coordinates in x, y and z were sourced from the swissALTI^{3D} project.

4.3.2 Determination of Stable Ground

The newest height information derives from the swissALTI³ᴰ project. In this area the measurements are from 2015 (figure 9). To make sure, that the additional GCPs aren't on the glacier, only points inside the stable ground (figure 15) were selected. The stable ground is the area, where there is no glacier since 2015. The extent was determined by visual comparison of SWISSIMAGE from 2016 but also considering the glacier advances observed on the Satellite Imagery. Some points were chosen outside the stable ground, because of the difficulty to find usable GCP. Those point were set at locations were only

Figure 15: GCP used for the SfM generation for the Helicopter survey flight on the fourth of September 2020. The GCPs are set inside the stable ground.

small changes from the swissALTI³ᴰ would be expected. For example, at locations with only little snow cover. Or where the glacier advanced during 2017/18 which is influencing the altitudes of swissALTI³ᴰ. For the different SfM projects, different GCP had to be chosen due to the difficulty to find them both, in the helicopter survey image and the Swissimage from 2018.

4.3.3 DEM Differencing

In order to detect spatial patterns of surface elevation change, the DEM from swissALTI³ᴰ (2015) was subtracted from the DEM derived from the helicopter flight on the 4th of September 2020. Additional for mass balance estimation, the difference of swissALTI³ᴰ (2015) to DHM 25 (1993) was calculated. According to the timespan between the chosen scenes, shorter- or longer-term spatial surface elevation change patterns can be detected. Difference raster shows the change of the surface elevation per grid cell and are calculated as follows:

$$\Delta h = DEM_{new} - DEM_{old}$$

4.4 Extrapolation of Climate Data

The weather station of *"Grimsel Hospitz"* is situated about 660 meters below the examined area of Ärlen Glacier. Due to the small size of the glacier, only one height point is taken into considerations for the following research.

For the temperature a decline of 0,65 °C / 100 m is assumed. This is a typical value used for simple extrapolations with altitude. And can be assumed because temperature declines linearly with height under dry adiabatic conditions (Klose and Klose, 2020). This results in a decline of 4,29 °C for all further temperature calculations concerning Ärlen Glacier.

According to Vuille (2011), mountain climates differ greatly in regional atmospheric circulation, which strongly influences wind systems, cloud cover, precipitation, and other factors. Regarding precipitation, high altitudes lead to orographic uplift or convective instabilities that result in regional increases in precipitation. This can lead to large errors in interpretation if weather stations located in the valley are taken into account (Ding, 1991). In this study, strong local precipitation events might have been overlooked. This could lead to interpretation errors because the triggering effect of heavy precipitation events could be underestimated.

4.5 Melt Calculations with PDDM

It can be assumed that the melting of snow and ice is related to air temperature, as long as the air temperature is above a critical threshold, which usually is close to the melting point of ice. More specific, the amount of snow or ice melted at a certain place, during a certain period, is assumed to be proportional to the sum of positive temperatures at the same place and in the same time period (Braithwaite, 2011). The amount of melt is then calculated by multiplication with a degree-day factor, typically between ca. 3 and 9 mm d^{-1} $°C^{-1}$ (Braithwaite and Zhang, 2000). Huybrechts, Letreguilly and Reeh (1991) already used a degree-day model to estimate mass balance forcing for their model of ice dynamics for the whole Greenland ice sheet, assuming degree-day factors of 3 and 8 mm d^{-1} K^{-1} for snow and ice respectively.

PDDMs are often used because of the wide availability of air temperature data, relatively easy interpolation and forecasting possibilities for air temperature, generally good model performance despite their simplicity and, computational simplicity (Hock, 2003 and Tsai and Ruan, 2018).

The simple positive degree day model assumed for this study is:

$$M = PDDMF \cdot (T - T_{melt})$$

Where M [cm/d of ice] is the depth of ice melted during one specific day, $PDDMF$ [cm d^{-1} °C^{-1}] is the positive degree day melt factor for the glacier (chapter 4.6), T [°C] is the temperature at the glacier and T_{melt} is the melting point of ice [°C] assumed to be 0.

4.6 Calibration of PDDM

For the case of Ärlen Glacier no in-situ measurements were available to estimate the positive degree day melt factor (PDDMF). To still approach a reasonable melt assumption values from literature (Fischer, Huss and Hoelzle, 2015) for (1980-2010), geodetic mass balance
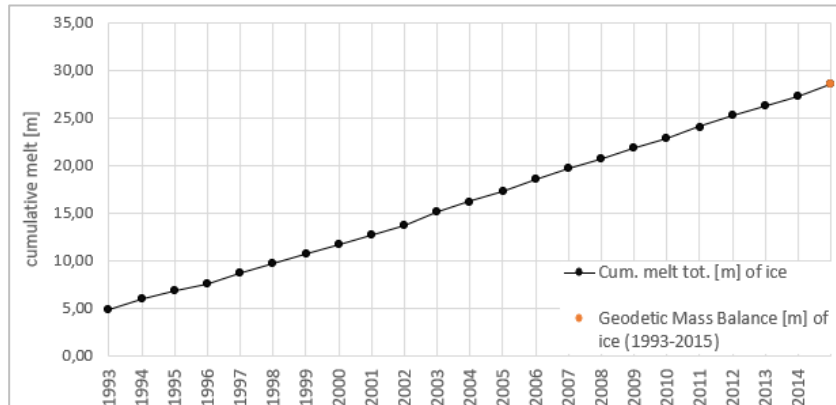
Figure 16: Calibration of PDDM with the geodetic mass balance calculated with the difference of swissALTI^{3D} and DHM25 (chapter 4.7).

between (1993-2015) and in-situ melt measurements on the *Oberaar Glacier* (2004 and 2014 - 2018) were used for calibration and comparison. The estimation of the average degree day factor was done by dividing the total cumulative melt through the sum of PDDs (positive degree days) over the same time period. And also, by comparing the cumulative melt over the observed time period (geodetic, literature and field measurements) with the calculated melt from the PDDM. In the case of Ärlen Glacier the PDDMF is estimated to be 0,165 cm d^{-1} °C^{-1} (figure 16).

4.7 Geodetic Mass Balance

To calculate the geodetic mass balance the difference between the two available DEMs was calculated. Prior to the calculation of surface elevation changes, the swissALTI[3D] DEMs were resampled to a grid cell size of 25 m (Fischer, Huss and Hoelzle, 2015). Then the glaciers total volume change ΔV (m) for the respective survey period was calculated as follows: where $\widetilde{\Delta z}$ (m) is the average elevation change calculated from the difference between the swissALTI[3D] and the DHM25 DEMs within the area covered by the glacier in 1993 (A_{1993} (m^2)).

$$\Delta V = \widetilde{\Delta z} * A_{1993}$$

Then the geodetic mass balance rate (m w.e. yr^{-1}) was calculated with:

$$\dot{B} = \frac{\Delta V * c}{\bar{A} * \Delta t}$$

Where c is a conversion factor used to convert ΔV into mass change, $\bar{A}$ (m^2) the average area between 1993 and 2015 calculated as (A1993 + A2015) / 2 and Δt the length of the observation period (t1 - t2) in years. The conversion factor c varies from glacier to glacier depending on the length of the observation period, the respective mass balance and the firn compaction history. Due to the fairly long observation periods, is set as a constant of 0.85 corresponding to a density of volume change of 850 ± 60 kg m^3 (Huss, 2013), which is consistent with other studies (Sapiano, Arrison and Chelmeyer, 1998; Fischer, 2011 and Zemp *et al.*, 2013).

The method was used as described by Fischer, Huss and Hoelzle (2015) for comparability with their study within the timespan 1980 - 2010. Their results for the main hydrological catchments, range from 0.52 to 1.07 m w.e. yr^{-1} with an average of 0,62 m w.e. yr^{-1} and - 0,6 to - 0,5 m w.e. yr^{-1} for Ärlen Glacier.

5. Results

5.1 Glacier Front Positions since 1980
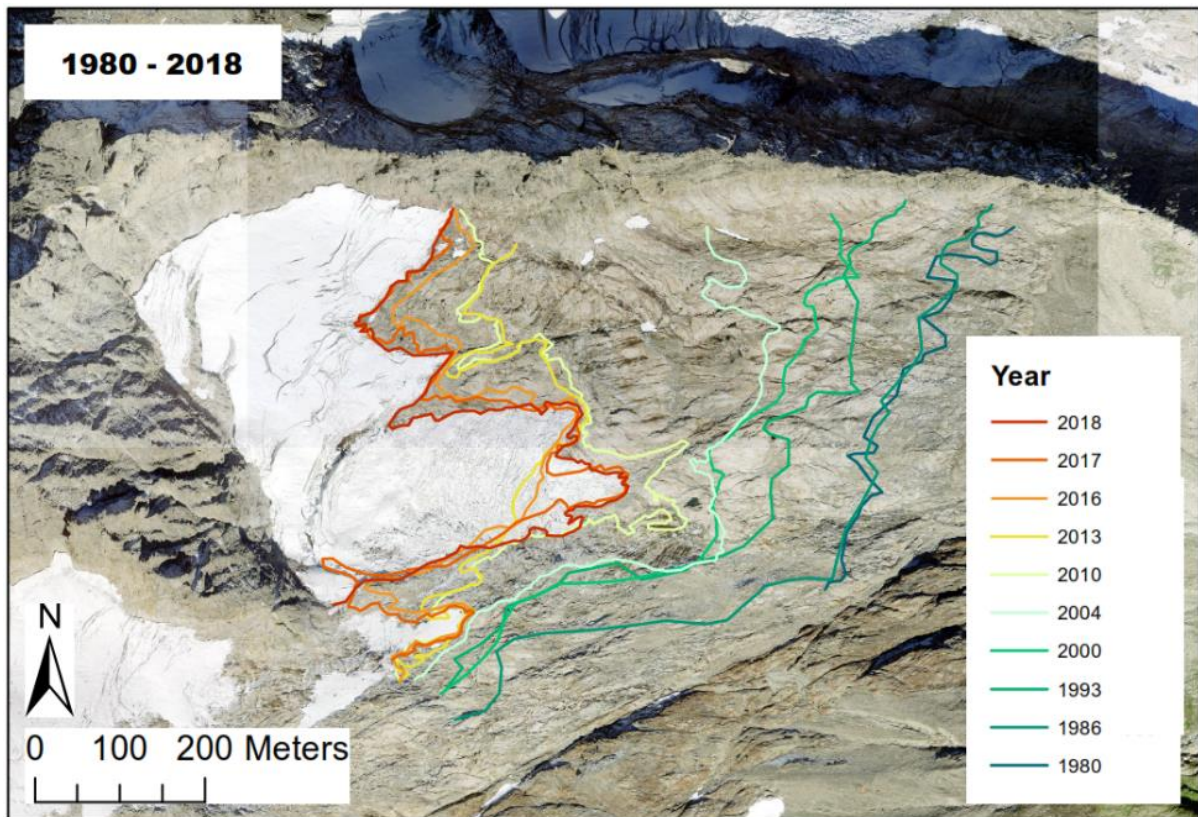
Figure 17: Glacier front positions drawn by hand in ArcGis, using orthophotos provided by Swisstopo from 1980 to 2018. 2017 is an additional Aerial Image from the Swissimage RS mission. The events later detected on Satellite imagery are not yet included and are discussed in chapters 5.2 and 5.3.

Figure 17 shows the rapid melting from 1980 to 2013 which is visible on all glaciers around the world. Interestingly at the glaciers tongue the advance stopped after 2013 and is even slightly advanced in 2016. Then the Swissimage RS orthophoto from 2017 shows the first advance detected with the Swissimage products.

The glacier advanced about 100 m during 2017 compared to 2016. In the following chapter the evolution of Ärlen Glacier is analysed more precisely with additional satellite imagery which allow a better resolution in time. The maximal retreat of the glacier is 384 m from 1980 to 2013. Which is a retreat of about 11,64 m per year. While there is almost no retreat from 1980 to 1986, rapid melting is visible from 1986 to 1993, where glacier retreat 90 m in only 7 years.
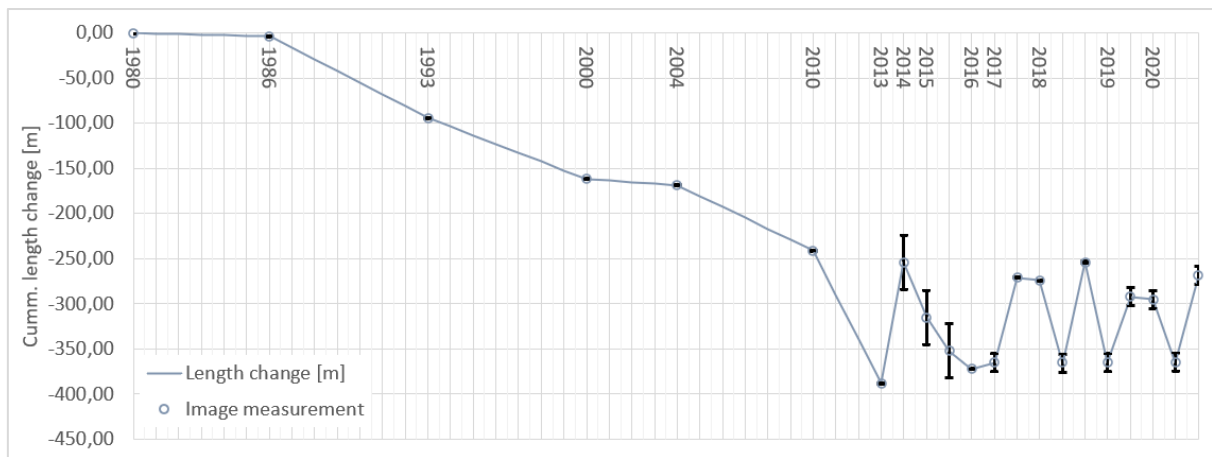
Figure 18: Length changes for Ärlen Glacier (1980 to 2020) with distances measured along center line for all available imagery. The error bars show the estimated uncertainty for each image, depending on the survey platform (chapters 3.5 and 3.6).

The front positions mapped with all available imagery is showed in (figure 18). The minimal length is reached in 2013 with advances in 2014, 2017/18 and 2019/20. Each reaching a maximum advance of about 100 m. After each advance the minimal length of 2013 is nearly reached again before a further advance appears. Over the whole time period the glacier retreated 388 m with the maximal retreat during 2013. The exact characteristics of the events are further discussed in the next chapter.

5.2 Observed Sliding Events

In the following chapter important events and states of the glaciers are listed. In order to relate the events to triggers from climate or bed geometry, the timing of the event is very important. In order to obtain the highest possible temporal resolution, all possible sources of freely accessible aerial and satellite images were considered for the following observations. A detailed list of available imagery and sources can be found in chapter 2. All used aerial images which are discussed but not presented in this chapter can be found in the appendix chapters IV, V and VI.

2010

- 21. Sept; The glacier is still below the critical terrain step. It is heavily crevassed but doesn't show any unusual forms (figure A62).

2013

- September 23; The glacier melt has passed a critical terrain level. On the right side of (figure 19), the first observed small ice breakoff is visible. In addition, very interesting crevasses are opening on the glacier. It can be clearly seen that the front is highly crevassed and will eventually break off. An unusual crevasse can also be seen in the upper part, where the large crevasse will open in the coming years (figure 19).
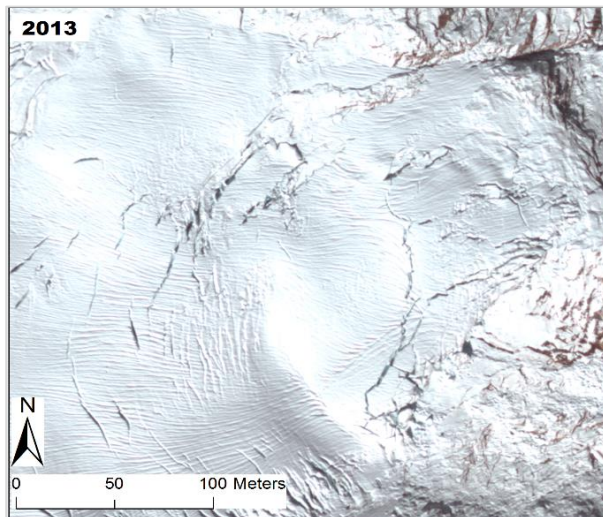
Figure 19: Swissimage RS from 2013. With RS the crevasses are still visible even, when the glacier is covered with snow which improves the interpretation.
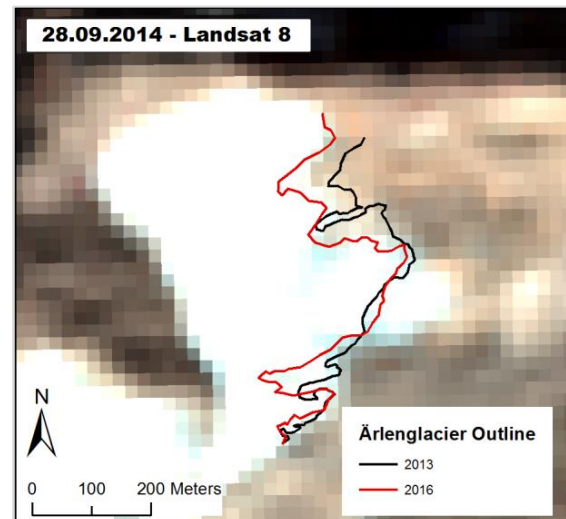
Figure 20: Landsat-8 image from the 28th of September 2014. Compared to the glacier outlines of 2013 and 2016 the glacier seems to have advanced. Because the Image is from late September and includes no snow cover the white area is assumes to be glacier ice.

2014

There is a lack of open-source data for the year 2014. This makes it hard to understand what exactly happened. But the really low-resolution image from Landsat-8 shows that the glacier advanced in comparison to 2013 (figure 20). The image is from the end of September where the snow cover should be at its minimum and the glacier outline is quite visible even with such a low resolution. The only information that can be obtained from this picture is that the slide started before September 28. This assumption is backed by amateur images taken during 2014 and 2015 (figure 21). Unfortunately, it cannot be confirmed, whether the slide affected the whole glacier or only the glacier tongue broke off over the terrain step.

2015

Two usable images from 2015 could be found from the Sentinell-2 mission (figure A64). One at the beginning and one at the end of August. It appears that the portion of the glacier that advanced in 2014 is melting but not reaching the critical terrain level. And there is no evidence of another slide event. After a random search on the Internet, another source came to light. An amateur geologist posted pictures (figure 21) from a field trip to Ärlen Glacier in fall 2015 (Weissenfluh, 2015), among them an interesting description of the condition of the glacier.

The following is a translation and summary of the description. *"Very impressive and frightening how the glacier disappears. The lower half of the glacier is completely shattered and slides down-hill on the smooth rock slab into the next terrain basin below. The upper part of the glacier has lost its grip and is sliding downward. The sliding was clearly audible. The ice cracked constantly and frequently and pieces broke off from the compact part of the glacier."*

Figure 21: The tongue of Ärlenglacier during 2015. The advanced tongue is very nicely visible. The assumption is, that the advance happened during 2014 and is now melting. Photo from Weissenfluh (2015).

This suggests that the glacier was also in an active phase with increased basal movement in 2015. And it can be suspected that the glacier showed similar dynamics as in 2017 to 2018. Because it is mentioned that the whole upper part was in an unstable state.

2016

For 2016, a high-resolution aerial photograph was taken by Swisstopo on September 7. The glacier does not show any unusual crevasses (figure 22). Compared to the last image from Swisstopo (2013) (figure 18), it could be assumed that the glacier did not slide and melted only slowly. This was also initially assumed, since there are no clear signs of glacier instability in 2014 and 2015.
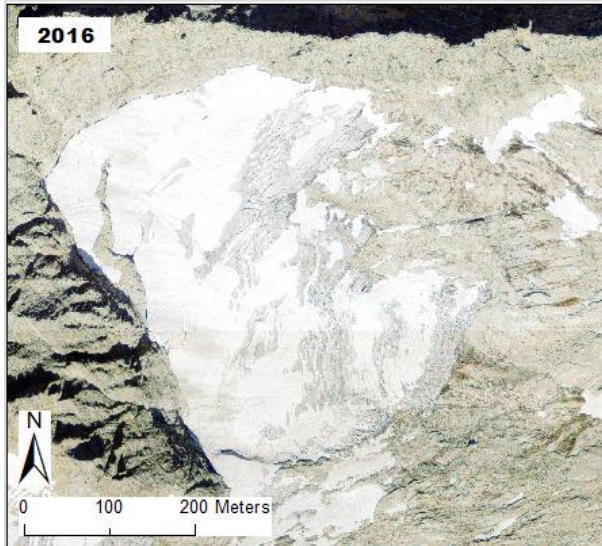
Figure 22: Swissimage from 2016. The glaciers tongue lays over the critical terrain step and the whole glacier looks extremely normal and without crevasses considering the past events.
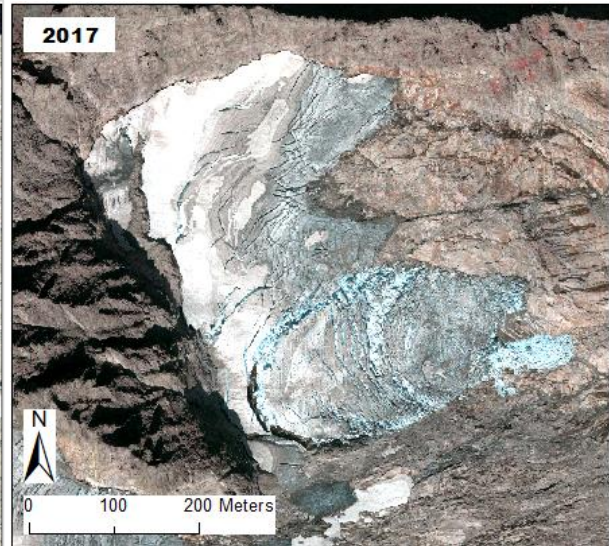
Figure 23: Swisstopo RS from 25th of August 2017. The opening of the listric breakout niche is clearly visible. The whole glacier is heavily crevassed and a small ice avalanche tumbled from the glaciers tongue into the terrain syncline.

2017

- 15. Aug.; Small ice avalanche at the glaciers tongue (figure A64).

- 23. Aug.; Whole unstable part starts to slide. Images (figure A64) shows a heavily crevassed glacier. The ground reaching listric breakout niche, opens up in the upper part of the unstable area. Further small ice avalanches at the glaciers tongue.

- 25. Aug.; Sliding continues. The ground reaching listric breakout niche opens up. The totally crevassed glacier is very nice visible on the aerial image from Swisstopo (figure 23).

- 29. Aug.; Unstable part is sliding further down. More small avalanches at the glaciers tongue (figure A64).

Due to snowfall and regular cloud cover, there were no more usable images in September and October 2017 to observe the further changes. However, the Sentinell-2 images from 2018 (figure A64) show that the slide probably stopped from October 2017 to mid-August 2018.

2018
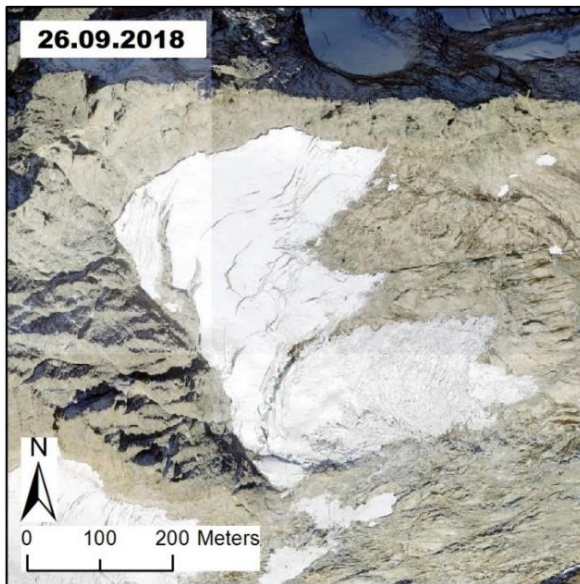
Figure 24: Swissimage from the 26th of September 2018. The listric breakout niche is clearly opened at the top. And the typical avalanche has tumbled at the glaciers tongue.

Figure 25: GeoEye image from the 23rd of October 2018. The opening of the listric breakout niche is as extreme as never before. And the whole unstable glacier part is sliding downwards.

- 09. Sep.; Glacier is at a similar state as at the end of 2017. In comparison there is melt at the glaciers tongue and the ending is nearing the critical terrain step (figure A64).

- 26. Sep.; Small avalanche at the glaciers tongue. Listric breakout niche crevasse at the top got bigger. Which shows that the glacier was sliding with increased speed (figure 24).

- 29. Sep.; Big ice avalanche at the glaciers tongue appeared (figure A64). The part of the tongue, advanced over the critical terrain step, breached off. Connection the rest of the glacier is lost.

- 07. Oct.; Gap between the broken off tongue and the unstable glacier part has closed. listric breakout niche at the top got bigger. Sliding of whole unstable part is clearly visible (figure A64).

- 09. Oct. - 19. Oct.; Listric breakout niche at the top is getting bigger and expanding to the southern part of the glacier.

- 23. Oct.; The World Imagery picture shows clearly how much the glacier advanced during the end of September and October of 2018 (figure 25).

- 30. Aug.; Advance of 2018 has melted away over the summer. Glacier reached the critical terrain step once again. Interestingly, the listric breakout niche at the top seems to have closed again. Maybe also just covered with snow from the last winter or recent snow events (figure A64).
- 04. Sep.; Small avalanches at the glacier tongue.
- 19. Sep., Melting at the tongue (figure 26).
- 27. Sep.; Avalanche at the tongue. Listric breakout niche at the top is also visible again (figure 27). Possibly only due to melting and no confirmed sliding on the unstable glacier part. Which is interesting, cause the glacier reached the critical terrain step. This leads to the assumption, that further factors need to be fulfilled to provoke the whole unstable part to slide.
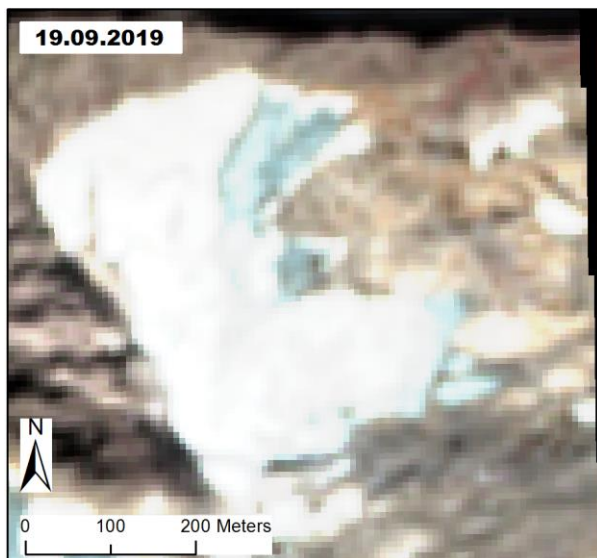
Figure 26: Sentinel-2 image from the 19th of September 2019. The glaciers tongue is rested at the critical terrain step as 2013 and 2016. Small ice avalanches or rest from the 2018 advance are visible in front of the glaciers terminus.
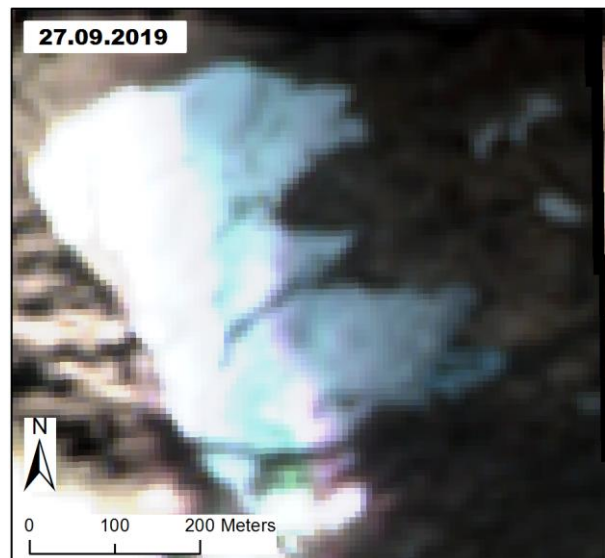
Figure 27: Sentinel-2 image from the 27th of September 2019. With a clearly visible listric breakout niche at the back and an ice avalanche at the glaciers tongue.

2020

The events in 2020 were observed precisely with the time lapse imagery and helicopter survey flights (figure 28). First the tongue, which is represented by the break off from 2019 melted during the summer. As it reached the point where it's not supported by the topography, the tongue broke off and the glacier end was once again at the critical terrain step (as 2013). The timing and velocity of the consequential sliding event is discussed in (chapter 5.4) in detail.

Figure 28: State of Ärlenglacier at the 22nd of September 2020. Image Taken during helicopter survey flight over the glacier.

5.3 Topography and Crevasses
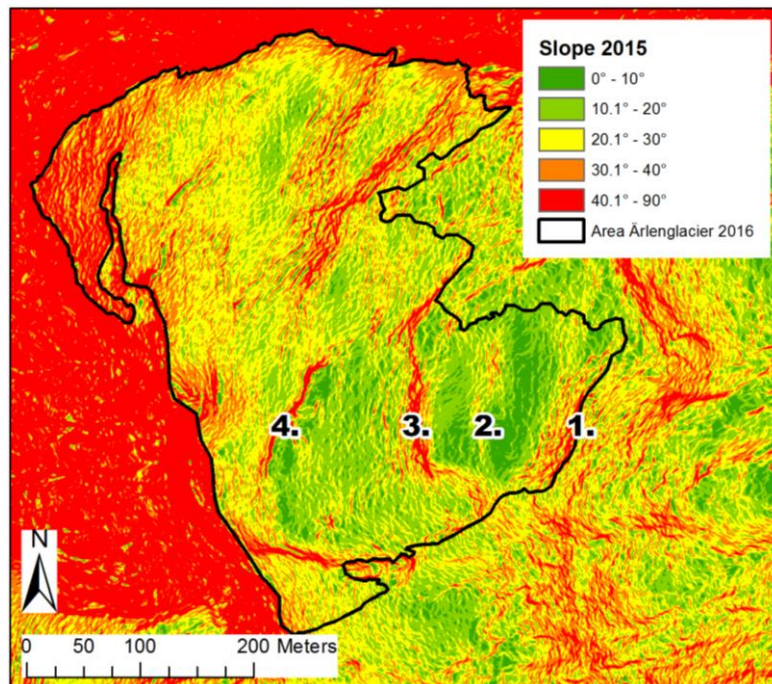
Figure 29: Slope of Ärlen Glacier classified in 10° steps, derived from swissALTI[3D]. With the front positions of 2016 for orientation. Numbers 1.-4. are at the locations of terrain steps , where heavy crevassing occurred during the slide events.

The lower part of Ärlen Glacier, which showed unstable behavior over the last years, is relatively flat. Characteristic are the steps (1. - 4.) (figure 29). As expected, the glacier was strongly crevassed and divided at the steep steps. Step (1.) is in this work referred to as the critical terrain step, and has a steepness of about 25°. The steps (2.) and (3.) were heavily crevassed during the slide events. Especially in 2017 (figure 23). At step (4.) the whole unstable part of the glacier separated from the rest of the glacier and a listric breakout niche opened starting during 2013.

The listric fracturing niche which started to form during 2013 and opened to the ground during 2017 is already clearly visible in swissALTI[3D] from 2015. Between the steeper terrain steps (2.), (3.) and (4.) the average slope is only about 16° and above step (4.) the average slope is slightly steeper with 22° (figure 29). The area between the terrain steps (1.) and (2.) is very flat with an average slope of only 12°. This flatter area shows where the glaciers terminus is located during 2015 which is just above step (1.) and therefore flattens the terrain in that area. Therefore, the bedrock topography is assumingly slightly steeper.

5.4 Flow Velocity Variations (2020)

5.4.1 Daily Flow Variations
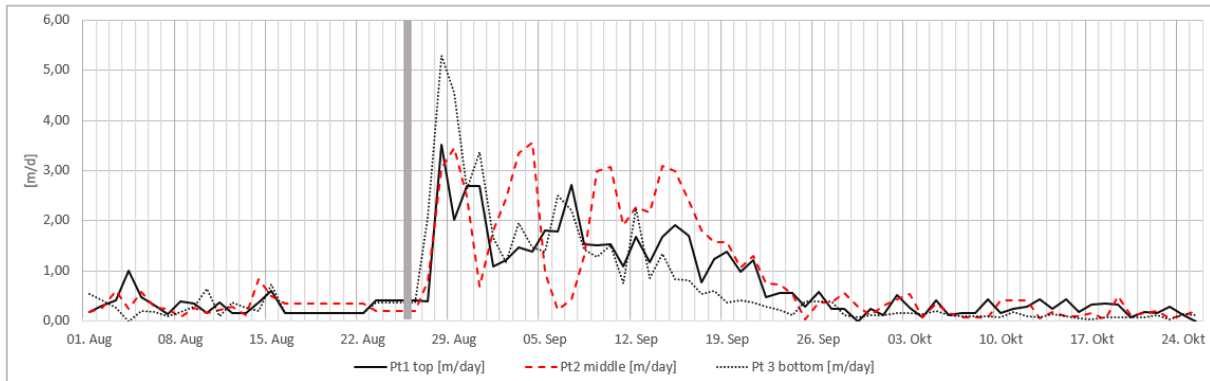
Figure 30: Observed speed changes [m/day] for Ärlen Glacier for three different points. One at the top (Pt1) one in the middle (Pt2) and one at the bottom of the unstable glacier part. The break off of the glacier tongue (26th of August 2020) is showed with a thick grey line.

After the break off of the glacier tongue (26th of August 2020) the glacier accelerates nearly exponentially. The delay of reaction from the brake off at Pt1 to the end of the unstable glacier part is nicely visible in figure 30. First the tongue brakes off, and then it takes about 1 day till the upper part of the glacier starts to flow with higher velocities. The movement continues with different variations until about the end of September, when the velocities return to normal, as observed before the break off. It is interesting to note the development of Pt2, which is discussed in chapter 6.2.1. The velocity increases for about 3 days and then decreases again for the same time period. This pattern is repeated 2 times and a third time with similarities.

The maximum of the observed velocities for each point (Pt1; Pt2; Pt3) are 3.51; 3.56 and 5.29 m/d. The means are 0,69; 0,81 and 0,64 m/d for the whole observed period, and 1,3; 1,61; and 1,31 m/d during the enhanced velocity period. Before the terminus break off the mean velocities where 0.31; 0.31; 0.27 m/d, and after the movement stopped at the end of September 0.24; 0.21 and 0.10 m/d. With a total distance of 59,48m; 69,72m and 55,44m (figure 31).
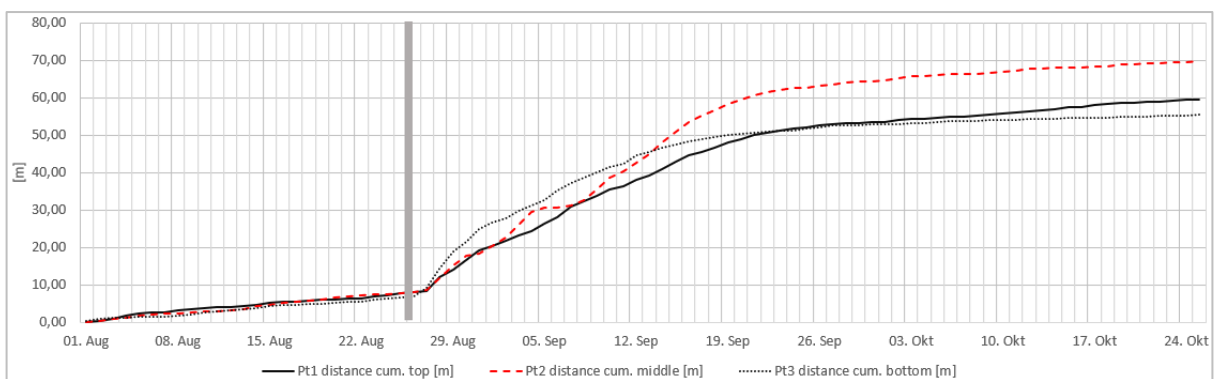
Figure 31: Cumulative change of Ärlen Glacier in [m] for the three observed points (Pt1 at the top, Pt2 in the middle and Pt3 at the bottom) of Ärlenglacier during the observed 2020 slide. The break off of the glacier tongue (26th of August 2020) is showed with a thick grey line.

50

5.4.2 Hourly Flow Variations

The hourly flow velocity variations of two time periods (September 03 - 05 and 13 - 15) were examined in detail. The time periods were chosen because of the weather conditions. Cloud-free days were selected to better understand the influence of melt water. The points Pt1 to Pt3 were chosen in the same area as for the daily flow variations (top, middle and bottom of the unstable glacier part) and the measurements are presented in this order. The results showed in (figure 32) are visualized with the difference from the mean velocity per hour for each point. This makes interpretation in terms of flow variations easier. For further interpretations the PDDM values are added to the figure. This is discussed in more detail in chapter 6.2.1.

03. - 05. of September the flow velocity means were 0,19; 0,24 and 0,41 m/h, with maximums at 0,48; 0,69 and 0,65 m/h.

13. - 15. of September the flow velocity means were 0,19; 0,40 and 0,31 m/h, with maximums at 0,41; 0,45 and 0,65 m/h.
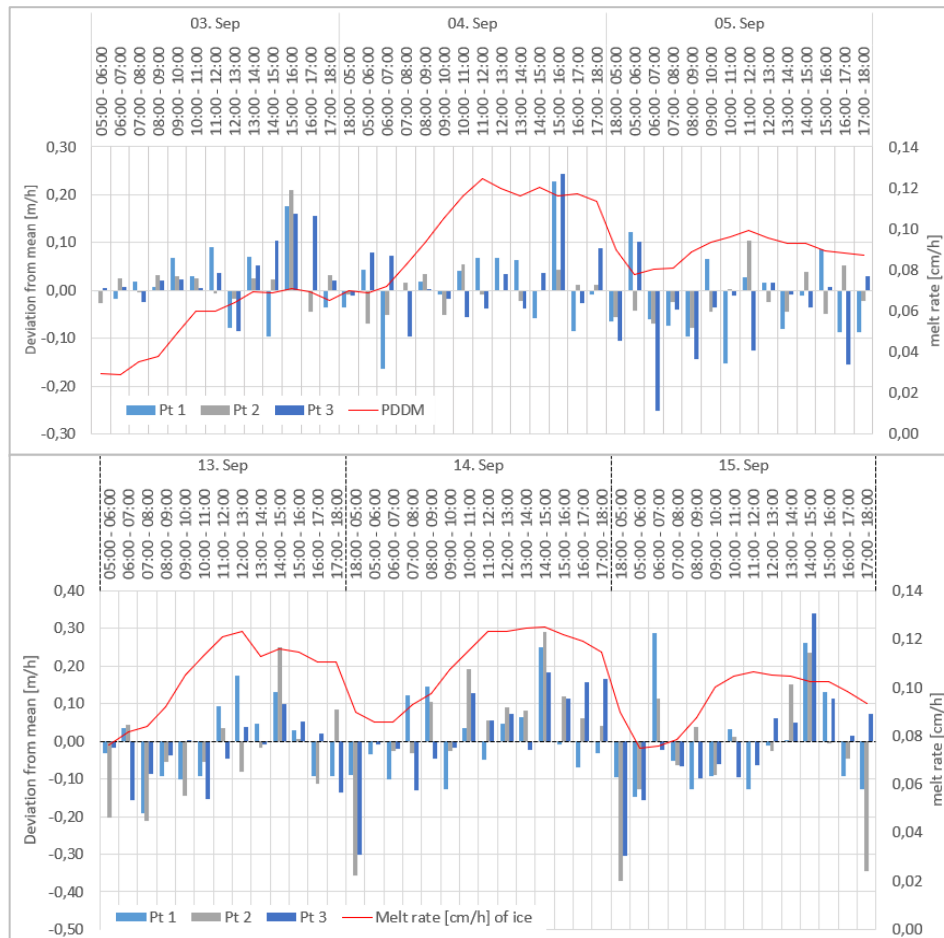
Figure 32: Deviation from mean flow velocity in [m/d] for Pt1 - 3 placed at the top, middle and bottom of the glacier. Including additional information of the melt in cm/h from the PDDM (Chapter 5.6). For the two time periods (03. - 05. Sep) and (13. - 15. Sep).

5.4.3 Flow Velocity (2018)

The high-resolution Satellite Image from World Imagery allowed a comparison with the SWISSIMAGE aerial orthoimage, both from 2018. Both images are showed in (figure 24 and 25). The high-resolution properties of World Imagery allowed the identification of crevasses and ice blocks on both images (figure 33) which made a velocity estimation possible over the whole time period.

Additional points were added both on the ground control and on the stable part of the glacier, to correct for contortions caused by the reprojection of the World Imagery to the LV03 coordinate system (tables A10 and A11).
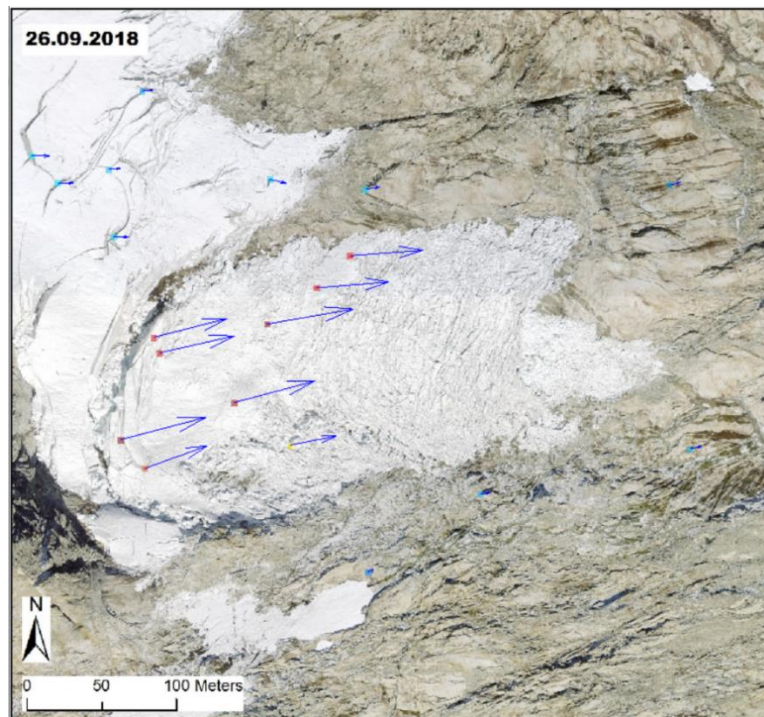
Figure 33: Displacement Vectors from Pointcatcher for 2018 from the 26th of September (SWISSIMAGE) to the 23rd of October (World Imagery).

Over the unstable part, the glacier moved 43,6 m with an overall average velocity of about 1,56 m/d. This occurred during the time period from September 26 to October 23. The stable part of the glacier moved 2,6 m during the same period, corresponding to a velocity of 0,1 m/d.

Compared to 2020, the movement of the area corresponding to the 2018 measurement would correspond to the approximate location of Pt1 (figure 33). This moved 59.48 m with an average of 1.24 m/d over the entire sliding period. The other points in the middle and end of the glacier moved (Pt2 = 69.72 m; 1.35 m/d) and (Pt3 = 55.44 m; 2.25 m/d).

Since the exact timing of the movement for 2018 is not known, the comparison with 2020 is lagging, but it shows that the distance for 2020 is similar, but perhaps somewhat overestimated.

5.5 Multi-Temporal DEMs from SfM

To identify the differences between the two DEMs, they were compared by subtraction, as described in chapter 4.3.3. In this way, it is possible to determine where mass loss or mass increase has occurred in the period between the two DEMs.

5.5.1 The 4th of September 2020 DHM - 2015 (SwissALTI[3D])
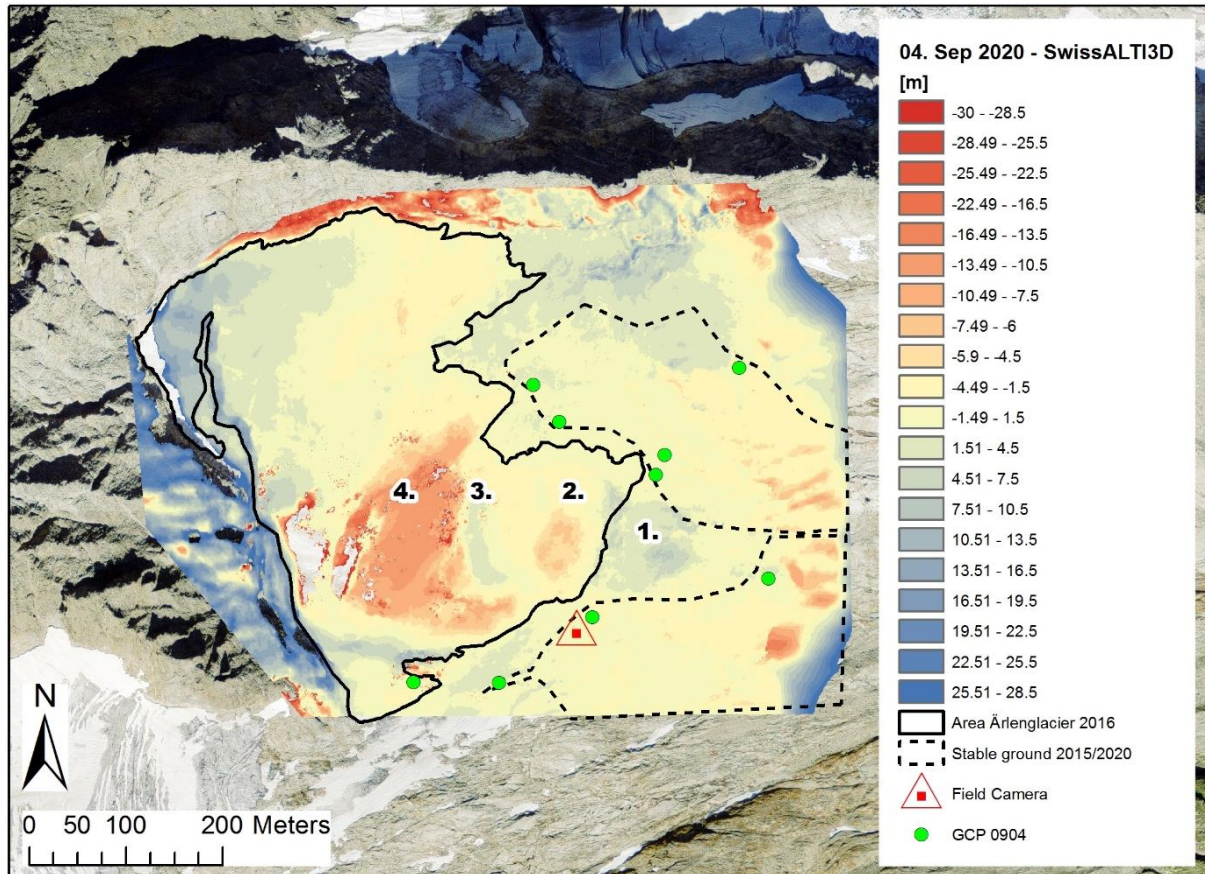
Figure 34: Comparison of the two DEMs, one from the September 4, 2020 helicopter survey flight and the other from SwissALTI[3D]. Areas with less mass than 2015 are shown in red, areas with more mass in blue. The points 1. to 4. are areas with interesting changes, which will be discussed in more detail.

The expected melt for the period (2015 - 2020) would be 6.21 m of ice according to the PDDM (chapter 5.6.2). Figure 34 shows the calculated height changes for the same time period. The points 1. to 4. show areas with interesting changes, which are discussed in detail below.

1. Area where the glacier is at an advanced stage during the survey flight on the fourth of September. The glacier advanced over an area of 10'114 m^2 with a height gain of about 3 to 8 m.

2. Hight loss in this area is about 5 to 7 m. The area is located at the front of the glacier of 2015. The relatively high height difference compared to the surrounding (ca. - 2 m) could be a sign of a dome that builds up at that area and is discussed in chapter 6.2.5. But they represent approximately the values expected by the melt model.

3. Interesting area with a slight height gain of about 3 m. Probably area where the mass sliding down from above is congested slightly due to the flat terrain below.

4. On the top of this area the listric breakout niche opens during the sliding events. This area shows a heavy mass and height loss. And is referred to as reservoir zone during this study. The height difference ranges from about - 6 m to - 12 m and maximums from up to - 17 m. The exact depth of the crevasse is quite poorly reproduced by the DEM, which is due to rather large errors in the area of the listric breakout niche. This reservoir area shows the strongest changes and is probably the area from which the largest part of the volume from the slide events originates. The mean elevation change is - 8.5 m, which results in a mass loss of about 218'374 m^3 in the 5-year period for this area.

Compared to the time-lapse image from the same day (figure 35), the height changes from figure 34 become quite reasonable, compared to the Swissimage from 2016 (figure 22).

Figure 35: Image from the time-lapse camera at noon of the 4th of September 2020. Compared to the DEMs differences of figure 34 the advanced state of the glacier is nicely visible.

5.6 Climate and Weather Variability

5.6.1 Temperature
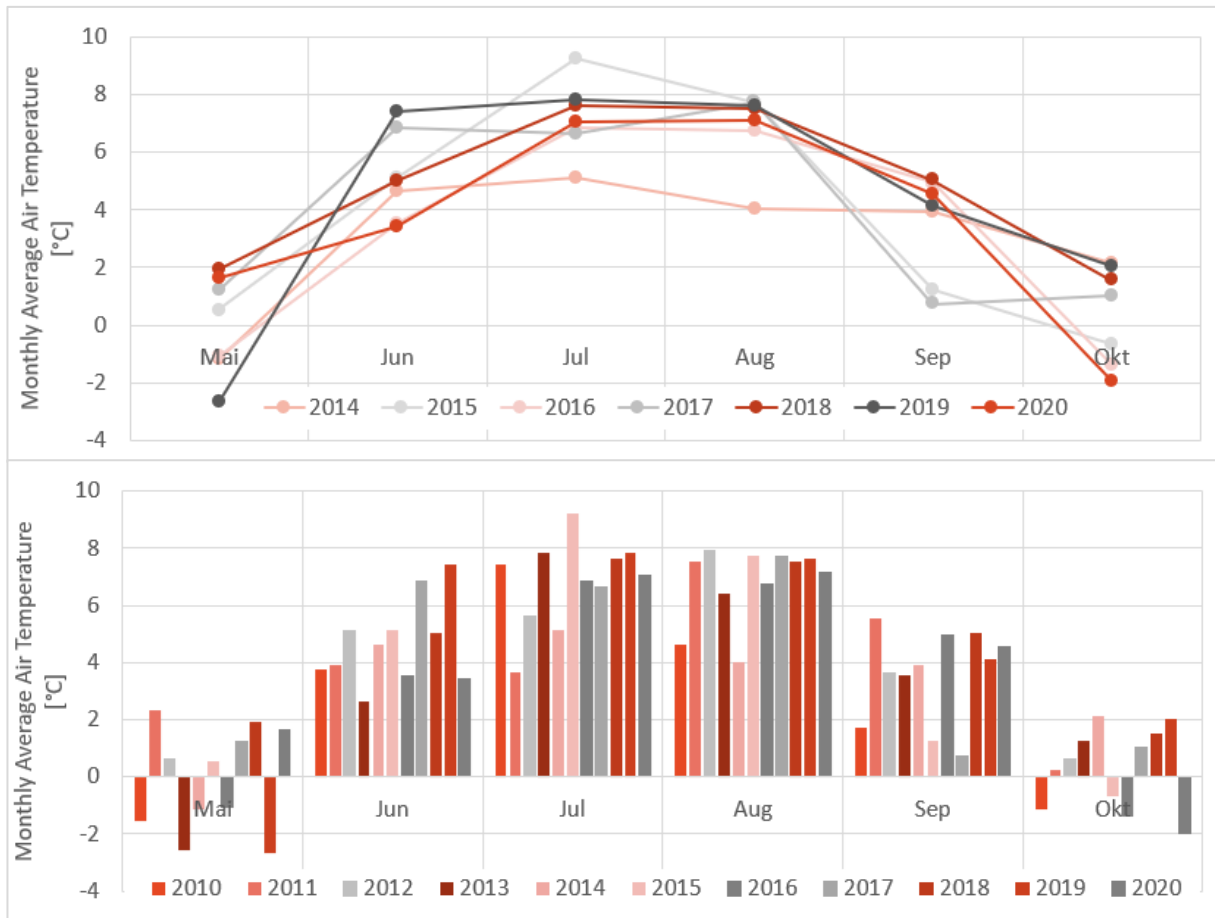
Figure 36: Monthly average air temperature extrapolated to Ärlenglacier from the Grimsel Hospitz weather station for the years 2014 to 2020 (upper) and 2010 to 2020 (bottom). More detailed temperature data can be found in the appendix (Figure A).

Years with an average temperature below 0 °C during October are 2010, 2015, 2016 and 2020. Year with temperature below 2 °C during September are 2010, 2015 and 2017.

For a better understanding of temperature variability, the temperature deviation from a norm was calculated. The norm is the average temperature between 1981 und 2010. The results (figure 37) shows that the majority of temperatures are generally above the norm, especially during the months of June through August, when temperatures are below normal only a few times in a 10-year period. The highest deviation occurred in June 2019, with an average temperature that was nearly 4 °C above the norm.
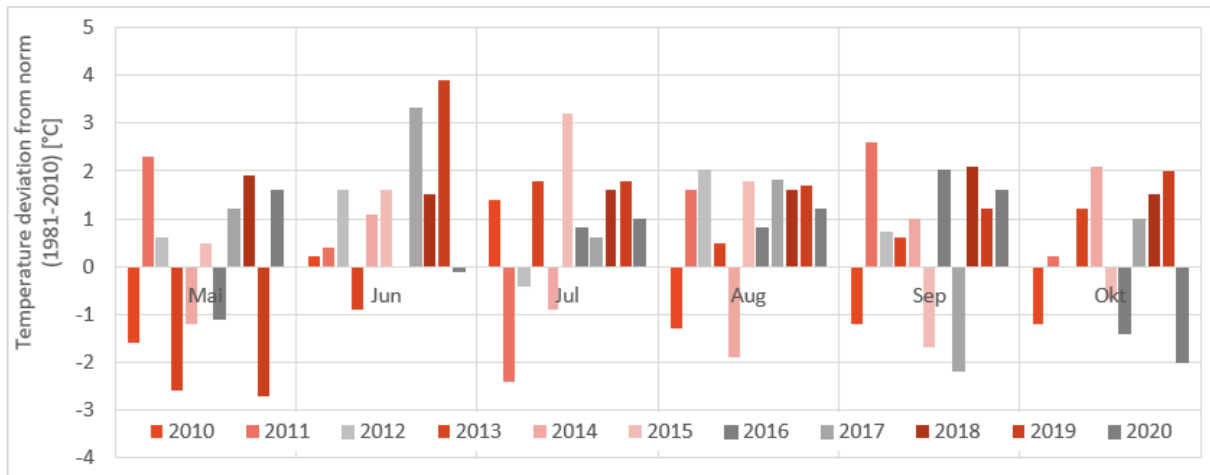
Figure 37: Temperature deviation from norm (1981 - 2010) from Grimsel Hospitz weather station extrapolated to Ärlenglacier.

5.6.2 PDDM and Melt

The PDDM for the time period 1989 to 2020 was calculated using the available weather data from *Grimsel Hospitz* and an average degree day factor of 0,165 cm d^{-1} °C^{-1} (chapter 4.7).

The positive degree day factor is quite lower as the typically assumed one (0,3 to 0,9 cm d^{-1} °C^{-1}). The reason lies probably in the steep topography around the glacier which provides a lot of shadow during the day. Or in an underestimation of the temperature decline with height in our extrapolation. Nevertheless, the approach with a calibration with the geodetic mass balance should provide quite a reasonable amount of melt in relation to temperature.

For comparisons over different time scales, the PDDM was also calculated in hourly variations to compare with hourly velocity changes (chapter 5.4.2). The estimated cumulative ice melt for the entire period (1989 - 2020) is 34.78 m (figure 38).
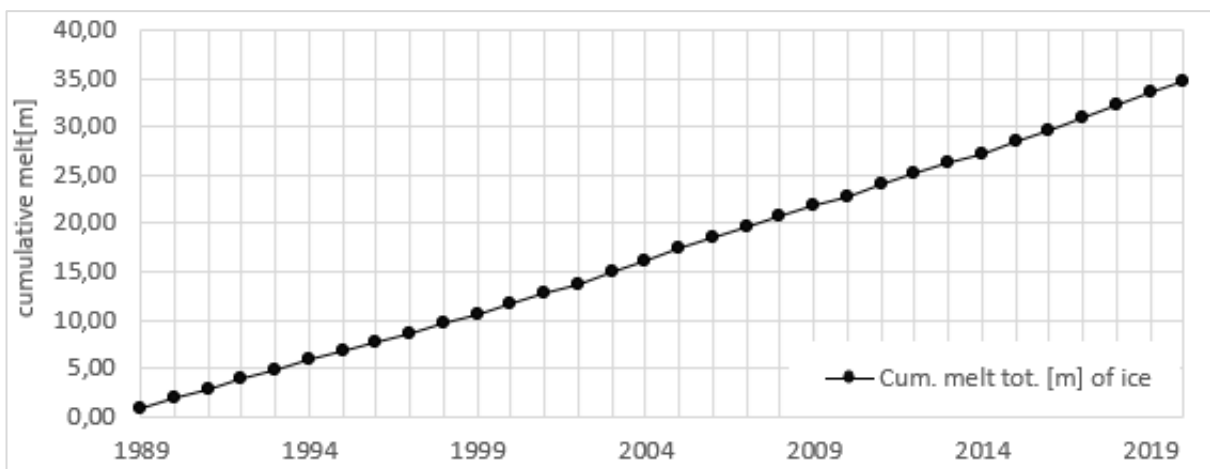
Figure 38: Cumulative melt [m] of ice over the time period (1989 - 2020) for Ärlenglacier. Calculated with PDDM (chapter 4.6) and calibrated with our geodetic mass balance (chapter 5.7).

The melt cumulative deviation from mean (1989 - 2020) (figure 39) shows nearly clear two phases where the majority of years are above average after 2002 and conversely. Yet 2013, 2014 and 2016 are below average. From there (2017 - 2020) all years are clearly above the mean. The highest melts were modelled for 2003 and 2018.
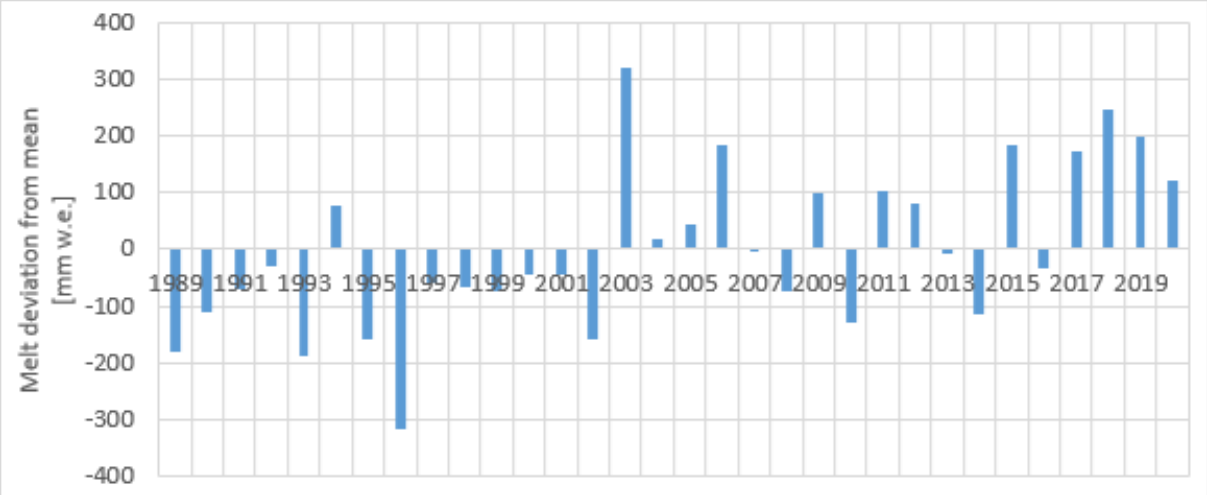
Figure 39: Cumulative melt deviation from mean (1989 - 2020). Bars above zero show years with more than average melt and years below zero are years with less modelled melt the average.

To understand the triggers and influencing factors for the glacier sliding instabilities at Ärlen Glacier the daily variations of the PDDM are really interesting and are presented below for the time span of 2014 to 2020 (figure 40). Interesting are the periods in which the sliding instabilities appeared during the years (August to October). Especially regarding the sequence of basal water pressure which is highly influenced by melt.
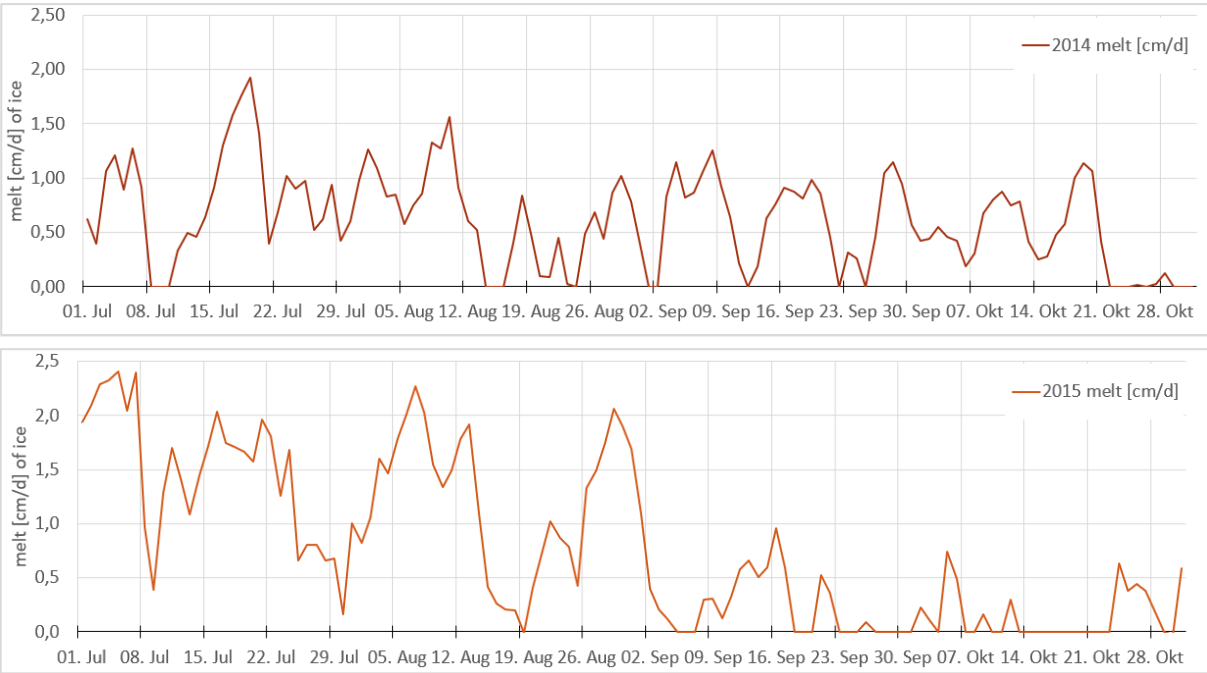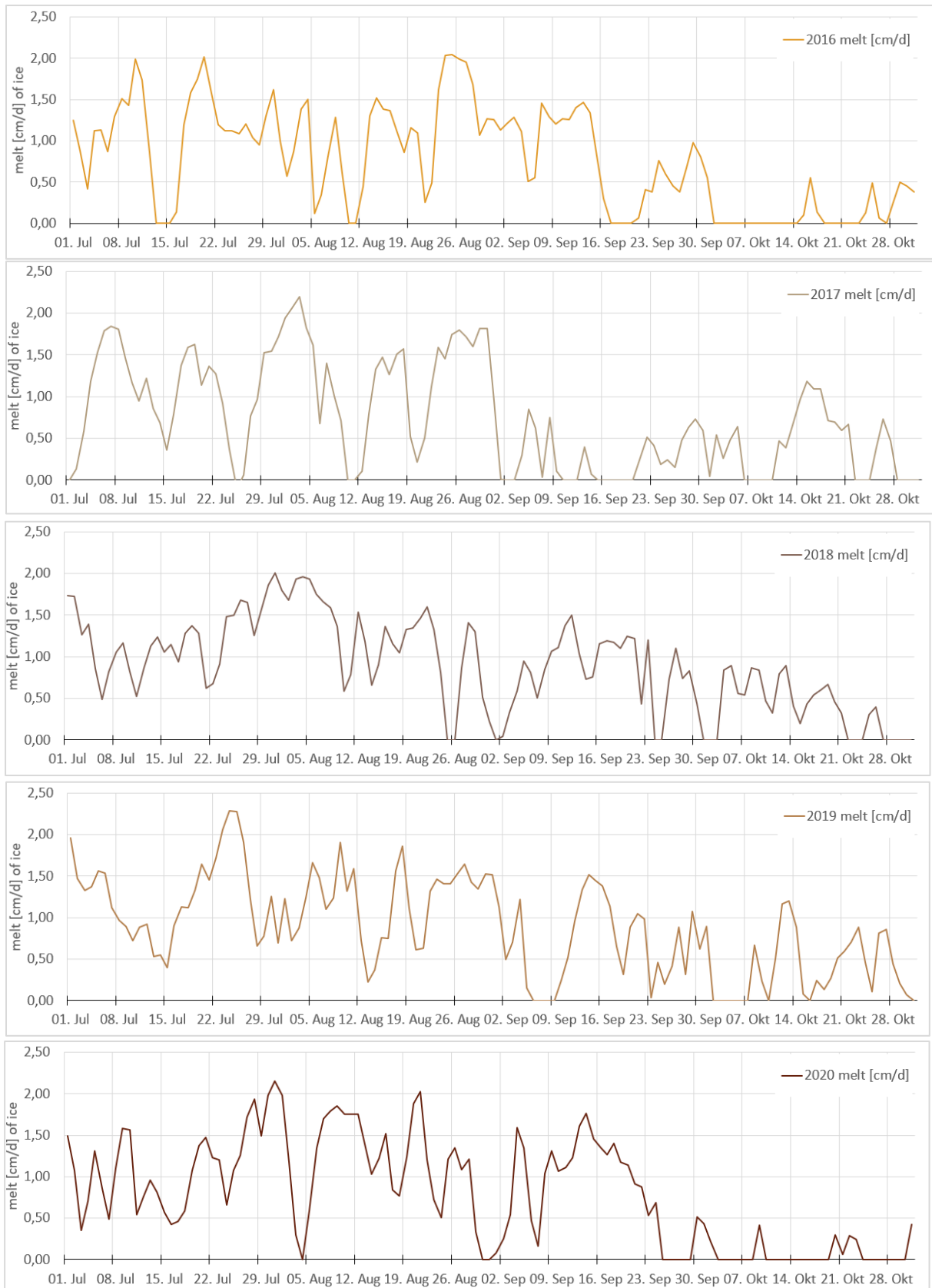
Figure 40: Melt in [cm/d] calculated with the PDDM for the years 2014 to 2020. Interesting are the places where the melt reaches zero which could be a part of a potential trigger chain for a sliding event (chapter 6), if the temperature and therefore the melt rises again.

5.6.2 PDMM

With the PDMM the main melt season is defined over the last 10 years (2010 - 2020). The main melt season at Ärlen Glacier is during July and August when the average melt lies at 33,72 and 33,81 cm w.e. d^{-1}.
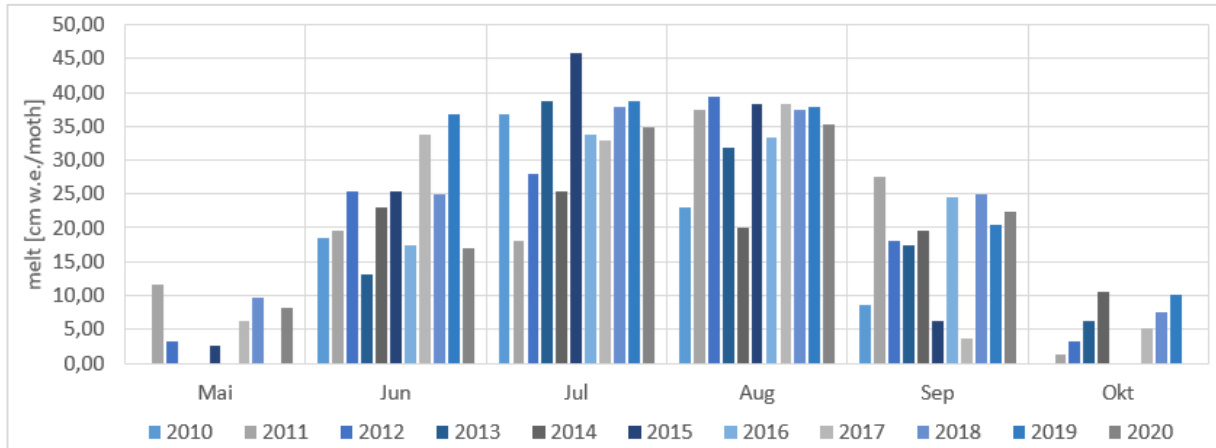
Figure 41: Positive degree month model, calculated with the monthly average temperature and the same degree day factor as for the PDDM (chapter 4.6).

5.6.3 Rain and Summer Water Availability

Rain is the sum of all precipitation events at the Grimsel Hospitz weather station where the extrapolated temperature at Ärlen Glacier is above 0 °C. This approach is chosen to exclude possible snowfall at the altitude of Ärlenglacier, because the main interest is the water availability. The results are quite prone to error due to strong local weather changes in mountain climates. The maximum was determined for 2014, the years 2017 and 2018 were slightly below average and 2019 and 2020 above average.
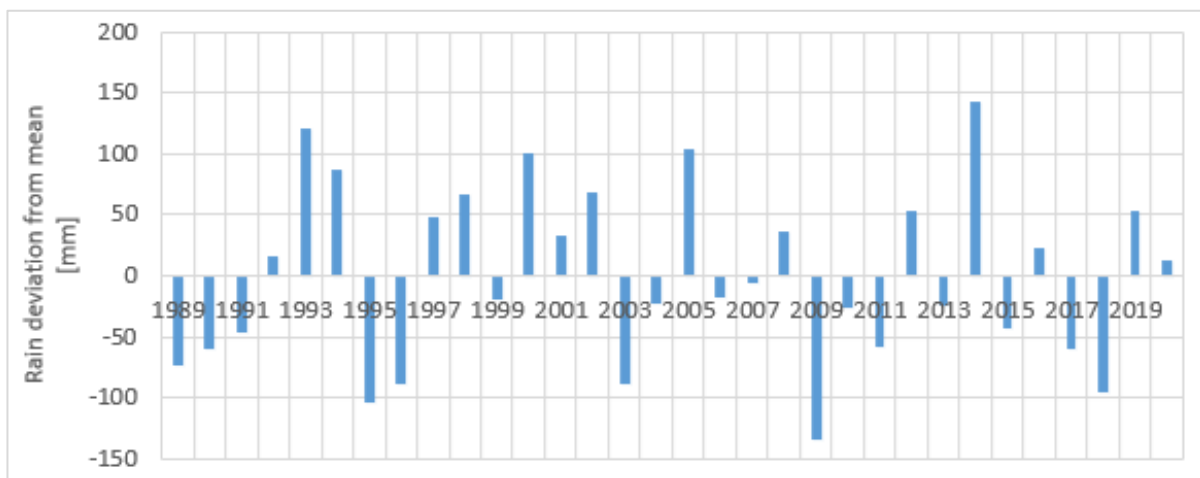
Figure 42: Cumulative summer rain (Mai - October) during the time period 1989 to 2020. Calculated by adding all rain events at Grimsel Hospitz weather station, when the extrapolated temperature at Ärlen Glacier was above 0 °C.

Daily rain variations during summer for the years with glacier instabilities (2014 - 2020) are showed in the appendix (figure A65). Rain events could be the necessary additions of water which trigger the glaciers instabilities. This effect is further discussed in chapter 6.2.

The summer water availability is the combination of melt from the PDDM and rain. The average since 1989 lies at 1379 mm w.e. with a maximum during 2019 of 1633 mm w.e and a minimum of 972 mm w.e. (1996) (table A12). Figure 43 shows years with a summer water availability above or beyond average.
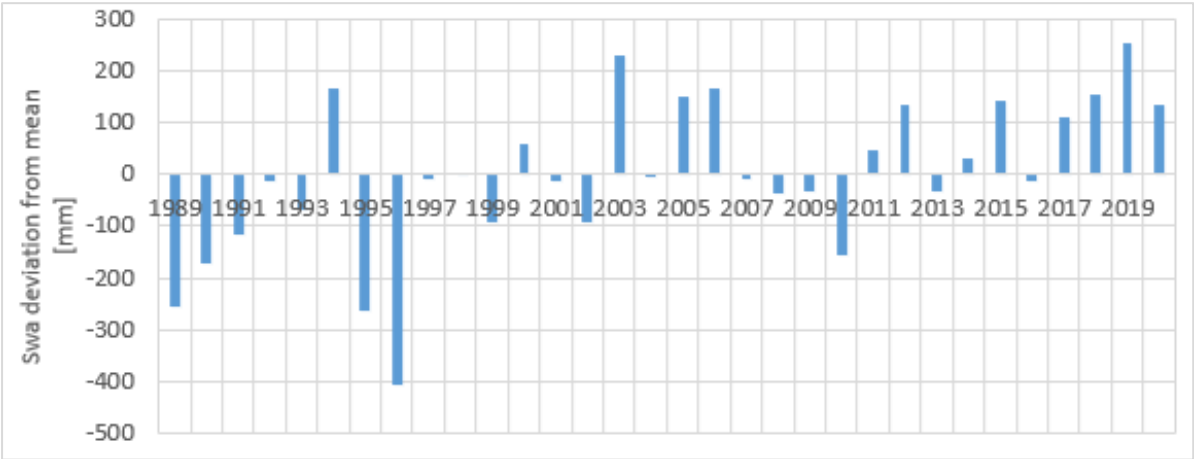
Figure 43: Summer water availability (1989 - 2020), calculated by adding the melt from the PDDM (figure 41) and rain (figure 42).

5.7 Geodetic Mass Balance (1993 – 2015)
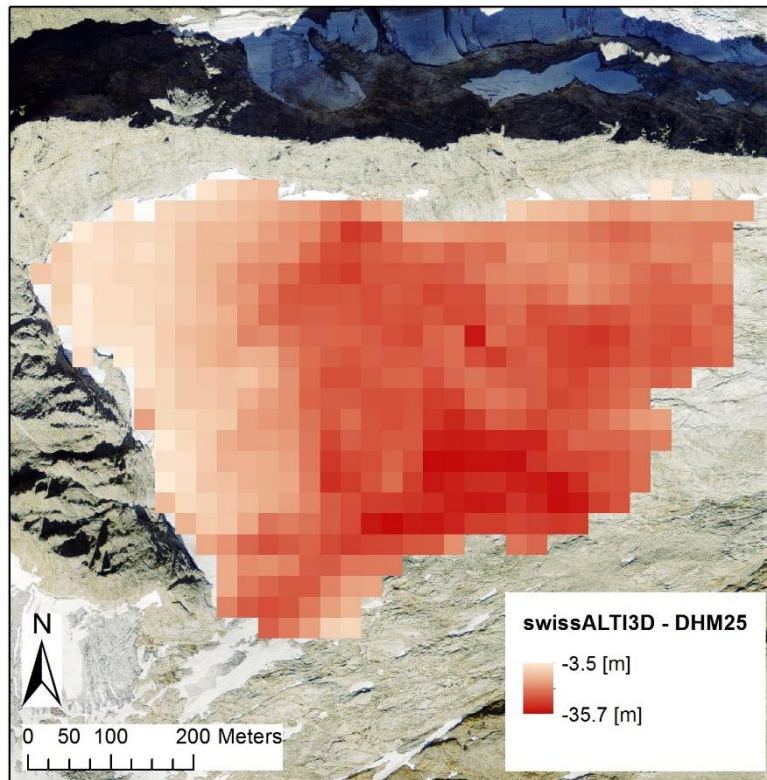
Figure 44: Geodetic mass balance for Ärlenglacier between 1993 and 2015 (swissALTI³D - DHM25). The resolution was set to 25 m to match the one of DHM25.

The following geodetic mass balance calculations were performed as described in chapter 4.7. The glaciated area was 323'770 m² in 1993 and 144'530 m² in 2015, which is a loss of more than half of the glaciated area (179'240 m²) in only 22 years.

$$\Delta V = -20{,}6\,m * 323765\,m^2$$

The total volume loss calculated for the period 1993 to 2015 ΔV is - 6'670'000 m³.

Then the geodetic mass balance rate (m w.e. yr⁻¹) was calculated with:

$$\dot{B} = \frac{\Delta V * 0{,}85}{234'149\,m^2 * 22}$$

The geodetic mass balance over the time period 1993 - 2015 $\dot{B}$ = - 1,1 m w.e. yr⁻¹. About - 1,3 m yr⁻¹ of ice. And an average elevation change of - 21 m.

6. Discussion

6.1 Classification of Instabilities at Ärlen Glacier

In temperate mountain glaciers, ice flow velocity is a glaciological parameter that responds very quickly to changes in forcing factors, but also depends strongly on topography. Since the strong retreat of glaciers, ice flow velocities have continuously decreased in recent decades (Nishimura *et al.*, 2013 and Stocker-Waldhuber *et al.*, 2018). The maximum flow velocity is located up-glacier in the middle of the valley where the ice is thick. Surface velocity decreases at the glacier margins and edges as ice thickness decreases (Nishimura *et al.*, 2013). To understand the nature of the mass movement of Ärlen Glacier, ice flow velocities and the timing of phases of enhanced flow are critical. Compared to other events, these parameters give a fairly good understanding of the forces responsible for the collapse of Ärlen Glacier.

6.1.1 Differences and Similarities with Glacier Surges

Several features of the instabilities at Ärlen Glacier are striking and resemble the surge-like instabilities of glaciers: Ärlen Glacier shows near-cyclic changes between active (2014 - 15, 2017 - 2020) and one observed passive phase (2016) of flow rates. The active phases have a duration of 2 and 4 years and are followed by passive phases that last 1 to 2 years. The active phases of surge-type glaciers are also often accompanied by an advance of the terminus (Truffer *et al.*, 2021). This could be observed over several years (2014, 2017, 2018, 2019 and 2020) at Ärlen Glacier. Also, the rapid mass shift from a reservoir to a depletion zone during the active phase is quite characteristic and could be observed very nicely at Ärlen Glacier. The 10- to 1,000-fold increase in flow rate due to basal sliding (Jiskoot, 2011) during active phases is very characteristic of surge glaciers. This enhanced flow can last for days to weeks. At Ärlen Glacier, the glacier moved at up to 5 m/d during a period of about one month. Surge glaciers are also highly crevassed and the sliding part is often completely disrupted, as observed at Ärlen Glacier during the period of increased flow, particularly visible in 2017 (figure 23).

All these similarities might indicate that what happened at Ärlenglacier could have a similar forcing as a glacier surge. However, normally glacier surges occur within well-defined climatic zones (Clarke *et al.*, 1986; Jiskoot, 2011 and Sevestre and Benn, 2015) , and the Swiss Alps are certainly not one of them. Moreover, a soft glacier bed seems to be a necessary condition (Harrison and Post, 2003 and Truffer *et al.*, 2021), which is not the case for the hard granitic rock at Ärlen Glacier. Also, the volumes of movement are much smaller than expected for surge-type glaciers.

The most important difference, however, is the occurrence of the slides in late summer and fall (August to October), followed by a slowdown at the end of the melt season to complete stagnation in winter when temperatures are constant at about 0 °C. This characteristic timing of events has many similarities to temperate ice avalanches as described by (Röthlisberger, 1981). One example that has many similarities is the events at Allalin Glacier. The reasons why these events are so similar are discussed in the following chapters. The link to surge-like motion can be made based on the velocities experienced by the mass movement, but most other characteristics do not match at all as discussed previously.

6.1.2 Velocity and Movement Compared to Glacier Observations in the Swiss Alps

The maximum velocities on the Rhône Glacier in 2005 - 2006 were 0.28 m/d (Nishimura et al., 2013). This is an example of the magnitude that can be expected for a normally flowing glacier in the Swiss Alps. Velocities decrease with ice thickness and glacier size, which means that lower velocities should be expected in the case of Ärlen Glacier. According to Röthlisberger, (1981) the Allalinglacier moves with typical winter velocities of 5 cm/d during quiet phases.

The time-lapse photogrammetry results from 2020 showed that the average velocities before the fast acceleration were 0.31; 0.31; 0.27 m/d (always Pt1; Pt2; Pt3). After the movement stopped in late September, the average velocities were 0.24; 0.21; and 0.10 m/d, respectively. These values are already quite high considering the small size and thickness of the glacier. The thickness of the unstable part was estimated in the field to be only about 5 to 10 meters. The maximum observed velocities for each point (pt1; pt2; pt3) are 3.51; 3.56 and 5.29 m/d, respectively. The average velocity during a part of the 2018 slide event was about 1.56 m/d for the unstable part of the glacier. The upper, stable part of the glacier moved at 0.1 m/d during the same period. This would be a reasonable rate for the entire glacier during the period from late September to late October, given the high October temperatures of 2018 (about 1.5°C above normal (1981-2010)) (figure 37).

According to Röthlisberger (1981), slide velocities of up to 4.5 m/d were measured at Allalin Glacier during active phases. These velocities were measured in the years following the catastrophic 1965 breakup and are of the same order of magnitude as the maximum velocities observed at Ärlen Glacier (3.51; 3.56 and 5.29 m/d) in 2020.

Surface velocity changes during such active phases resemble a power-law acceleration observed prior to the instabilities of unbalanced glaciers (Röthlisberger, 1981; Faillettaz *et al.*, 2008 and Faillettaz, Funk and Vincent, 2015). A similar trended acceleration was also observed over the entire unstable part of Ärlen Glacier in 2020 after the glacier tongue broke off on August 26 (figure 45).

According to Röthlisberger (1981), in the case of Allalingletscher, the slides follow each other in intervals of one, two or three years. For Ärlen Glacier the same alternation between active and passive phases could be observed very nicely and is discussed in comparison to the surge-type glaciers above.
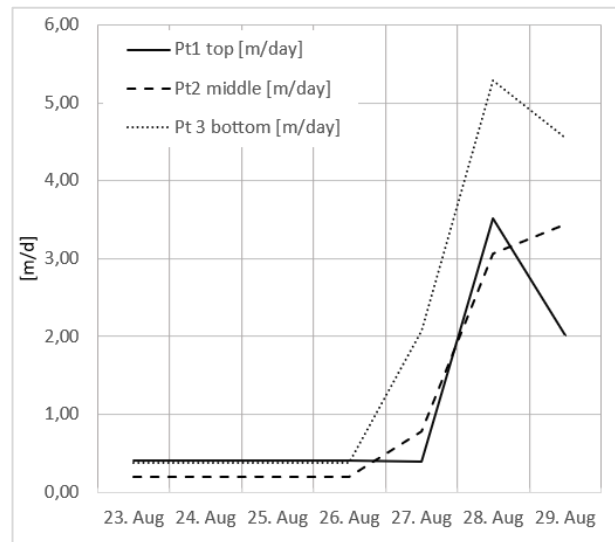
Figure 45: Power-law acceleration observed at Ärlenglacier after the terminus broke off at the 26th of August 2020, for the three observed points from top to bottom of the glacier (Pt1 to Pt3). The delay of the acceleration from the bottom to the top is very nicely visible. The vertical axis lines are placed at midnight.

These active phases, observed before and after 1965, did not always result in large ice avalanches as in 1965 (Röthlisberger, 1981). In 1967, a listric breakout niche formed in the same area where the glacier had broken off in 1965, but the glacier only sagged and did not form an avalanche. Reasons given are that the glacier may have been supported by a cone of ice debris formed by a small avalanche at the end of the glacier, or that the slide was less intense and the supporting end of the glacier was not pushed over the critical terrain step. Another reason would be the different mass distribution (Röthlisberger, 1981).

Only when sufficient ice has accumulated in the rear part of the slip area acceleration occurs. This area, where the listric outburst niche opens, thus has the function of a reservoir. If this reservoir empties significantly during a strong slide, it will take longer to reach the next slide than after a short incomplete slide. Typically, it takes one to two quiet years after a strong slide (Röthlisberger, 1981). This could be one reason why the glacier did not slide in 2016 and showed such a "normal" appearance and behavior. Also, after the severe slide of 2018, it took longer for it to be triggered again in late fall 2019. It was then immediately stopped by the cold temperatures, only to continue sliding in 2020. During severe slides, the moving mass separates from the bottom of the serac zone and bedrock emerges according to Röthlisberger (1981) in observations at Allalin Glacier after the catastrophic avalanche of 1965. This effect could be nicely observed at Ärlen Glacier during several years (chapter 5.2).

6.1.3 Similarities to Ice Avalanches from Temperate Ramps

Ice avalanches from temperate ramps were presented in (chapter 2.2.5). Since there are many similarities with the events at Ärlen Glacier, this chapter compares the most important features of such instabilities with the findings from our study at Ärlen Glacier. First, however, there is one characteristic feature at Ärlen Glacier that is not consistent with the findings of ice avalanches from moderate ramps, namely the very shallow slope.

According to Iken (1977); Alean (1984) and Haeberli et al. (1989) a necessary condition is that the avalanche area is located on a steep and even slope. This is not the case with Ärlen Glacier, which made the instabilities quite unexpected. However, Haeberli et al. (1989) mention that in warm ice, where a water film between ice and rock allows basal sliding, ice avalanches can occur at a slope as low as 25°. According to Röthlisberger (1981), in the case of Allalin Glacier, the landslides occur in an area with a slope of only 22°. This may be consistent with the steepness of the first step of the terrain at the glacier tongue, and may explain the small ice avalanches that have occurred there repeatedly over the years. But this decrease in critical slope with increasing temperature and decreasing elevation (Haeberli et al., 1989) is a start to understanding the processes at Ärlen Glacier.

Even though the slope seems to be too shallow for an ice avalanche from a moderate ramp based on the literature mentioned above, many other features fit very well with the descriptions of such events as at Allalin Glacier (chapter 2.3).

According to Haeberli et al. (1989) and Röthlisberge (1981), major ice avalanches from temperate ramps seem to be restricted to the late melt period. The timing of the onset of glacial avalanches at Ärlen Glacier was narrowed down to before the end of September (2014), mid to late August (2017), around September (2018), the second half of September for (2019), and August 26 for 2020 (chapter 5.2). Other than for 2020, the exact dates are not known due to the temporal resolution of the available imagery. However, it appears that slip instabilities always begin sometime between late August and late September. This corresponds to the late melt season according to our PDMM (chapter 5.6.2), where melt typically declines dramatically in early September.

Röthlisberger (1981) mentions that sliding usually stops at the beginning of winter, between mid-September and mid-November. On Ärlen Glacier in 2020, the active phase stopped around the end of September (figure 46), when temperatures dropped. In other years, the end of the active phase could not be determined due to snow cover, making the satellite images useless for such interpretations.

However, comparisons of glacier condition in the fall and summer of the following year seem to clearly indicate that glaciers ended their active phase sometime in September of 2017, stalled and continued again in late summer of 2018 (chapter 5.2).
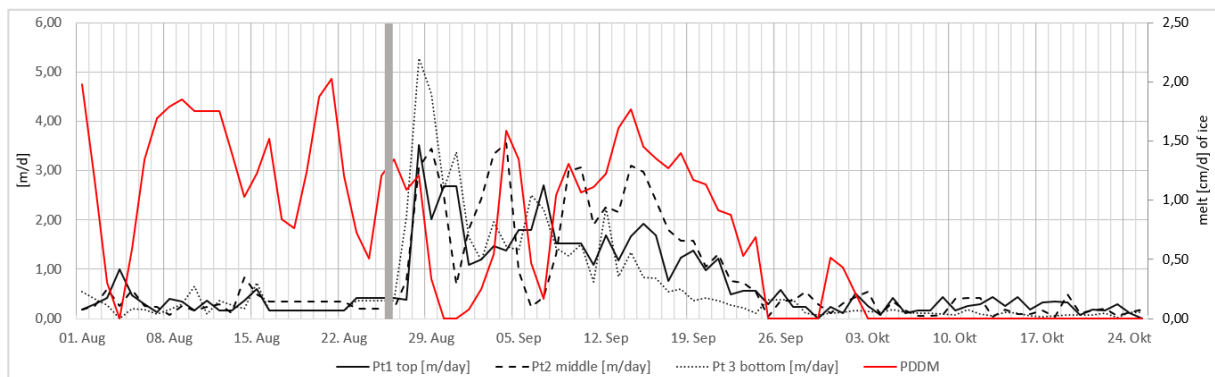
Figure 46: Velocities of the three different points [m/d] assessed with time-lapse photogrammetry compared to the melt calculated with the PDDM [cm/d] during the time period with enhanced velocities of 2020. The end of the active period accords very nicely with the dropping temperatures in the end of September. The break off of the glacier tongue (26th of August 2020) is showed with a thick grey line.

Other than the glaciers steepness, the criteria for sliding instabilities on (steep) temperate glacier tongues according to Faillettaz, Funk and Vincent (2015) are met:

1. A critical geometrical configuration at the glacier tongue is necessary (steep slope, no frontal abutment, and convex shape of bed topography). ➔ The frontal abutment disappears each time when the glacier melts over the critical terrain step. Which seems to be the most important factor because the slides appear always after the critical terrain step is reached.

2. The glacier should have gone through an active phase. ➔ Several active phases were observed at Ärlen Glacier (chapter 5.2).

3. The subglacial drainage network has to be distributed. ➔ The hard granite bedrock implies that the subglacial drainage network is distributed in the case of Ärlen Glacier.

4. A colder period with decreasing runoff is needed (reduces efficiency of drainage network and favours fracturation process). ➔ Such colder periods, where melt dropped to zero or close to zero, could be observed during each year with enhanced sliding at Ärlen Glacier (figure 40). For 2020 (figure 46) such a period could be the temperature drop around the 4th of August (below 0 °C) or even less strong temperature drops after the midst of August where temperatures reached a mean of about 4 °C during the 24th of August. Which is just two days before the fast flowing dynamics started.

5. A pulse of subglacial water flow is a probable trigger for the catastrophic break-off event. For 2020 (figure 46) shows that melt raises again just before the collapse starts. Also for the other years, this figures of temperature and melt dropping to nearly 0 and then rising again can be observed during all years, not excluding years with no sliding instabilities (figure 40).

These similarities clearly show that despite the flat slope, Ärlen Glacier exhibits almost the same dynamics as glacial avalanches from temperate ramps. We therefore suggest that glacier sliding instabilities can be triggered with the same mechanics as described above at lower slopes than previously thought. The difference being, that the flat slope prevents the ice mass from developing higher velocities and become an ice avalanche. Thus, Ärlen Glacier is experiencing the active phase, but fortunately is not steep enough to develop into an ice avalanche.

The temporal limitation of the active phase leads to the assumption of a climate influence (Röthlisberger, 1981). The different triggers and influences are discussed in detail in the next chapters and compared with climate factors and literature.

6.2 Possible Triggers for Mass Movements at Ärlen Glacier

Possible causes for events like Ärlen Glacier experienced from 2014 to 2020, were noted by Röthlisberger (1981) pertaining to the events at Allalin Glacier and other glacier observations. Table 3 shows those possible triggers of glacier avalanches and how they typically appear.

Table 3: Explaining appearances (vertical) of glacier avalanches and their probable causes (horizontal) according to Röthlisberger (1981).

	Mass distribution	Temperature	Water
Slip only during Summer		X	X
Slip not every year	**X**	?	
Start arbitrary (June – October)	X	?	
Stagnation at beginning of Winter (Sept. – Nov.)		?	**X**

The first obvious choice would be the influence of temperature. But as Faillettaz, Funk and Vincent (2015) determined, the stagnation during fall is hard to explain only with cooling. The reason for this is that the ice could only cool fast enough to freeze solidly to the rock at the front, edges and at the bottom of crevasses. This means that in years with early snow, the glacier would not freeze further and the sliding would not stop because of the insulating properties of the snow.

The observations at Ärlen Glacier are consistent with these findings, and the velocity data show that the glacier stopped immediately after the snowfall on September 26, 2020, and also slowed down massively after the snowfall on August 30 (figure 46). This indicates that temperature has an indirect effect via meltwater. When there is no meltwater, the glacier stops (Faillettaz, Funk and Vincent, 2015).

67

According to Faillettaz, Funk and Vincent (2015) there is strong evidence that the onset of the acceleration phase cannot be controlled by meltwater, but that sliding during a given year is dependent on mass distribution. As observed at Ärlen Glacier, Allalin Glacier also accelerates sometime during summer and fall, strengthening this assumption.

The mass distribution and the geometry of the glacier can be determined as the cause of a slide in a given year. However, other conditions must be present for the entire process to occur. The various factors and triggers that contribute to the sliding properties at Ärlen Glacier will be discussed in detail in the next chapters.

6.2.1 Flow Velocity and Water Pressure

Hagg (2020) discussed the seasonality of basal sliding, assuming that it depends mainly on meltwater, with the conclusion that the maximum is reached during the particularly high occurrence of meltwater. However, the importance of high pressures in subglacial cavities, which reduce the roughness of the bed and facilitate the sliding process, was also pointed out. According to the theory of water pressure in intra- and subglacial channels by Röthlisberger (1972), water pressure at the base of the glacier is more important than melt volume. Water pressure is highest in spring when the subglacial drainage system is not yet well developed (Röthlisberger, 1972). These assumptions are based on observations on alpine glaciers, where basal movement is highest in spring and early summer (May - June), when meltwater production increases. In summer (July - August), they are generally lower despite the higher meltwater input (Lüthi, Walter and Werder, 2020).

The same effect is also defined by Faillettaz, Funk and Vincent (2015) as trigger for ice avalanches and instabilities as observed at Ärlen Glacier. A colder period is needed to reduce runoff and the efficiency of the subglacial drainage network. This effect could not only favor the fracturing process discussed by Faillettaz, Funk, and Vincent (2015), but also trigger faster flow velocities due to higher subglacial water pressure after a colder period when temperature and meltwater increase again.

Figure 47 shows the relationship between flow velocity, melt and rain at Ärlen Glacier from August to October 2020. The point in the middle of the glacier was chosen for comparison because it is in the area that represents most of the flowing mass of the glacier and shows the most interesting dynamics. The onset of increased sliding appears to be controlled primarily by the small avalanche at the end of the glacier, which represents a loss of stabilization for the entire glacier. After that, both curves behave very similarly.

The very rapid second acceleration, after the melt has decreased to zero at the end of August, could be a consequence of the reduced efficiency of the runoff system. This causes the glacier to react very quickly after water has entered the system again. After this rapid acceleration, both curves show a very similar behavior until both melt and velocity come to rest at the end of September.
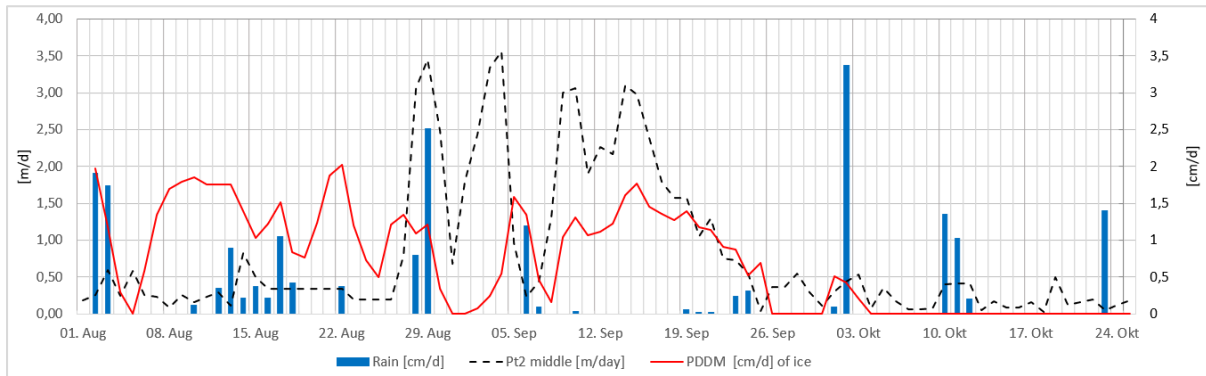
Figure 47: Comparison of flow velocity [m/d] of Pt 2 in the middle of the glacier, the modelled melt [cm/d] and rain [cm/d] during the same time period (2020).

The divergence of the two curves after the 26th of August could also be explained by errors in the temperature extrapolations due to the very regional climate characteristics of mountainous regions. The listric fracture niche extending to the ground probably also has an amplifying effect on glacier velocity because it delivers meltwater directly to the subglacial drainage network, which could also partially explain the rapid response correlation with melt. Another effect that influences velocity is the topography of the glacier bed, which could have a damming effect on the very flat part.

A study by Sugiyama and Gudmundsson (2004) investigated short-term velocity variations during the ablation season in Lauteraar Glacier, Bernese Alps, Switzerland, and showed that the horizontal surface current velocity oscillates daily and correlates with the water level in a borehole. This observation suggests that flow oscillations are mainly controlled by local water pressure, which amplifies basal movements. Specifically, flow velocity was found to decrease more when water level decreases than it increases when water level increases (Sugiyama and Gudmundsson, 2004).

Short-term fluctuations were also studied during periods of good weather on the Ärlen Glacier. These show the control of runoff fluctuations by melt in the case of this glacier. Normally the connection is made with subglacial water pressure, but because of the listric outburst niche extending to the ground at the top of the unstable area, the influence of melt may be more direct than is normally assumed for glaciers. The more rapid decrease in velocity with decreasing water and increase in velocity with increasing meltwater is also visible in figure 48.
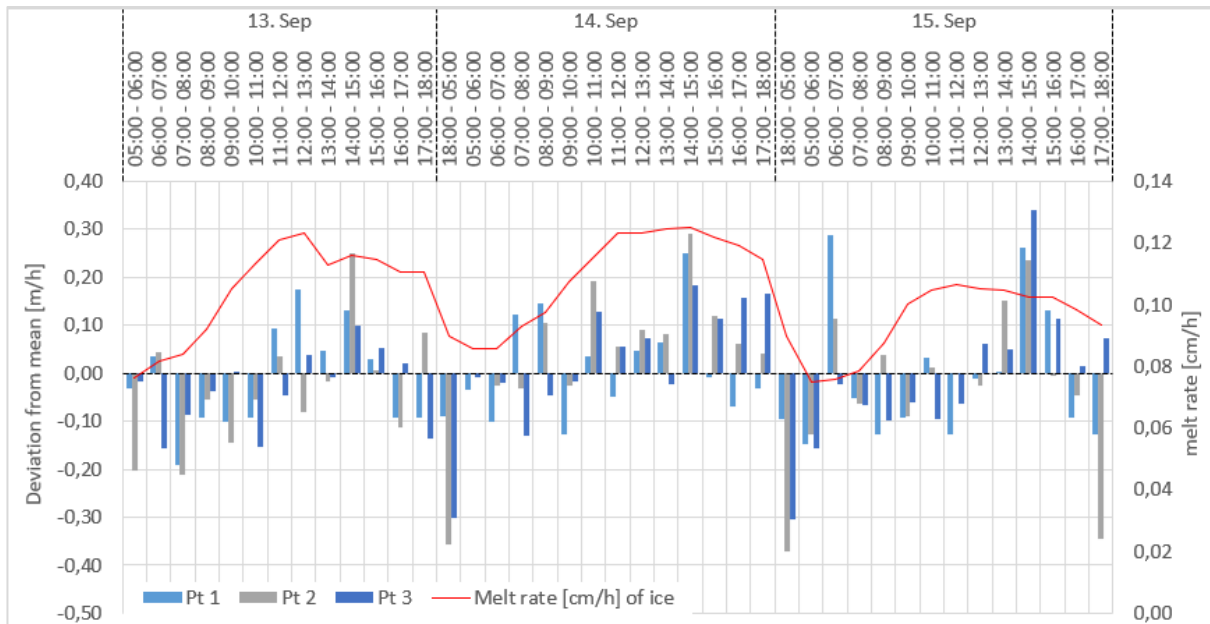
Figure 48: Velocity [m/h] deviation from mean for the points Pt1 - 3 situated from the top to the bottom of Ärlen Glacier. Mean for Pt1 = 0,19; Pt2 = 0,40 and Pt3 = 0,31. Compared to melt from the PDHM [cm/h] of ice. The deviation from mean makes the velocity fluctuations connection to melt and water pressure visible.

6.2.2 Initiation of Active Phase

According to Faillettaz, Funk and Vincent (2015) and Röthlisberger (1981) the glacier should have gone through an active phase during the year in which a ramp-type glacier avalanche happens. Faillettaz, Funk and Sornette (2012) note, that the onset of the active phase is induced by an increase in subglacial water flow. To understand the long-term changes in subglacial waterflow, we calculated the melt with a PDDM and additionally the summer water availability by adding rain at the height of Ärlen Glacier.
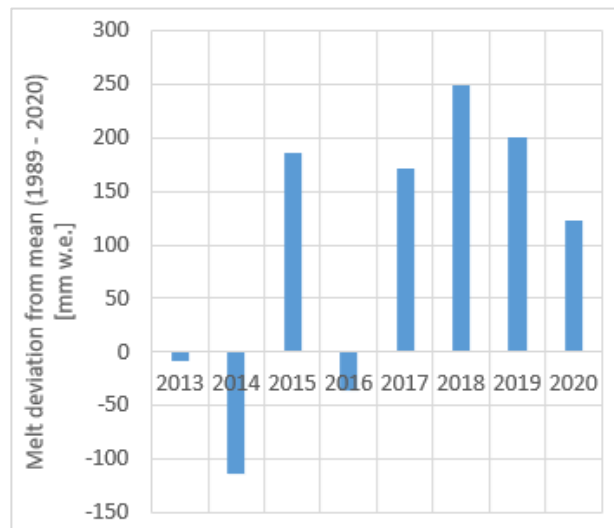
Figure 49: Melt deviation from mean from 2013 to 2020. The mean is calculated between 1989 and 2020 and is 997 mm w.e..

Figure 49 shows an obvious increase in meltwater after 2015 with an exception of 2016. This shows a strong connection with years in which an active phase was observed and melt. 2016 being the only year after 2013 with no active phase observations.

The clear exception provides the year 2014. To understand the possible active phase we have to look at the summer water availability (figure 50) as supposed by Jacquemart *et al.* 2020. This suddenly illustrates 2014 as a year with above average water availability. The low melt during 2014 can be explained with extremely bad weather during summer. Especially during July of 2014 a lot of areas in Switzerland experienced extreme precipitation. The Ärlen Glacier area was particularly hard hit, with cumulative precipitation between 200 and 300 percent of the norm (1981-2010) (MeteoSchweiz, 2015).
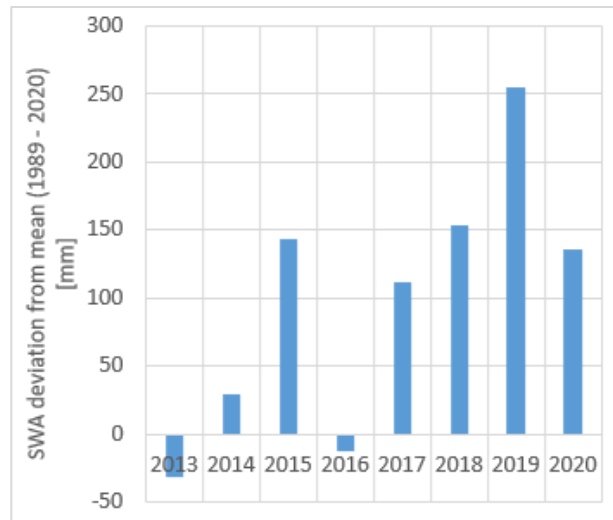
Figure 50: Summer water availability from 2013 to 2020. Calculated by addition of melt and rain events at the height of Ärlenglacier (extrapolated temperatures). The mean is 1379 [mm] for the time period (1989 - 2020).

Those extreme precipitation events of summer 2014 can explain why the glacier could enter an active phase even with relatively low melt during summer. How important those extreme precipitation events were in regard to the whole process of instabilities cannot be assessed with our data. But, the precipitation events took place during the first observed instabilities which shows a probable connection.

6.2.3 Influence of Glacier Geometry on the Instability

The topography of the glacier bed and the geometry and extent of the glacier are interrelated factors that strongly influence glacier stability. The extent and topography of Ärlen Glacier are a prime example of their importance in major glacier instabilities.

According to Faillettaz, Funk and Sornette (2012) and Faillettaz, Funk and Vincent (2015), the geometric extent of the glacier has a major influence on instability. Here, the critical condition for major instabilities at the glacier tongue is when the glacier terminus rests on a steep slope and the front abutment fails. This effect was nicely observed in the case of Ärlen Glacier for the events from 2014 to 2020. The observations of the extent of Ärlen Glacier shows the importance of this control for the instabilities (figure 51). The state of 2013 is just above the critical terrain step (25°) and it clearly shows, that the glacier needs to reach this step before the enhanced sliding starts again. During 2020 this effect could be studied precisely thanks to the time lapse camera. As soon as the glacier terminus loses its abutment the whole glacier starts to flow fast. It is also the reason why the glacier probably didn't advance during 2015.

With the heavy advance of 2014 the summer temperatures weren't hot enough to melt the whole ice advanced over the critical terrain step. This shows the importance of terminus abutment, because the glacier most likely was in an active phase as described by Weissenfluh (2015) while walking near the glacier during late summer of 2015.
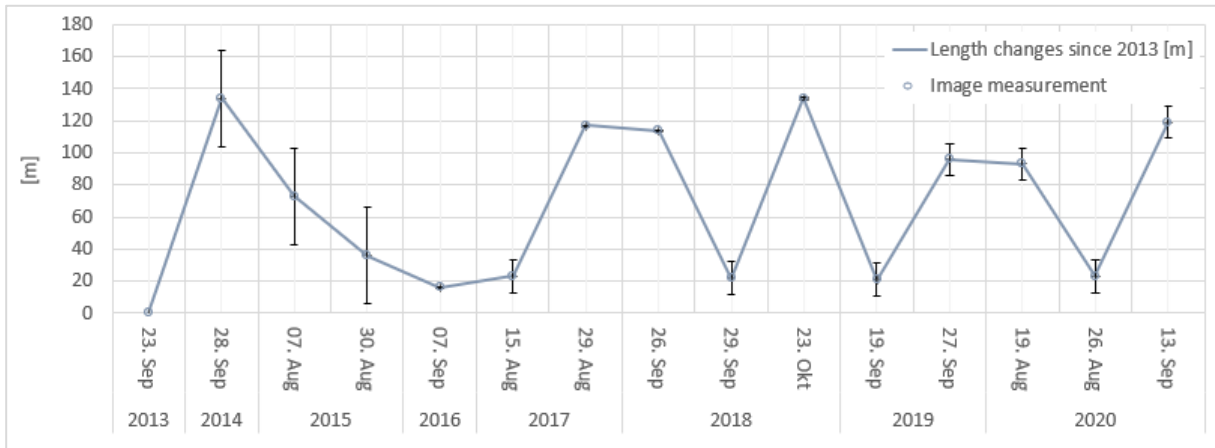
Figure 51: Extent of the Terminus of Ärlenglacier since 2013, whereby 0 is the state of the glaciers tongue during 2013. Positive values symbolize glaciers advances and negative values glacier retreat. The error bars show the estimated uncertainty for each image, depending on the survey platform (chapters 3.5 SWISSIMAGE and 3.6 Open-Source Satellite Imagery. Measurements were done with all available aerial imagery, from Swisstopo data to the different satellite imagery (chapters 3.5 SWISSIMAGE and 3.6 Open-Source Satellite Imagery.

Also, during 2019 the glacier started the enhanced slip velocities only late in September after the advanced ice from the big event of 2018 was melted again. During 2016 the glaciers terminus melted over the critical terrain step but didn't slide till 2017. Which shows that the topography is a necessary condition, but an active phase of the glacier is also needed to start a total collapse with enhanced slip velocities. Figure 51 doesn't show 2 of the retreats over the critical terrain step, because they weren't observed definitely on satellite and Swisstopo imagery. But the time lapse imagery shows a retreat over the critical terrain step for the 26th of August of 2020. For 2018 the Sentinel-2 images show a break-off at the glaciers tongue and the following loss of stabilization at the 29th of September (figure A64). The oscillations, with a two-year interruption after 2014 and an annual recurrence starting in 2017, show the importance of the control by terminus stabilization for the events at the Ärlen Glacier (figure 51).

According to Röthlisberger (1981) terminus stabilization can be achieved either from support of down-slope ice ore from cold ice margins frozen to bedrock if the starting zone is not (yet) at the terminus. In the case of Ärlen Glacier, if the glacier is above the critical terrain level, stabilization could also be given due to the flat topography in this area, as shown in figure 52.

The flat area above the critical terrain level causes the glacier to pile up in a most impressive manner during periods of increased basal movement, such as in 2020 (figure 52).For the years 2018, 2019 and 2020 the support from downslope ice vanished after melting. But for 2014 and 2017 the terminus support was probably pushed over the critical terrain step after assumably a vault formed beyond the glacier during the time of enhanced velocity, as proposed for Allalin Glacier (Röthlisberger, 1981 and Pralong and Funk, 2004).

According to the observations on Allalin Glacier by Faillettaz, Funk and Vincent (2015), the glacier must not only be above the critical terrain level,

Figure 52: Impressive tower of ice which was piled up during the sliding events of 2020. Picture was taken at the 4th of September 2020.

but also have sufficient mass in the reservoir zone (area beyond the listric breakout niche). This results in the glacier taking longer to reach the next slide (1-2 years) after a strong slide than after a short incomplete slide.

The emptying of the reservoir zone is visible by comparing the DHMs from 2015 to 2020 (chapter 5.5.1) where the glacier showed a mean hight difference of - 8.5 m over only 5 years which sums up to a mass loss of ca. 218'374 m^3. Compared to the geodetic mass balance (chapter 5.7) from 1993 to 2015 where the melt lies at - 1,3m yr^{-1} the reservoir zone at Ärlen Glacier had an average height loss of 1,7 m yr^{-1}.

A crescent-shaped outburst niche is often observed after a glacier collapse. This phenomenon is due to the fact that the stopped glacial vault was able to support itself at both ends of the arch. The loss of support on abutments is one of the most important reasons for the initiation of glacial or ice avalanches (Röthlisberger, 1981).

6.2.4 Role of Subglacial Drainage Network Topology

Similar glacier instabilities are strongly affected by the subglacial hydrology, because infiltrated meltwater causes a lubrication of the bed, which decreases the basal friction (Faillettaz, Funk and Vincent, 2015). In this process, the subglacial drainage network must be distributed (Faillettaz, Funk and Sornette, 2012) because it then affects a major part of the glacier tongue. Conversely, a channelized drainage network would affect only a limited area of the glacier. Figure 53 shows the hard, slippery bedrock, which is not only very slippery itself, but also provides for a very well-distributed subglacial network topology that appears to be an important precondition for instabilities across the entire glacier tongue.

Figure 53: Slippery granite bedrock beyond Ärlenglacier. Here showing an area still covered by ice during 2013.

It is even conceivable that in the flat area at the front, just above the critical terrain level, a lens of water forms below the glacier, as described by Röthlisberger (1972) for glaciers with a very flat bed, reducing basal friction even further. Also the effect that water can access the subglacial drainage net-work directly via the listric fracturing niche increases the subglacial water pressure and therefore the drag at the glaciers bed. Figure 54 shows well how water accesses the subglacial drainage network very directly through the listric fracturing niche.
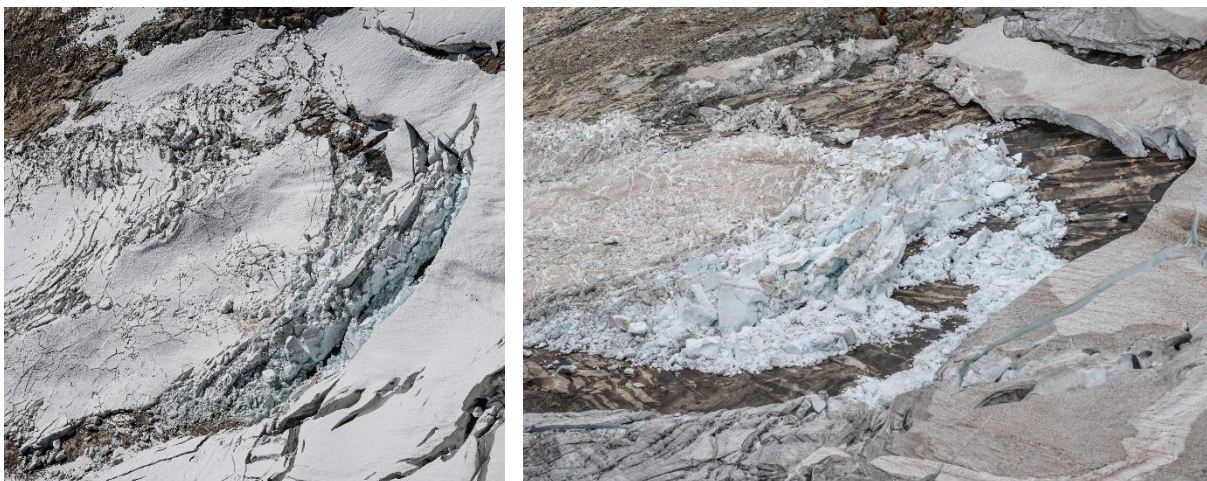
Figure 54: Opening of the listric fracturing niche with images from the two helicopter survey flights (04th of September and 22nd of September 2020).

6.2.5 Sequence of Basal Water Pressure

For a catastrophic break-off, as observed for Allalin Glacier in 1965 and 2000, the glacier must be in an active phase with strongly increased basal movement, and this active phase must be abruptly terminated by a sudden reconnection of the glacier to its bed. Furthermore, it appears that once the glacier is reconnected to its bed, an additional water pulse is required to trigger the instability (Faillettaz, Funk and Sornette, 2012 and Faillettaz, Funk and Vincent, 2015). During the cold period with reduced runoff and rapid recoupling of the glacier to the bedrock, intensive crevassing of the glacier tongue is initiated (Faillettaz, Funk and Sornette, 2012). This effect is related to the diminishing fluidity of ice as temperatures drop (Glen, 1958).

The velocities measured at Ärlen Glacier during 2020 (average: 3.51; 3.56 and 5.29 m/d) are similar to velocities measured during active phases at Allalin Glacier (max.: 4,5 m/d according to Röthlisberger (1981)). This could lead to the assumption that Ärlen Glacier does not need the sequence of basal water pressure to start the enhanced basal motion (active phase) and therefore does not exhibit catastrophic break-off. But comparing the velocities before the terminus break off (means Pt1 - Pt3: 0.31; 0.31; 0.27 m/d) to the maximum velocities at Rhône Glacier during 2005 – 2006 (0,28 m/d from Nishimura *et al.* 2013) the velocities at Ärlen Glacier seem to show an active phase regarding the thin layer of ice and topography at Ärlen Glacier compared to Rhône Glacier, both factors strongly influencing the glaciers velocity.

Nevertheless, our data do not clearly show that the sequence of basal water pressure is necessary in the case of Ärlen Glacier. This is especially the case for the years 2018 to 2020, where it only matters if the glacier tongue loses its stabilization after the break-off and the new break-off is above the critical terrain step. This can be seen particularly well for 2020, when the entire glacier begins to slide immediately after terminus break-off. Then the last cold period is about one month ago and also an increased meltwater input cannot be clearly defined (figure 55).
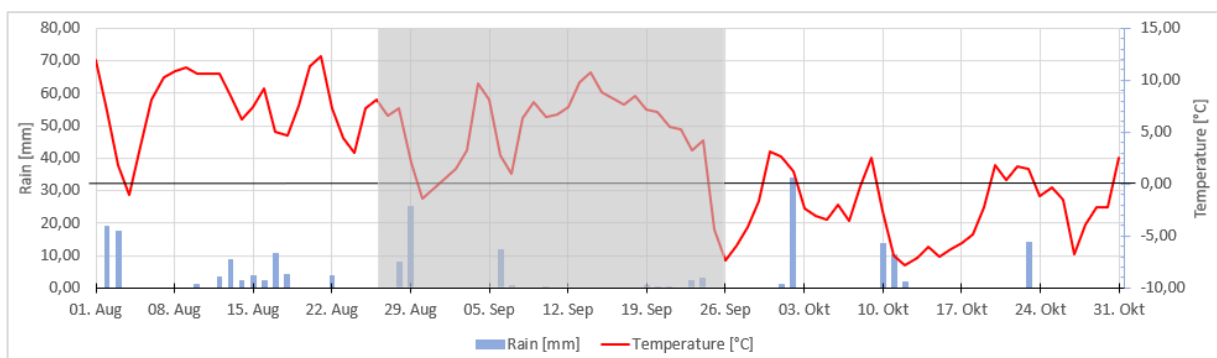
Figure 55: Estimated rain and temperature at the height of Ärlen Glacier during August till October of 2020. The time period where enhanced basal motion was observed is showed with a grey box.

For the 2014 (figure A65) and 2017 (figure 56) events, such a process chain is plausible, and there are sufficient possible temperature declines followed by increases in water availability during the periods when the glacier instabilities occurred in those years. However, the exact timing of the sliding events is not known, so the relationship cannot be clearly established. However, for the years after 2017, we assume that the listric fracture niche has not closed again, especially after the severe slide of 2018. This firstly separates the unstable part of the glacier from the rest, making enhanced fracturing practically unnecessary, and secondly allows melt and rainwater to directly enter the subglacial drainage system.

This makes the front part of the glacier independent since 2017, and our research shows that the most important factor then is terminus stabilization due to previous events. However, the sliding instabilities are still strongly influenced by the availability of meltwater, which allows the increased velocities due to reduced basal resistance and stops the sliding when subglacial meltwater vanishes with lower temperatures.
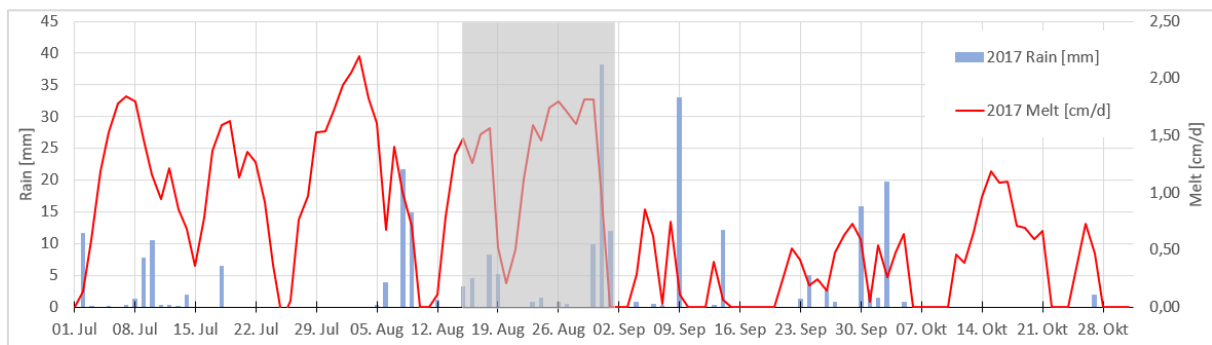
Figure 56: Estimated rain and temperature at the height of Ärlen Glacier during July till October of 2017. The time period in which enhanced basal motion is assumed due to aerial and satellite images, is showed with a grey box.

Enhanced fracture mechanisms also have an impact on sliding velocities, as observed on August 30, 2020 (figure 47), where glacier velocity quickly rebounded after slowing at temperatures below 0 °C. This may also contribute to the strongly crevassed appearance of Ärlen Glacier, which was outstandingly evident in 2017 (figure 23). This phenomenon shows the combination of reduced ice flow at colder temperatures and increased flow velocities after the subglacial drainage system became inefficient due to colder temperatures and freezing.

For the events of 2014 and 2017, a sequence of basal water pressure triggering the events seems quite plausible. The temporal and visual similarities with Allalin Glacier and the ramp-type glacial avalanches discussed in this paper reinforce this assumption. Unfortunately, the data in 2014 and 2017 are so sparse that these similarities cannot be confirmed beyond doubt, but they seem very plausible.

It is reasonable to assume that the sequence of basal water pressure is necessary in the case of an intact glacier but loses significance when part of the glacier is detached. During 2018 the unstable part of the glacier detached with a separation from the rest of the glacier of nearly 60 m (figure 25). The observed glacier velocities are 0.31; 0.31; 0.27 m/d during august of 2020 (chapter 5.4.1). This are the velocities during an active phase with enhanced basal motion and can only be assumed for a short period of the year depending on temperature and subglacial water availability. Assuming much lower velocities for the rest of the year, the two glacier parts didn't reconnect in the following years (2019 and 2020). The opening has been filled with snow during the winter, and ice falling down from the upper edge of the listric fracturing niche. This leads to the appearance of a reconnected glacier on images, but the opening contains only snow, firn and unconnected blocks of ice which have different physical properties then glacier ice (figure 57).

Figure 57: In the middle of the image is the area where the listric fracturing niche opened during 2017/18. The upper edge of the fracturing niche is nicely visible on the right side, while the rest of the glacier is on the left side. Image is from the helicopter survey flight on the 4th of September 2020.

6.3 Relevance of Ärlen Glacier for Glacier Related Natural Hazards in the Alps

In a more general context, slope and bedrock instabilities due to permafrost degradation, rockfall, landslides, snow avalanches, or glacier instability are common in high mountain regions such as the Swiss Alps (Gill and Malamud, 2014). Because temperature and precipitation changes have numerous effects, including altering glacier extent, snowpack extent and duration, and permafrost distribution and thermal properties, climate change is likely to influence the frequency and magnitude of such mass movements (Stoffel and Huggel, 2012).

The events at Ärlen Glacier show many links to current climate changes. Most obvious is the strong correlation of instabilities with the extent of the glacier. In this context, other factors such as water availability, subglacial water pressure, and ice overburden pressure are also influenced by climate change, which presumably makes such events more likely, as suggested by Helanow *et al.* 2021 in developing a glide law for hard-bedded glaciers. Their conclusion is that weather or climate changes that increase sliding velocity or decrease effective pressure (water pressure in the cavity, subtracted from ice overburden pressure) would reduce resistance to sliding and thus promote faster flow and glacier instability, including glacial surge propagation.

Regarding glacier stability, Faillettaz, Funk and Vincent (2015) also concluded that the stability of some glaciers could be affected in the near future due to changes in the thermal regime at the ice-rock interface or changes in geometric extent.

Ärlen Glacier is a perfect example of the increased possibilities of glacier instability. Due to its small extent and flat topography, such glacial features are unexpected. This shows that with the melting of glaciers over terrain steps and increased water availability, even very small alpine glaciers can suddenly develop instabilities and release mass movements of up to an estimated 1 million m^3 of ice for Ärlen Glacier in 2014.

Although, such instabilities are rare, they have a potential to cause major disasters, especially when they are at the beginning of a process chain involving other materials such as snow (snow avalanche), water (flood) and/or debris (mudflow) (Gill and Malamud, 2014).

6.3.1 Potential Future Hazard of the Ärlenglacier

Instabilities at Ärlen Glacier were first noticed because a water intake was built below the glacier. This raises the question of the potential danger of these instabilities. Fortunately, the topography below the glacier has trapped the advances in a terrain syncline every time since 2014.

Because the glacier advanced over several years, the mass loss is much more significant than would be expected for a glacier without advances. Advancement beyond the terrain depression is therefore unlikely with respect to potential future slides. It is likely that the detached segment of the glacier will slide each fall after the tongue has melted above the critical terrain level until either there is not enough mass to trigger further sliding or the detached segment has completely melted. The detached ice will melt over the next few years, leaving no trace of the interesting dynamics that the glacier displayed over several years. The only effect will be, that the glacier will disappear quicker than just with the enhanced melting most glaciers experience.
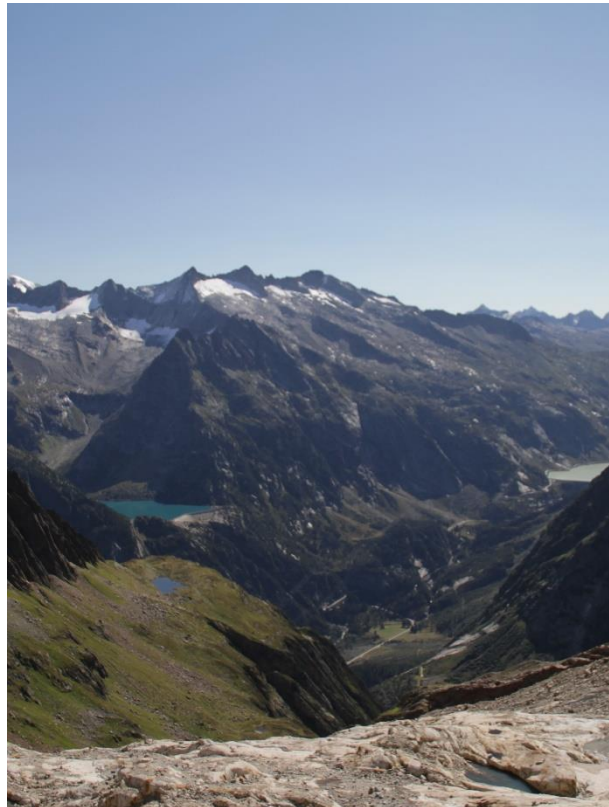
Figure 58: View from the bottom of Ärlenglacier down into the valley containing the Grimsel Pass Street and the power plant Hangholz.

According to Röthlisberger (1997), slides at glacier tongues or tongue sections are not a frequent but a widespread phenomenon in the Alps. However, they often do not appear in the data because step tongues in particular are not included in the survey network. This can also be true for small alpine glaciers, which are often neglected in survey networks. The example of Ärlen Glacier shows that a major glacier instability was not detected for almost four years (2014-2018).

Fortunately, the topography and geometric characteristics of the glacier prevented the ice avalanche from breaking loose and precipitating into the valley. However, the question arises as to how a similar event would develop under less optimal conditions. To estimate the potential ice volume of such an event, we used the ice thickness estimates of Grab *et al.* (2021), who estimate an average ice thickness of 21 m for Ärlen Glacier in 2016 (data available at Grab (2020)). Glacier thickness was estimated for all of Switzerland based on extended ground radar data and glaciological models.

At this estimated average ice thickness, the unstable material that moved in 2017/18 was about 963'396 m^3. This means that the total unstable ice volume for 2014 is estimated to be about 1 million m^3. For the closely monitored 2020 event, the unstable ice volume was already much lower due to melting, which was also enhanced by continuous inflows. In the field, the ice thickness was estimated to be only 5 to 10 m, resulting in an unstable ice volume of 337,978 m^3. This shows the strong melting of about two thirds of the total mass.

Comparison with the catastrophic event at Allalin Glacier in 1965, when nearly 2 million m^3 of ice broke off, shows that the volume of unstable ice at Ärlen Glacier poses a major hazard potential when combined with steeper topography below the glacier. A similar event could also pose a major hazard with respect to glacial lake outbursts floods (GLOFs) if a lake is located beyond an unstable glacier or if a debris flow could be triggered. If such an event is at the beginning of a process chain involving other materials such as water and/or debris, the disaster potential is enormous (Gill and Malamud, 2014) .

Although the Ärlen Glacier never posed a threat and the unstable ice will melt in the coming years, other glaciers could develop into unstable situations and become dangerous. And as Faillettaz, Funk and Vincent (2015) noted in their study of Allalin Glacier, timely detection of such newly developing critical situations is a challenge in hazard assessment.

6.3.2 Assessment of Possible Hazard Warning Signs and Monitoring Methods

The research done after the catastrophic break off at Allalin Glacier lead to the important finding that the sliding at the tongue doesn't start immediately, but that the unstable ice mass accelerates during days to weeks (Pralong and Funk, 2004). According to Röthlisberger (1981), such active phases with strongly intensified basal sliding were observed at Allalin Glacier and the neighboring Hohlaub Glacier every few years, but usually without catastrophic break-off. Usually, these phases start between June and October and end between September and October. The reason why the active phase leads to a termination is possibly an unfavorable mass distribution. However, the stepped topography was probably also decisive for the fact that the arch formed at the end of the glacier was pushed over the terrain step and lost its abutment.. Observations of a listric fracture niche indicate that the glacier found an abutment on the lateral flanks at a critical equilibrium (Röthlisberger, 1981).

Unfortunately, the variations in flow velocity could only be estimated during the slide event of 2020, when the glacier was already separated from the upper part. More interesting in terms of natural hazards would be to know how the flow velocities developed in 2014 and 2017. However, due to the many similarities to the events at Allalin Glacier, we assume that the terminations have many similarities, even if the avalanches descended faster due to the much steeper slope.

According to Faillettaz, Funk, and Vincent (2015), events such as the Allalin Glacier disaster, which involve a chain of processes, are difficult to detect at an early stage, and timely evacuation is often the only efficient way to secure the potentially endangered area. Reliable prediction of such events is therefore desirable, but remains a challenge because the physical processes involved are not yet fully understood.

Pralong and Funk (2004) have addressed the possibility of predicting glacial avalanches. Their findings in relation to events similar to those at Ärlen Glacier and Allalin Glacier are discussed in the following sections. For successful prediction of a glacial slide, the dangerous development must first be recognized. Clues from mountaineers and the local population can be a useful source. Because glaciers are constantly changing, they may reach a critical mass distribution sooner or later. Glaciers that exhibit recurrent instability can be monitored with aerial imagery to predict a recurrence of the event. The recurrence of the 2000 event at Allalin Glacier could also be predicted because the glacier reached the identical extent. However, such critical developments can also occur with unknown glaciers, as can be seen in the case of the Ärlen Glacier. This is very actual, because the past years have been characterized by strong changes in glacier extent and this trend will continue. Therefore, early detection of glacier-related hazards is a topic that needs attention in the future.

The preparation phase for dangerous events can according to Pralong and Funk (2004) often be documented with regular aerial imagery. This critical mass distribution can be detected if glaciers melt over terrain steps and show enhanced crevassing as observed at Ärlen Glacier during 2013 prior to the breakoff during 2014. Whereby glaciers with hard bed-rock seem to be an important factor for break-offs with bigger ice volumes. Therefore hard-bedded glaciers, melting over terrain steps need to be monitored more closely in future, even if they seem flat and small as the example of Ärlen Glacier shows. Especially if such glaciers are in a situation where they could affect infrastructure or trigger a process chain like a glacier outburst flood.

If a critical mass distribution is found, Pralong and Funk (2004) suggest detailed survey measurements, as was also done after the discovery of instabilities at Ärlen Glacier. The development of the glaciers must be monitored at weekly to monthly intervals with the help of helicopter flights or automatic cameras. When more accurate prediction is required due to vulnerable infrastructure, measurements with a theodolite and electronic distance measurements are a proven method. A fix installed digital camera as installed at Ärlen Glacier can show the glaciers development in daily to hourly intervals. At Trift Glacier in 2003, a permanently installed digital camera allowed the observation of a glacier break-off at a similar terrain step.

This method provides the possibility to timely recognize a glacier slip and measure the corresponding acceleration of the unstable ice mass. However, acceleration is not always predictive of an ice avalanche, since active phases do not always lead to catastrophic termination. Pralong and Funk (2004) therefore conclude that, with current knowledge, it is only possible to predict when ice break-off can generally be expected. However, a precise prediction is not possible at present.

6.4 Uncertainties, Challenges and Limitations

6.4.1 Error Estimations for Front Positions

Low resolution satellite images make it difficult to plot front positions. It is hard to tell if a pixel is still ice or just a bit of ice. This is especially difficult with Landsat-8 images. Here the pixel size is about 30 m. Therefore, the estimated error 30 m for Landsat-8 images and about 10 m for Sentinel 2. The error is estimated to be the size of one pixel. Based on the estimate, the pixel takes the value of the majority of the land cover.

The georeferencing of the satellite imagery is a source of uncertainties depending on the projection of the images and the coordinate system used. By comparing the satellite images with SWISSIMAGE the errors seem to be up to 10 m ad the edges of the glacier and probably lower at the center of the glacier due to topographic effects where the topography is very steep.

The subjective centerline (chapter 4.1) leads to a rather large subjectivity of the glacier length. But for this research, the glacier advances and retreats are more relevant. And these can be observed quite well with a centerline that lies in the middle of the glacier.

6.4.2 Temporal Resolution of Images

A big limitation for this thesis was the temporal resolution of the available imagery. For 2020 the time-lapse camera provided very high resolution observations which could be used to understand the processes happening at Ärlen Glacier. But, for the other years the availability of imagery was very limited, depending on the revisit time of the satellite and weather conditions. This made it challenging to detect the exact timing of sliding events. Nevertheless, in most cases a useful image could be found for each month during the researched time period which provided a great contribution to understand the events at Ärlenglacier.

6.4.3 Point Tracking and Topographic Effects for Velocity Measurements

Due to the time intensive method of tracking pixels manually, only one point per measurement was considered. For further research, an average over several pixels in the same area would probably provide results less sensitive for errors. Over the whole time period, the influence of point selection gets smaller because the whole glacier is moving. However, this is particularly problematic for hourly variations, where point selection can have a big impact on the results because the motion is not homogeneous over the entire glacier. Further, registration problems arise when tracked features change their appearance (e.g. due to varying snow cover and light conditions) or are obscured totally by clouds or fog (James, How and Wynn, 2016).

Because hourly variations in flow velocity could be observed very nicely (chapter 5.4.2) with deviations from the hourly mean velocity of max. 0.2 m the inaccuracy of the manual point selection is assumed to be at about 0,2 m/h. For days with limited visibility due to bad weather the inaccuracy gets higher and often the points cannot be found at all due to low visibility or darkness.

Severe random errors can occur unless the angle between the axis of the lens and the direction of horizontal motion is determined (Harrison *et al.*, 1992). According to James, How and Wynn (2016), in order to process sequential feature observations to derive velocities within an image sequence, an updated DEM should be used for each image. However, normally only a single DEM is available, with the problem that any surface changes in the direction of the camera cannot be differenced. Because the unavailability of recent enough DEMs and the later discussed uncertainties in the SfM DEMs the simple approach was chosen. This can lead to errors in velocity estimation, but the important accelerations and decelerations of the sliding motion can still be analysed well. Other effects affecting the precision of the measurements are, that the glaciers movement towards the camera or away from it cannot be measured with our 2D approach. The combination of these effects leads to an estimated uncertainty of about 1 m/d, also regarding the velocity fluctuations during the measurements.

6.4.4 Processing of Helicopter Imagery

The DHM generated with SfM shows quite big errors at the boarders and at the top of the glacier (figure 34). The RMSE estimations from Agisoft PhotoScan for the difference between 2015 and September 4 2020 are showed in table 4. The Z error, representing height lies at 1,24 m. Which is quite a good value for the low input of images and control points. However, the main differences in volume between the years are readily apparent and provide clues as to how such a mass flow works.

Table 4: RMSE estimates of control points by Agisoft PhotoScan for the DEM on September 4.

Count	X error (m)	Y error (m)	Z error (m)	XY error (m)	Total (m)
10	5.56036	3.69267	1.23587	6.67484	6.78828

The processing of helicopter images with Agisoft PhotoScan is really dependant of the quality, quantity and distribution over the image of the GCPs. A major challenge was to find good enough GCPs because the area which was assumed to be stable since 2015 (swissALTI^{3D}) and 2020 was quite small on a lot of pictures which limited the amount of useful GCPs. The GCPs painted around the glacier could be used with the additional hight information measured in the field. Nevertheless, the process of finding enough GCPs was challenging and required a lot of comparison between the different images.

For the second helicopter flight on the 22nd of September, the goal to construct another DEM to observe short-term elevation changes during the slide was missed. The processing of a DEM precise enough to compare with the other DEMs available could not be achieved. The reasons are assumingly the low quantity of images and the small amount of overlapping areas. Another reason could be, that the section photographed contains mainly glacier, which leaves only a small area to put the GCPs. This issues could be solved with more experience with the requirements of Agisoft PhotoScan and appropriate planning of the survey flights.

7. Conclusion and Outlook

7.1 Conclusion

The focus of this study was on the mass movement of a small alpine glacier, the Ärlen Glacier. At the beginning of the work, it was assumed to be a singular mass movement with first signs of instability in 2018, which then finally occurred in late summer and autumn 2020. However, after studying aerial and satellite imagery and on-site observations (in one case by an amateur geologist), the data showed that the glacier had already undergone an initial slide event in 2014. This initial event was then followed by an interplay of advance and retreat of the glacier tongue over the next six years (figure 18). Timing, surface elevation changes, and velocity variations during mass movements were analyzed and compared with climate data and other similar events, particularly in the Swiss Alps, such as Allalin Glacier. This chapter summarizes the main results of these investigations, organized according to the underlying research questions.

- **What were the main triggers for this mass movement?**

The research on Ärlen Glacier clearly shows that each time the glacier reaches a critical terrain level, a slide occurs and the glacier terminus advances by about 100 meters (figure 51). After retreating nearly 400 m, the terminus of the glacier reached this critical terrain step in 2013. The first advance followed directly in 2014, so the most important factor for the instabilities is glacier retreat, which can be attributed to warmer temperatures due to climate change. However, several factors must interact to trigger a sliding event, as demonstrated by quiescent years such as 2016, when the glacier was above terrain step but did not advance. As seen with other glaciers such as Allalin, it takes a sequence of basal water pressures to trigger such events. After the lower part of the glacier lost its connection to the rest of the glacier in 2017/18 (chapter 5.2), this sequence of basal water pressures became less important and the main factors were the stabilization of the glacier terminus and the availability of subglacial water (chapter 6.2.5).

- **How big was the influence of meltwater for this process?**

The timing of the slide events was always in late summer and autumn (chapter 5.2), indicating that there is a correlation with temperature and thus meltwater. For the slide event during 2020, the correlation with meltwater could be accurately observed based on velocity measurements (chapters 5.4.1 and 5.4.2). The comparison between flow velocity and meltwater in 2020 clearly shows that the amount of melt controls the speed of the slide, especially when the meltwater vanishes, the glacier slows down very quickly and comes to a complete stop during prolonged cold periods. The comparison also showed that the onset of the 2020 event was not triggered by the influence of meltwater.

85

Nevertheless, meltwater is a necessary precondition and enhances basal sliding during the event. In this case, the influence is very direct, which could be an effect where listric fracture niches reach the ground where meltwater or rain can directly enter the subglacial water system of the glacier.

In the events before 2018, when the connection with the rest of the glacier was lost, meltwater probably had a greater triggering effect. Unfortunately, no measurements were made at the time and conjectures can only be made based on comparisons with similar events such as Allalin Glacier and some satellite imagery, as well as an in-situ description by an amateur geologist (chapter 5.2). Most scientific work on this type of glacial slide seems to agree on the assumption that a sequence of basal water pressure is necessary to trigger a so called ramp-type avalanche. This sequence involves an active phase in which the movement of the glacier is enhanced due to subglacial water pressure. The active phase must then be interrupted by an abrupt period of low meltwater, during which the glacier recouples to its bed. During the recoupling phase, intense fracturing of the tongue occurs as the fluidity of the ice decreases with falling temperatures (chapter 2.2.5). A high-resolution Swissimage RS aerial image from 2017 (figure 23) nicely shows such a highly fissured glacier. After feedback, a phase of faster flow must begin due to increased subglacial water availability, which can then lead to a catastrophic break-off event if the unstable part is above a terrain level.

Such sequences of basal water pressure can be found in the meteorological data for almost every year in late summer and fall (figure A65). Which, in combination with the visual appearance of the glacier, especially in 2017 (figure 23), seems to be a strong indication that Ärlen Glacier was affected by this sequence of basal water pressure. The sliding events in 2014 also indicate that it is not only meltwater that should be considered in relation to groundwater pressure. In 2014, summer temperatures and melt were relatively low (figure 43), but it was one of the rainiest summers, especially in the Bernese Alps region where Ärlen Glacier is located. We hypothesize that this had a large impact on the instability of the glacier and that water availability is a better variable to monitor subglacial water pressure because it includes rain events.

- **What is the influence of the polished sloping bedrock as a sliding interface?**

Of course, polished rock has a low coefficient of friction, which facilitates the sliding of the glacier at the base. But for glacial avalanches, the polished bedrock has an additional effect. The polished and regular surface allows for a distributed subglacial drainage network that facilitates the sliding of entire portions of the glacier tongue, or in our case, the entire tongue (chapter 6.2.4). In a channeled subglacial drainage network, only smaller parts of the glacier would be affected, making sliding of entire parts of the glacier unlikely.

- **What was the geometric displacement for this rapid sliding events?**

The comparison of the two DHMs (2020-2015) (figure 34) clearly shows how much ice mass has disappeared in the lower part of the unstable area, just below the listric fracture niche. The difference in elevation ranges from about -6 to -12 m with maximum values of up to -17 m (chapter 5.5). This reservoir area exhibits the most severe changes and is probably the area from which most of the ice volume for the slide events originates. The average height difference is -8.5 m, which results in a mass loss of about 218,374 m^3. Whereby the slide event of 2014 is not considered.

In the back, the listric fracture niche opened twice, once in 2018 and once in 2020, by about 40 meters (figures 25 and 54). The 2018 opening began in 2017, when sliding activity suddenly ceased due to cold autumn temperatures and the vanishing of meltwater (chapter 5.6.1). The shape of the listric fracture niche shows that the glacier found abutments on the sides of the glacier during the unbalanced period before the breakup. Due to the low resolution of the satellite imagery, it was not possible to determine if the listric fracture niche opened in 2014 or if the glacier simply sagged in this area. In addition, persistent poor weather in 2014 limited the availability of satellite imagery during the period of interest. However, the high-resolution swissALTI3D DHM shows a deep trench in the area where the listric fracture niche later opened (figure 29). This suggests that increased fracturing occurred in this area in 2014. However, whether the area merely sank in or whether the fracture reached the ground could not be determined during this study.

In 2014, the glacier tongue advanced about 130 m (chapter 5.1). With every advance the glaciers tongue experiences increased melting due to its lower position which leads to a high mass loss. Hence, the advance became smaller in 2018 with 100 m and in 2020 with only 55 m.

Event velocities were measured during the 2020 slide event from the first of August through the end of October using a time-lapse camera system (chapter 5.4). The maximum observed velocities for each point (pt1; pt2; pt3, corresponding to the upper, middle, and lower parts of the glacier) are 3.51; 3.56; and 5.29 m/d, respectively. The mean values are 0.69; 0.81 and 0.64 m/d during the whole observation period. And 1.3; 1.61; and 1.31 m/d during the period with increased velocity. Before the termination of the term, the mean velocities were 0.31; 0.31; 0.27 m/d. And after the termination of the movement at the end of September, 0.24; 0.21 and 0.10 m/d. The total distance traveled was 59.48 m, 69.72 m, and 55.44 m, respectively.

In 2018, two high-resolution images taken on September 26 and October 23 allowed comparative velocity measurements (chapter 5.4.3). Although the exact state of the glacier during the sliding period is unknown, the images show that the glacier was in a period of enhanced basal sliding between the two exposures. The average distance traveled during the study period is 43.6 m with an overall average velocity of about 1.56 m/d. The stable part of the glacier moved 2.6 m during the same period, corresponding to a velocity of 0.1 m/d.

With an estimated average ice thickness of 21 m (Grab *et al.*, 2021), the amount of unstable material moved in 2016 is 963,396 m^3. This means that the total unstable ice volume for 2014 is estimated to be about 1 million m3. For 2020, the ice thickness in the field was estimated to be only 5 to 10 m, resulting in an unstable ice volume of 337,978 m^3. This means that two-thirds of the unstable ice mass has already melted as it is exposed to warmer temperatures as it sinks further below the ELA.

- **How important is the control of terminus stabilization?**

As the glacier advances periodically and presumably loses its connection to the upper part, the role of terminus stabilization changes. Velocity calculations with time-lapse photogrammetry in 2020 show that there is an immediate response to the loss of stabilization when the lower part of the glacier abruptly breaks off (chapter 5.4.1). It only takes one day till the middle part of the glacier reacts and only two days till the upper part of the glacier shows a power law acceleration. We assume that this shows that the glacier is supported only by the terminus of the glacier, which rests in the syncline where the glacier advance normally ends. With an intact glacier where the ice is still connected, a sequence of basal water pressure with enhanced fracturing may be needed as a trigger as described for Allalin Glacier (chapter 2.3). During the sliding events of 2014 and 2017 at Ärlen Glacier we assume that those mechanisms had an important role as a trigger. Therefore, if the connection to the rest of the glacier is lost, the terminus stabilization becomes the most important triggering factor, while subglacial water availability controls the speed and duration of the event.

Since the glacier was still connected to the rest, the triggering mechanisms become more complex. Because we can only compare the timing and occurrence of the events and no other data are available for the period prior to 2018, the main conclusions come from comparing ramp-like glacier terminations and the events at Allalin Glacier, which showed very similar behavior. In the case of Allalin Glacier, studies have shown that an important factor is the stepped terrain with a critical terrain step (chapter 6.1.3). In this case, the terminus of the glacier rests above a steep slope (figure 29).

During the active phase with increased basal sliding velocities, the glacier is thought to form a subglacial vault at the front, the abutment of which is pushed over the terrain step. The extent of Ärlen Glacier in 2013 and later in 2016 shows very similar features (figures 19 and 22). Stabilization at the tongue could be due to cold ice margins frozen to the ground or simply to the very flat topography above the terrain step.

- **How does the speed and movement of this process compare to other glacier observations?**

Although Ärlen Glacier has many similarities to other glacial slides such as Allalin Glacier in 1965 and 2000, the velocity and movement observed in 2020 in particular show very unique characteristics. The main reason for this is that velocity observations on such small glaciers are rare due to their expected low activity. During the 2020 slide event, as expected, Ärlen Glacier showed an increase in velocity with increasing groundwater pressure on daily and hourly time scales. The maximum velocities measured during the slide (3.51; 3.56 and 5.29 m/d: upper, middle and lower parts of the glacier, respectively) (chapter 5.4.1) appear to be similar to the slide velocities of up to 4.5 m/d measured at Allalin Glacier during active phases. However, given the small size of Ärlen Glacier and the assumption that sliding velocity depends on basal shear stress and effective pressure, it is clear that an active phase on Ärlen Glacier would be much slower than on the larger Allalin Glacier, especially given the flatter slope. We hypothesize that the measured velocities prior to termination, with mean velocities of (0.31; 0.31; 0.27 m/d: top; middle and bottom of the glacier, respectively), indicate an active phase in the Ärlen Glacier size scale. What at Allalin Glacier comes down as an ice avalanche tumbling down to the valley, at the much shallower Ärlen Glacier results in a mini-surge-like advance of the tongue. Faster velocities cannot be achieved because of the flat topography, but the slippery bedrock combined with high basal water pressure and a very thin glacier can sustain the slide until the tongue stabilizes the ice mass when it reaches the syncline at the base of the terrain step (chapter 6.2.3). With steeper topography, the unstable ice mass would most likely develop into an ice avalanche and tumble down the valley.

- **What is the importance of this event for glacier related natural hazards in the Alps?**

The Ärlen Glacier demonstrates the importance of studying alterations in the flow dynamics of glaciers, especially given the rapid changes that glaciers have undergone in recent decades. Given the small size and shallow slope of the glacier, such mass movement was completely unexpected and demonstrates the potential danger of even such small, unsuspected glaciers. The Ärlen Glacier shows that glacier sliding instabilities increase due to glacier retreat, and especially that small, shallow alpine glaciers with hard bedrock should not be neglected when assessing potential glacier-related natural hazards, especially when their terminus melts over a terrain step.

The number of small alpine glaciers in the Swiss Alps is huge and most of them are located in remote areas where sliding does not affect infrastructure or population. However, some of them could be dangerous, and early detection and close monitoring could prevent catastrophic consequences.

The main objective of this work was to quantify the temporal and spatial patterns of mass movements at Ärlen Glacier. Since the glacial history studies showed that the glacier has a completely different history than expected, the focus shifted from one event to several events over several years. Nevertheless, the pattern found showed a correlation with other slide events such as Allalin Glacier or more general ramp-type ice avalanches. This was achieved by analyzing the temporal behavior of the glacier over the years and also during single events. The photogrammetric analysis of the 2020 events was very challenging, and the potential errors in the results are quite substantial. A large number of subjective point tracings were required because of inconsistent data due to changes in weather and light conditions. Still, interesting patterns could be analyzed and compared with other studies. While the photogrammetric calculation is error-prone and subjective, the results compared to other scientific work showed that the errors were less than expected and temporal and spatial patterns were clearly evident.

7.2 Outlook

Measurement data of glacier terminations in such good temporal resolution as collected at Ärlen Glacier in 2020 are rare and offer opportunities for further research. This especially in combination with the findings that the event started much earlier than expected. Ärlen Glacier also raises some questions about subglacial water flow, a topic that is not yet fully understood. Velocity data from this study could contribute to a better understanding of subglacial water flow, especially in the specific case where water can enter directly through the ground into the ground reaching fracturing trench on the back side of the unstable part of the glacier. The potential of high-resolution satellite imagery is also evident in the additional analyses that were possible for 2018. The ability to detect and even monitor dangerous glaciers with satellite imagery is a cost-effective approach, but the question of efficiency could be part of further studies.

The results from photogrammetric methods used in this thesis show that this technology provides a very efficient way to precisely research mass movements. This is especially useful in mountain environments, where accessibility is difficult. The possibility to create DHMs with only a few images, gives the possibility to investigate changes in volume on various glaciers without a big time and money input. While, the possibility to track pixels over time-lapse imagery is an efficient way to use available monitoring images to research glacier flow dynamics. Photogrammetric methods show a growing popularity in mountain natural hazard research and with further developments and specifications their usage will improve for applications in this field.

Ärlen Glacier also highlights opportunities for more research. Because of its simple geometric properties, the glacier offers great potential for numeric modelling. Combined with the velocity measurements in 2020 and the timing of events since 2014, a modelling approach could reproduce the events and analyse the significance of the various triggers. This could lead to a better understanding of the instabilities in glacier sliding due to climate change. Another interesting research question might be how dangerous glaciers could be identified from aerial photographs or even topographic and geologic ground features and how many of these potentially dangerous glaciers are located in areas where severe damage could occur.

8. References

Agisoft (2018) 'Agisoft PhotoScan User Manual: Professional Edition', *Agisoft LLC*, p. 127. Available at: http://www.agisoft.com/pdf/photoscan-pro_1_4_en.pdf [Accessed December 21, 2020].

Ahn, Y. and Box, J. E. (2010) 'Instruments and Methods Glacier velocities from time-lapse photos: Technique development and first results from the Extreme Ice Survey (EIS) in Greenland', *Journal of Glaciology*, 56(198), pp. 723–734. doi: 10.3189/002214310793146313.

Alean, J. (1984) 'Untersuchungen über Entstehungsbedingungen und Reichweiten von Eislawinen', *Mitteilungen der Versuchsanstalt für Wasserbau, Hydrologie und Glaziologie*, (74).

Allaby, M. (2008) *Glen's power flow law*, Edited by M. Allaby, Oxford University Press. Available at: https://www.oxfordreference.com/view/10.1093/oi/authority.20110803095854948 [Accessed May 17, 2021].

Benn, D. I. *et al.* (2019) 'A general theory of glacier surges', *Journal of Glaciology*, pp. 1–16. doi: doi.org/10.1017/jog.2019.62.

BKW (2018) *Grimselwelt: Ein wahrer Kraftort*. Available at: https://blog.bkw.ch/grimselwelt-ein-wahrer-kraftort/ [Accessed August 02, 2021].

Braithwaite, R. J. (2011) 'Degree-days', in *Encyclopedia of snow, ice and glaciers*, V.P. Singh, P. Singh, and U.K. Haritashya, Editors. 2011, Springer: Dordrecht, The Netherlands, pp. 196–199.

Braithwaite, R. J. and Zhang, Y. (2000) 'Sensitivity of mass balance of five Swiss glaciers to temperature changes assessed by tuning a degree-day model', *Journal of Glaciology*, 46(152), pp. 7–14. doi: 10.3189/172756500781833511.

Le Bris, R. and Paul, F. (2013) 'An automatic method to create flow lines for determination of glacier length: A pilot study with Alaskan glaciers', *Computers and Geosciences*, 52, pp. 234–245. doi: 10.1016/j.cageo.2012.10.014.

Clarke, G. K. C. (1987) 'Fast glacier flow: ice streams, surging, and tidewater glaciers', *Journal of Geophysical Research*, 92(B9), pp. 8835–8841. doi: 10.1029/JB092iB09p08835.

Clarke, K. C. *et al.* (1986) 'Characteristics of Surge-Type Glaciers', *Journal of Geophysical Research*, 91(B7), pp. 7165–7180.

Colgan, W. *et al.* (2016) 'Glacier crevasses: Observations, models, and mass balance implications', *Reviews of Geophysics*, pp. 207–250. doi: 10.1002/2017RG000559.

Davies, B. (2020) *Surging glaciers*. Available at: http://www.antarcticglaciers.org/glacier-processes/glacier-flow-2/surging-glaciers/ [Accessed December 02, 2020].

Davies, B. (2021) *Stress and strain*, *Stress and strain*. Available at: http://www.antarcticglaciers.org/glacier-processes/glacier-flow-2/glacier-flow-ii-stress-and-strain/ AntarcticGlaciers.org [Accessed January 11, 2021].

Ding, Y. J. (1991) 'Precipitation Conditions for the Development of the Present Glaciers on the Norhtern Slope of Karakorum', *GeoJournal*, 25(2/3), pp. 243–248.

ESA (2021) *EO Browser*. Available at: https://apps.sentinel-hub.com/eo-browser/?zoom=10&lat=41.9&lng=12.5&themeId=DEFAULT-THEME&toTime=2021-09-09T21%3A28%3A23.974Z [Accessed August 15, 2021].

Esri (2021) *World Imagery*. Available at: https://www.arcgis.com/home/item.html?id=10df2279f9684e4a9f6a7f08febac2a9 [Accessed August 16, 2021].

European Space Agency (2015) *SENTINEL-2 Data access and management*, *Sentinel Online Handbook*. Available at: https://sentinel.esa.int/documents/247904/1848117/Sentinel-2_Data_Products_and_Access [Accessed August 14, 2021].

Evans, S. G. *et al.* (2009) 'Catastrophic detachment and high-velocity long-runout flow of Kolka Glacier, Caucasus Mountains, Russia in 2002', *Geomorphology*, 105(3–4), pp. 314–321. doi: 10.1016/j.geomorph.2008.10.008.

Evans, S. G. and Clague, J. J. (1994) 'Recent climatic change and catastrophic geomorphic processes in mountain environments', *Geomorphology*, 10(1–4), pp. 107–128. doi: 10.1016/0169-555X(94)90011-6.

Faillettaz, J. *et al.* (2008) 'Evidence of log-periodic oscillations and increasing icequake activity during the breaking-off of large ice masses', *Journal of Glaciology*, 54(187), pp. 725–737.

Faillettaz, J., Funk, M. and Sornette, D. (2012) 'Instabilities on Alpine temperate glaciers: New insights arising from the numerical modelling of Allalingletscher (Valais, Switzerland)', *Natural Hazards and Earth System Science*, 12(9), pp. 2977–2991. doi: 10.5194/nhess-12-2977-2012.

Faillettaz, J., Funk, M. and Vincent, C. (2015) 'Avalanching glacier instabilities: Review on processes and early warning perspectives', *Reviews of Geophysics*, 53(2), pp. 203–224. doi: 10.1002/2014RG000466.

Falaschi, D. *et al.* (2019) 'Brief communication: Collapse of 4Mm3 of ice from a cirque glacier in the Central Andes of Argentina', *Cryosphere*, 13(3), pp. 997–1004. doi: 10.5194/tc-13-997-2019.

Fischer, A. (2011) 'Comparison of direct and geodetic mass balances on a multi-annual time scale', *Cryosphere*, 5(1), pp. 107–124. doi: 10.5194/tc-5-107-2011.

Fischer, M., Huss, M. and Hoelzle, M. (2015) 'Surface elevation and mass changes of all Swiss glaciers 1980-2010', *Cryosphere*, 9(2), pp. 525–540. doi: 10.5194/tc-9-525-2015.

Freers, T. F. (1997) 'Crevasse', in *Geomorphology. Encyclopedia of Earth Science.* Berlin, Heidelberg: Springer Berlin Heidelberg, pp. 222–223. doi: 10.1007/3-540-31060-6_74.

Gill, J. C. and Malamud, B. D. (2014) 'Reviewing and visualizing the interactions of natural hazards', *Reviews of Geophysics*, 52, pp. 680–722. doi: 10.1029/88EO01108.

Glaister, R. M. (1951) 'The Ice Slide on the Glacier du Tour', *Journal of Glaciology*, 1(9), pp. 508–509.

Glen, J. W. (1958) 'Glen_1958_The flow law of ice.pdf'. Physics Department, Birmingham University, England, pp. 171–183.

Grab, M. (2020) *Swiss Glacier Thickness – Release 2020*. doi: https://doi.org/10.3929/ethz-b-000434697 [Accessed August 17, 2021].

Grab, M. *et al.* (2021) 'Ice thickness distribution of all Swiss glaciers based on extended ground-penetrating radar data and glaciological modeling', *Journal of Glaciology*, pp. 1–19. doi: 10.1017/jog.2021.55.

Haeberli, W. *et al.* (1989) 'Assessing Risks from Glacier Hazards in High Mountain Regions: Some Experiences in the Swiss Alps', *Annals of Glaciology*, 13(September 2014), pp. 96–102. doi: 10.1017/s0260305500007709.

Haeberli, W. *et al.* (2004) 'The Kolka-Karmadon rock/ice slide of 20 September 2002: An extraordinary event of historical dimensions in North Ossetia, Russian Caucasus', *Journal of Glaciology*, 50(171), pp. 533–546. doi: 10.3189/172756504781829710.

Hagg, W. (2020) 'Eisbewegung', in *Gletscherkunde und Glazial- geomorphologie*. Springer Berlin Heidelberg, pp. 29–46.

Harrison, W. D. *et al.* (1992) 'The determination of glacier speed by time-lapse photography under unfavorable conditions', *Journal of Glaciology*, 38(129), pp. 257–265. doi: 10.1017/S002214300000366X.

Harrison, W. D. and Post, A. S. (2003) 'How much do we really know about glacier surging?', *Annals of Glaciology*, 36, pp. 1–6. doi: 10.3189/172756403781816185.

Helanow, C. *et al.* (2021) 'A slip law for hard-bedded glaciers derived from observed bed topography', *Science Advances*, 7(20), p. eabe7798. doi: 10.1126/sciadv.abe7798.

Herreid, S. and Truffer, M. (2015) 'Earth Surface Automated detection of unstable glacier flow and a spectrum of speedup behavior in the Alaska Range Special Section ':, *Journal of Geophysical Research : Earth Surface*, 121, pp. 64–81. doi: 10.1002/2015JF003502.

Hock, R. (2003) 'Temperature index melt modelling in mountain areas', *Journal of Hydrology*, 282(1–4), pp. 104–115. doi: 10.1016/S0022-1694(03)00257-9.

Honegger, R. (2020) *Surface Elevation Change at Marine-Terminating Outlet Glacier Eqip Sermia, Western Greenland in Relation to Front Position, Flow Velocity and Climate*. University of Zürich.

How, P. *et al.* (2020) 'PyTrx: A Python-Based Monoscopic Terrestrial Photogrammetry Toolset for Glaciology', *Frontiers in Earth Science*, 8(February), pp. 1–17. doi: 10.3389/feart.2020.00021.

Huggel, C. *et al.* (2004) 'An assessment procedure for glacial hazards in the Swiss Alps', *Canadian Geotechnical Journal*, 41(6), pp. 1068–1083. doi: 10.1139/T04-053.

Huss, M. (2013) 'Density assumptions for converting geodetic glacier volume change to mass change', *The Cryosphere*, 7(3), pp. 877–887. doi: 10.5194/tc-7-877-2013.

Huybrechts, P., Letreguilly, A. and Reeh, N. (1991) 'The Greenland ice sheet and greenhouse warming', *Paleogeography, Paleoclimatology, Paleoecology (Global and Planetary Change Section)*, 89, pp. 399–412.

Iken, A. (1977) 'Movement of a large ice mass before breaking', *Journal of Glaciology*, 19(8).

Jacquemart, M. *et al.* (2020) 'What drives large-scale glacier detachments? Insights from Flat Creek glacier, St. Elias Mountains, Alaska', *Geology*, 48(7), pp. 703–707. doi: 10.1130/G47211.1.

James, M. R., How, P. and Wynn, P. M. (2016) 'Pointcatcher software: Analysis of glacial time-lapse photography and integration with multitemporal digital elevation models', *Journal of Glaciology*, 62(231), pp. 159–169. doi: 10.1017/jog.2016.27.

Jiskoot, H. (2011) 'Dynamics of glaciers', *Encyclopedia of Snow, Ice and Glaciers*. doi: 10.1007/978-90-481-2642-2_127.

Jóhannesson, T., Raymond, C. and Waddington, E. (1989) 'Time–Scale for Adjustment of Glaciers to Changes in Mass Balance', *Journal of Glaciology*, 35(121), pp. 355–369. doi: 10.3189/s002214300000928x.

Kääb, A. *et al.* (2018) 'Massive collapse of two glaciers in western Tibet in 2016 after surge-like instability', *Nature Geoscience*, 11(2), pp. 114–120. doi: 10.1038/s41561-017-0039-7.

Kääb, A. *et al.* (2021) 'Sudden large-volume detachments of low-angle mountain glaciers – more frequent than thought?', *The Cryosphere*, 15(4), pp. 1751–1785. doi: 10.5194/tc-15-1751-2021.

Klose, B. and Klose, H. (2020) *Meterologie*, *Michel de Certeau*. Springer Spektrum. doi: 10.2307/j.ctvvb7mbf.9.

Konz, M. (2011) 'Serac', in *Encyclopedia of Snow, Ice and Glaciers*. Springer, pp. 1027–1028.

Lüthi, M., Walter, F. and Werder, M. (2020) *Basal motion*, *Physics of Glaciers*. Geographisches Institut, 3G, Universiät Zürich; Versuchsanstalt für Wasserbau, Hydrologie und Glaziologie VAW, ETH Zürich.

Margreth, S. and Funk, M. (1999) 'Hazard mapping for ice and combined snow/ice avalanches - two case studies from the Swiss and Italian Alps', *Cold Regions Science and Technology*, 30(1–3), pp. 159–173. doi: 10.1016/S0165-232X(99)00027-0.

Messerli, A. and Grinsted, A. (2015) 'Image georectification and feature tracking toolbox: ImGRAFT', *Geoscientific Instrumentation, Methods and Data Systems*, 4(1), pp. 23–34. doi: 10.5194/gi-4-23-2015.

MeteoSchweiz (2015) 'Klimareport 2014', in *Bundesamt für Meteorologie und Klimatologie MeteoSchweiz*. Zürich, p. 80. Available at: https://www.meteoswiss.admin.ch/content/dam/meteoswiss/de/service-und-publikationen/Publikationen/doc/klimareport_2014_DE_web.pdf [Accessed July, 15 2021].

Nishimura, D. *et al.* (2013) 'Changes in Ice-Flow Velocity and Surface Elevation from 1874 to 2006 in Rhonegletscher , Switzerland', *Arctic, Antarctic, and Alpine Research*, 45(4), pp. 552–562. doi: 10.1657/1938-4246-45.4.552.

Paul, F. (2015) 'Revealing glacier flow and surge dynamics from animated satellite image sequences : examples from the Karakoram', *The Cryosphere*, 9, pp. 2201–2214. doi: 10.5194/tc-9-2201-2015.

Paul, F. (2019) 'Repeat Glacier Collapses and Surges in the Amney Machen Mountain Range, Tibet, Possibly Triggered by a Developing Rock-Slope Instability', *Remote Sensing*, 11(6), p. 708. doi: 10.3390/rs11060708.

Pralong, V. A. and Funk, V. M. (2004) 'Können Eisabbrüche vorhergesagt werden?', in *14th International Conference on Engineering Surveying*, pp. 1–12. Available at: http://www.iv2004.ethz.ch/programm/Session/S_14_IV2004.pdf.

Regamey, B. (2017) 'SWISSIMAGE RS : Die Schweiz in all ihren Farbbereichen', *Geomatik Schweiz*, 9, pp. 313–315.

Röthlisberger, H. (1972) 'Water Pressure in Intra- and Subglacial Channels', *Journal of Glaciology*, 11(62), pp. 177–203. doi: 10.3189/s0022143000022188.

Röthlisberger, H. (1981) 'Eislawinen und Ausbrüche von Gletscherseen', *Jahrbuch der Schweizerischen Naturforschenden Gesellschaft, wissenschaftlicher Teil*, 1978.

Röthlisberger, H. (1997) *'Normale' und aussergewöhnliche Gletscherveränderungen*, *Gletscherschwankungen im Alpenraum*. Zürich.

Sapiano, J. J., Arrison, W. D. H. and Chelmeyer, K. A. E. (1998) 'Elevation, volume and terminus changes of nine glaciers in North Alllerica', *Journal of Glaciology*, (146).

Sevestre, H. *et al.* (2018) 'Tidewater Glacier Surges Initiated at the Terminus Journal of Geophysical Research : Earth Surface', *Journal of Geophysical Research : Earth Surface*, 123, pp. 1035–1051. doi: 10.1029/2017JF004358.

Sevestre, H. and Benn, D. I. (2015) 'Climatic and geometric controls on the global distribution of surge-type glaciers : implications for a unifying model of surging', *Journal of Glaciology*, 61(228), pp. 646–662. doi: 10.3189/2015JoG14J136.

Stocker-Waldhuber, M. *et al.* (2018) 'Ice flow velocity as a sensitive indicator of glacier state', *The Cryosphere Discussions*, (March), pp. 1–18.

Stoffel, M. and Huggel, C. (2012) 'Effects of climate change on mass movements in mountain environments', *Progress in Physical Geography*, 36(3), pp. 421–439. doi: 10.1177/0309133312441010.

Sugiyama, S. and Gudmundsson, G. H. (2004) 'Short-term variations in glacier flow controlled by subglacial water pressure at Lauteraargletscher, Bernese Alps, Switzerland', *Journal of Glaciology*, 50(170), pp. 353–362. doi: 10.3189/172756504781829846.

Swisstopo (2005) *Produktinformation DHM25*. Available at:
http://www.swisstopo.admin.ch/internet/swisstopo/de/home/products/height/dhm25.html
[Accessed July 19, 2021].

Swisstopo (2018) 'swissALTI3D. Das hoch aufgelöste Terrainmodell der Schweiz', p. 17. Available at:
file:///C:/Users/RietK/Downloads/swissALTI3D_detaillierte Produktinfo_201802_DE.pdf [Accessed
July 22, 2021].

Swisstopo (2019) 'swissALTI3D Ausgabebericht 2019', pp. 1–7.

Swisstopo (2020) *Swissimage - Das digitale Farbphotomosaik der Schweiz*. Available at:
https://www.swisstopo.admin.ch/de/geodata/images/ortho/swissimage10.html#58_156948213685
6 [Accessed July 22, 2021].

Truffer, M. *et al.* (2021) 'Glacier Surges', in Haeberli, W. and Whiteman, C. (eds) *Snow and Ice-Related
Hazards, Risks, and Disasters*. 2nd Editio. Amsterdam: Elsevier Inc., pp. 417–466. doi:
https://doi.org/10.1016/B978-0-12-817129-5.00003-2.

Tsai, V. C. and Ruan, X. (2018) 'A simple physics-based improvement to the positive degree day
model', *Journal of Glaciology*, 64(246), pp. 661–668. doi: 10.1017/jog.2018.55.

U.S. Geological Survey (2016) 'Landsat 8 Data Users Handbook', *Nasa*, 8(June), p. 97. Available at:
https://landsat.usgs.gov/documents/Landsat8DataUsersHandbook.pdf [Accessed Fevruary 07, 2021].

Vuille, M. (2011) 'Climate Variability and High Altitude Temperature and Precipitation',
in *Encyclopedia of snow, ice and glaciers*, V.P. Singh, P. Singh, and U.K. Haritashya, Editors. 2011,
Springer: Dordrecht, The Netherlands, pp. 153–156.

Weissenfluh, W. (2015) *Ärlengletscher*. Available at:
https://www.grimselkristall.ch/strahlergeschichten/11-ärlengletscher-2015/ [Accesses August 05,
2021].

Zemp, M. *et al.* (2013) 'Reanalysing glacier mass balance measurement series', *Cryosphere*, 7(4), pp.
1227–1245. doi: 10.5194/tc-7-1227-2013.

9. Appendix

I. Ground Control Points

Table A5: Coordinates of Ground control points. Measured in the field with precision GPS (04. Sep 2020).

Nummer	Objekt	xKoordinate	yKoordinate	zKoordinate	Bemerkung
1	Fixpunkt	2 663 258,5	1 163 897,0	2 583,1	
2	Fixpunkt	2 663 272,8	1 163 899,5	2 575,8	
3	Fixpunkt	2 663 274,4	1 163 908,1	2 573,4	
4	Fixpunkt	2 663 297,4	1 163 902,8	2 568,6	
5	Fixpunkt	2 663 307,0	1 163 908,7	2 565,3	
6	Fixpunkt	2 663 329,2	1 163 907,7	2 556,8	
7	Fixpunkt	2 663 339,7	1 163 906,0	2 550,4	
8	Fixpunkt	2 663 368,4	1 163 895,7	2 538,2	
10	Fixpunkt	2 663 500,5	1 163 939,2	2 492,5	
11	Fixpunkt	2 663 488,2	1 163 981,0	2 505,2	
12	Fixpunkt	2 663 403,1	1 164 020,5	2 550,1	
13	Fixpunkt	2 663 311,3	1 164 062,4	2 578,2	
14	Fixpunkt	2 663 249,4	1 164 077,9	2 596,0	
100	Kamera	2 663 316,5	1 163 880,4	2 570,8	Objektiv 173 cm ab Terrain

Figure A59: Location of GCP (blue squares) and time-lapse camera (red triangle). Background is the SWISSIMAGE from 2018.

II. Calibration of Time Lapse Imagery, from Pixel in Meters

Table A6: Points used for calibration of the time lapse photogrammetry.

GCP Nr	X	Y	Δ x	Δ y	Distance [P	Distance [m]	one pixel [m]
1	551,38	534,99					
3	756,56	565,31	205,18	30,32	207,41	19,39	0,09
4	1166,42	743,92	409,86	178,61	447,09	23,69	0,05
5	1587,84	900,33	421,42	156,41	449,51	11,29	0,03
6	2436,59	1136,70	848,75	236,37	881,05	22,22	0,03
7	2746,68	1252,10	310,09	115,40	330,87	10,63	0,03
8	3372,40	1336,79	625,72	84,69	631,43	30,49	0,05

Point Nr	X (pt 1-3)	Y (pt 1-3)	X (Rpt 1-3)	y (Rpt 1-3)	Δ x	Δ y	Distance [Pixel]	Distance [m]	one pixel [m]
Pt1	1399,81	525,45	1908,69	591,21	-508,88	-65,76	513,11	47,05	0,09
Pt2	1952,25	679,03	2779,74	897,14	-827,49	-218,11	855,75	75,94	0,09
Pt3	2800,86	1015,54	3195,49	2,00	-394,63	1013,54	1087,66	70,14	0,06

Table A7: Distance from front of the picture (Δy) . Assumed a linear decline of m/pixel with distance from nearest image edge.

Table A8: Min max and mean of distance to nearest image edge (Δy) for the different pixel/meter

	y max		
Distance from closest edge [y max]	1534,00		
GCP Nr	Δy [pixel]	one pixel [m]	
1	-999,01	0,09	
3	-968,69	0,09	
4	-790,08	0,05	
5	-633,67	0,03	
6	-397,30	0,03	
7	-281,90	0,03	
8	-197,21	0,05	
Point Nr	Δy (pt 1-3)	Δy (Rpt 1-3)	one pixel [m]
Pt1	-1008,55	-942,79	0,09
Pt2	-854,97	-636,86	0,09
Pt3	-518,46	-1532,00	0,06

one pixel [m]	min	max	mean
0,03	-281,90	-633,67	-437,62
0,05	-197,21	-790,08	-493,65
0,06	-518,46	-1532,00	-1025,23
0,09	-636,86	-1008,55	-901,81
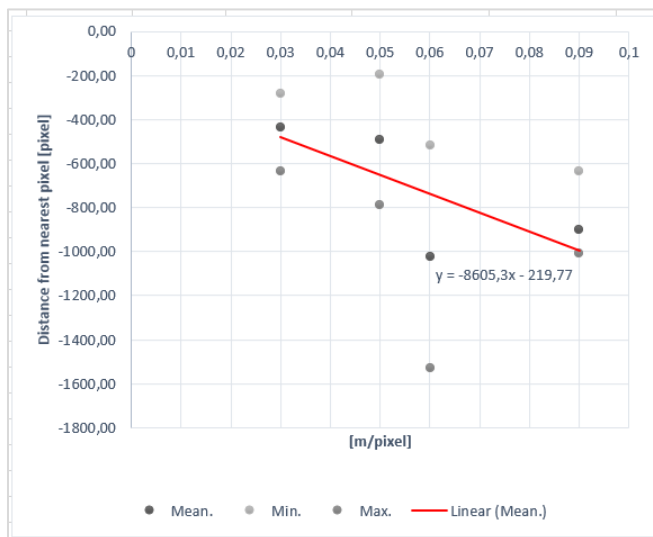
Figure A60: Distance reference points for calibration of the time lapse distance measurements. Including the linear calibration line, y = - 8605,3x - 219,77.
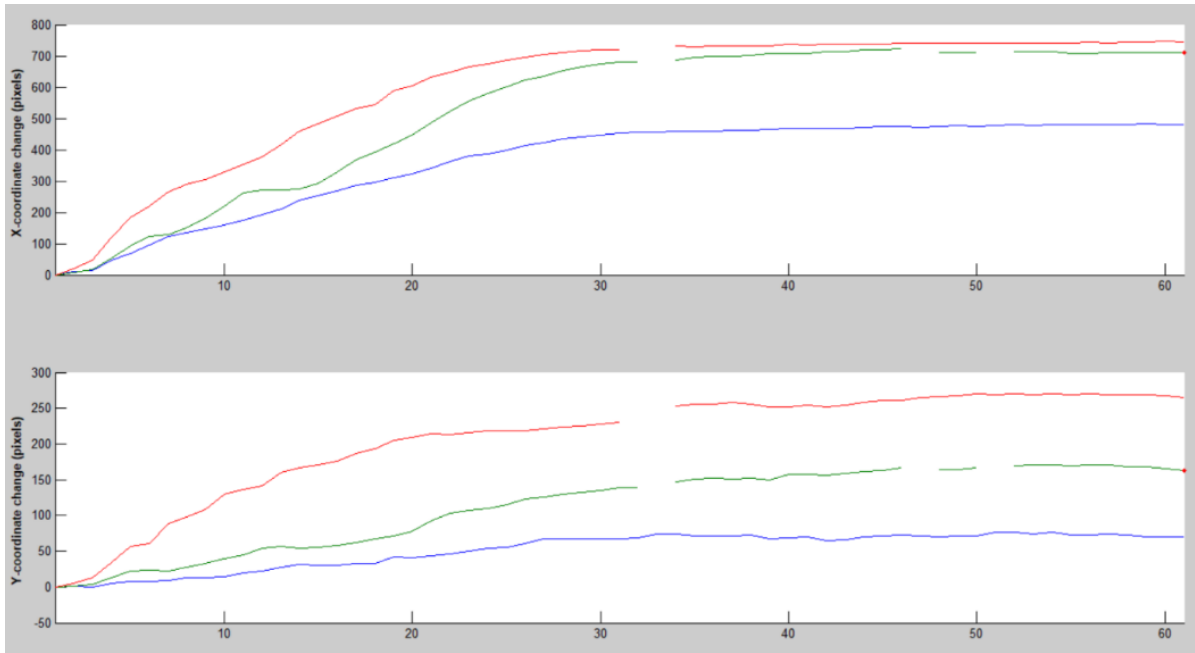
Figure A61: Changes in x- and y-coordinates from 3 tracked points (upper (Pt1-blue), middle (Pt2-green) and lower (Pt3-red) part of moving glacier) during the event period, tracked with pointcatcher. The output from pointcatcher gives the x and y coordinate for each tracked point on every picture.

III. Length Changes of Ärlen Glacier

Table A7: Length changes of Ärlen Glacier with start point 1980. The measurement was taken along the Center Line (chapter 4.1). The line "Date" contains the date on which the image, considered for the measurement, was taken.

Year	Date	Length [m]	Cumm. Length change/N	Cumm. Length change [m]
1980		899	0.00	0
			-0.67	
			-1.34	
			-2.01	
			-2.68	
			-3.35	
1986		895	-4.00	-4
			-16.86	
			-29.72	
			-42.58	
			-55.44	
			-68.30	
			-81.16	
1993		805	-94.00	-94
			-103.72	
			-113.44	
			-123.16	
			-132.88	
			-142.60	
			-152.32	
2000		737	-162.00	-162
			-163.75	
			-165.50	
			-167.25	
2004		730	-169.00	-169
			-181.00	
			-193.00	
			-205.00	
			-217.00	
			-229.00	
2010		658	-241.00	-241
			-290.00	
			-339.00	
2013	23. Sep	511	-388.00	-388
2014	28. Sep	645	-254.00	-254.00
2015	07. Aug	584	-315.00	-315.00
	30. Aug	547	-352.00	-352.00
2016	07. Sep	527	-372.00	-372
2017	15. Aug	534	-365.00	-365.00
	29. Aug	628	-271.00	-271.00
2018	26. Sep	625	-274.00	-274.00
	23. Okt	645	-254.00	-254.00
2019	19. Sep	534	-365.00	-365.00
	27. Sep	607	-292.00	-292.00
2020	19. Aug	604	-295.00	-295.00
	13. Sep	630	-269.00	-269.00

IV. High Resolution Images from Swisstopo and GeoEye
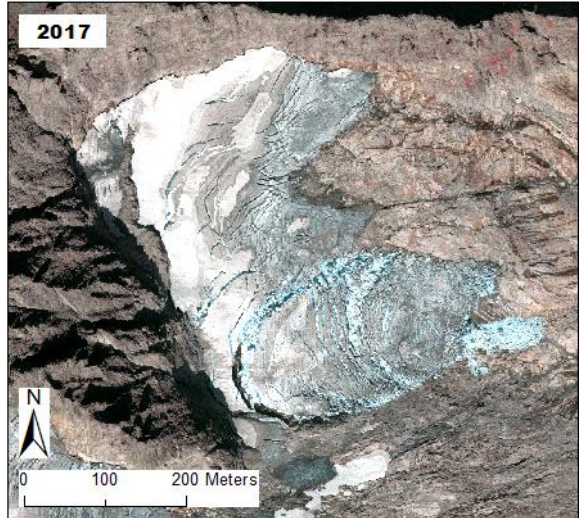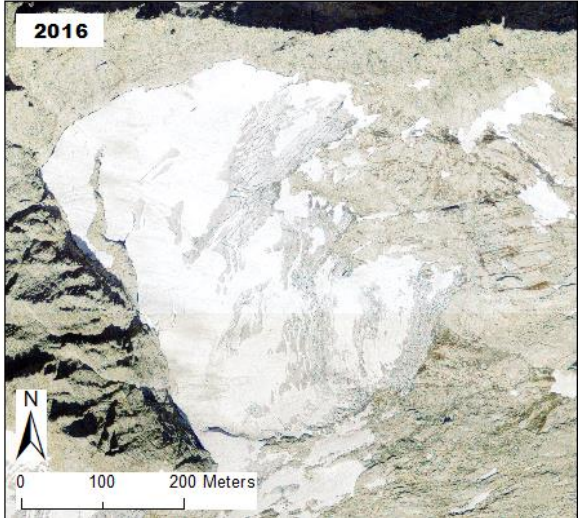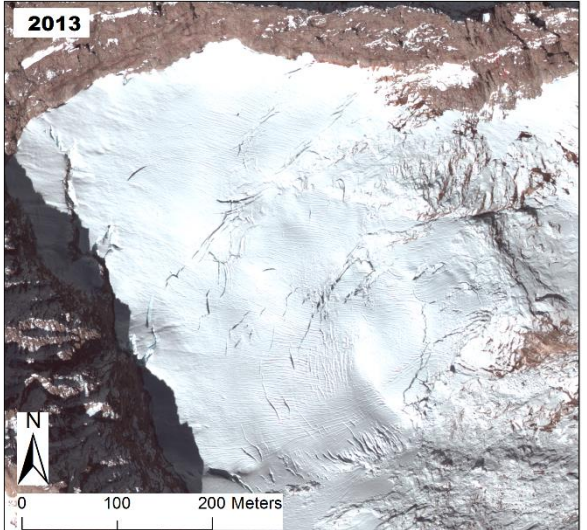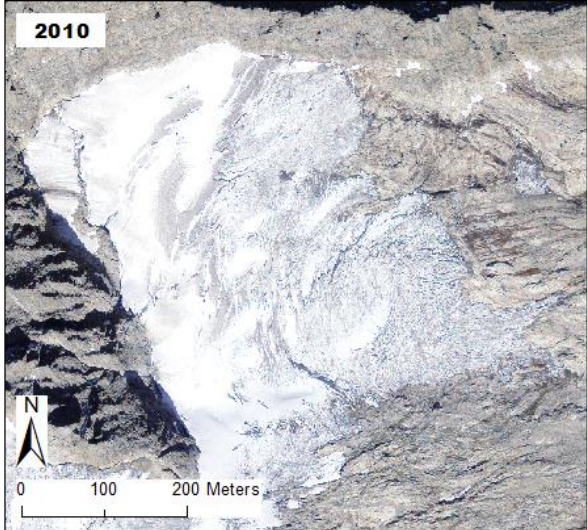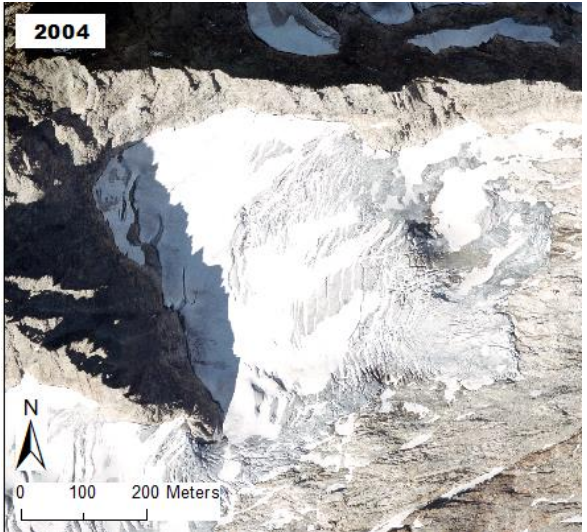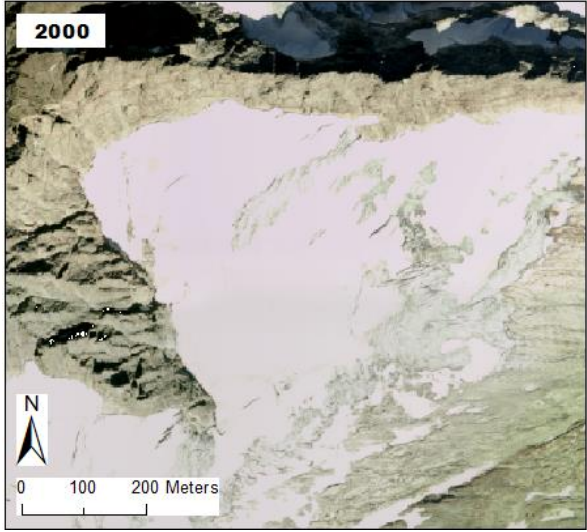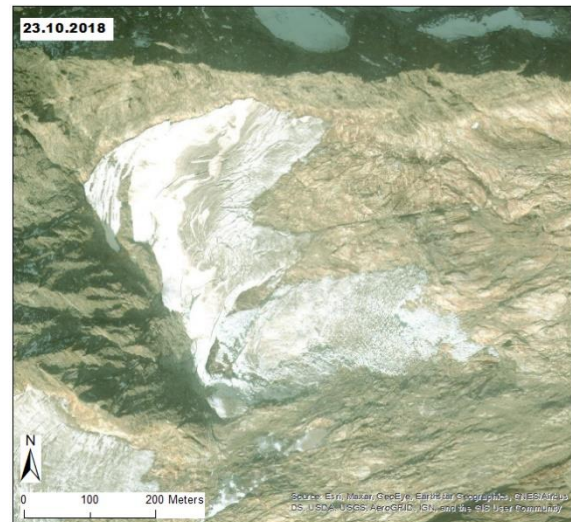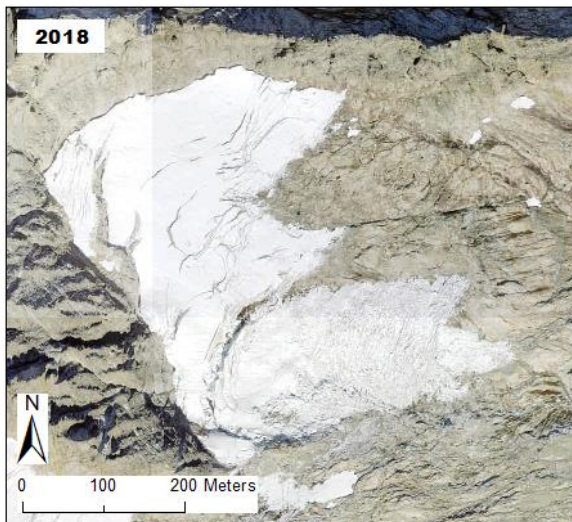
Figure A62: "Zeitreise" Product of Swisstopo including Orthophotos from the Ärlen Glacier (2''' – 20018). 2013 is Swissimage RS und 2017 is from a "Luftbildstreifen". The image from 2018 has a very high resolution and could be accessed over GeoEye base layer from Esri (Esri, DigitalGlobe, GeoEye, i-cubed, USDA, USGS, AEX, Getmapping, Aerogrid, IGN, IGP, swisstopo, and the GIS User Community).

V. High Temporal Resolution Landsat-8 (2014/15) and Planet Labs
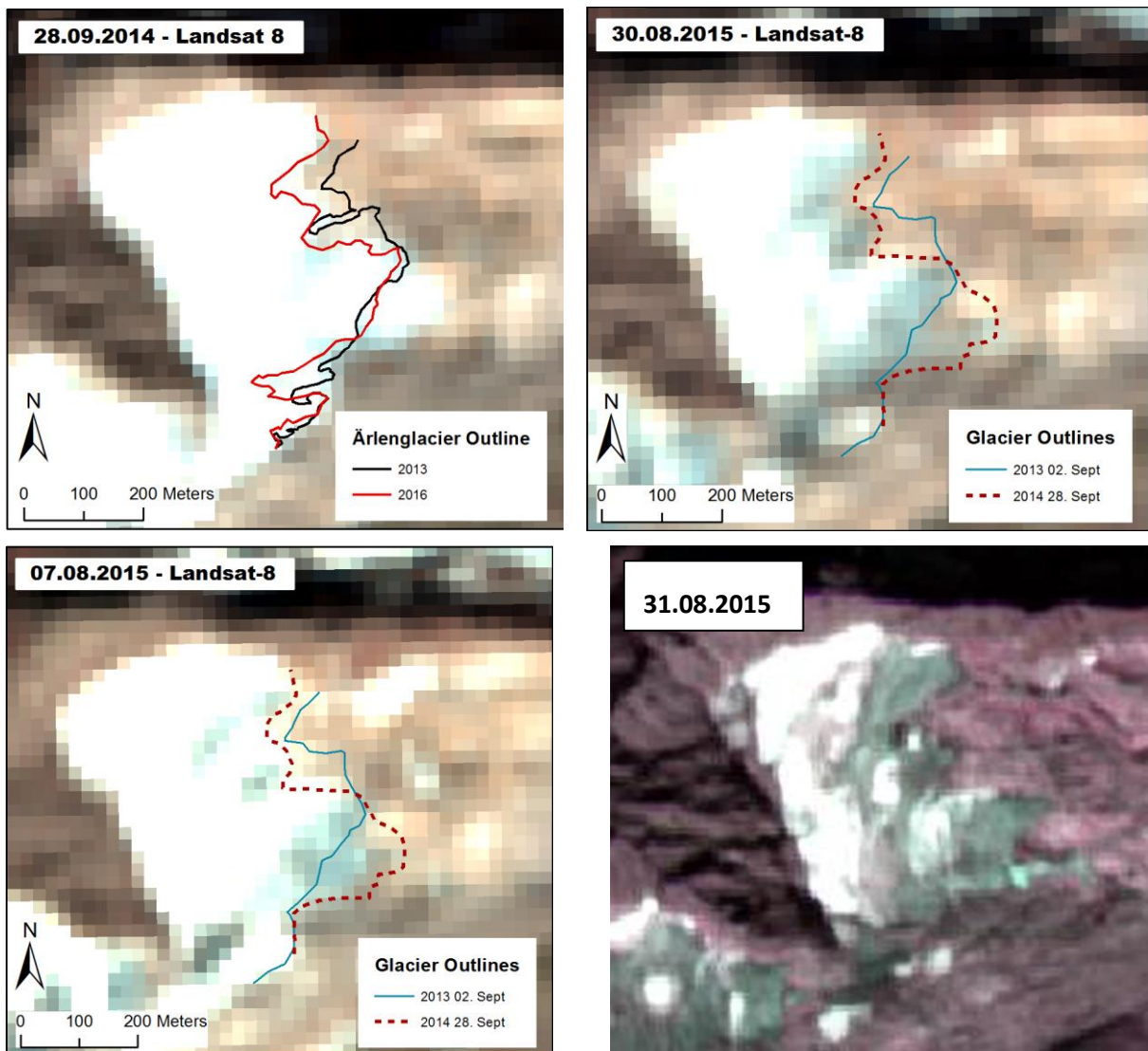
Figure A63: Additional Satellite data. For 2014 from the Landsat-8 Mission in verry low resolution. For an better overview the Outlines from 2013 and 2016 are includes in the image and an advance from both stages is visible also with this very low resolution. And Planet Labs image during 31 August 2015, where the rest of the advances of 2014 are clearly visible.

VI. High Temporal Resolution Sentinel-2 Images (2017/20)

15.08.2017

23.08.2017

09.09.2018

27.09.2018

29.09.2018

12.10.2018
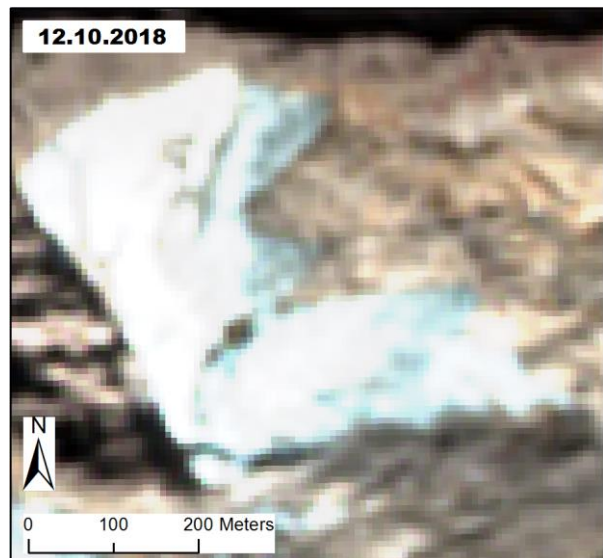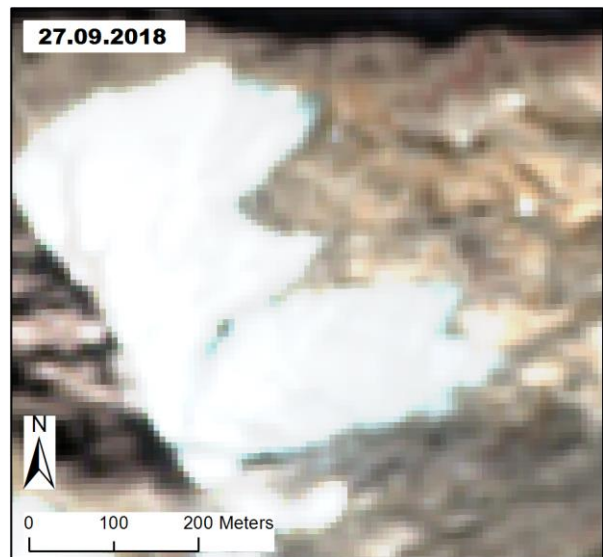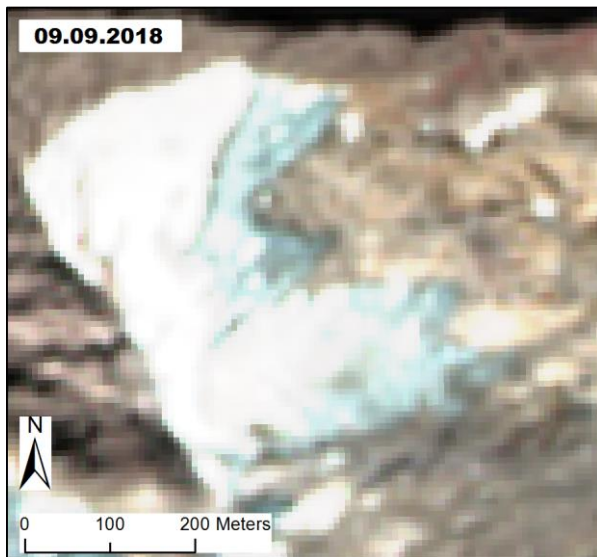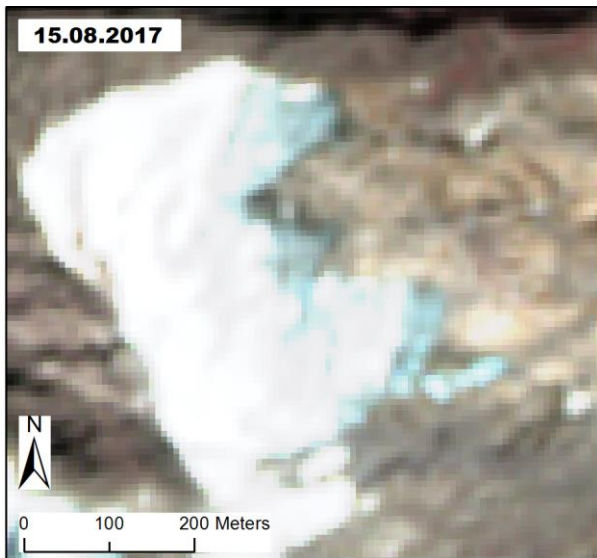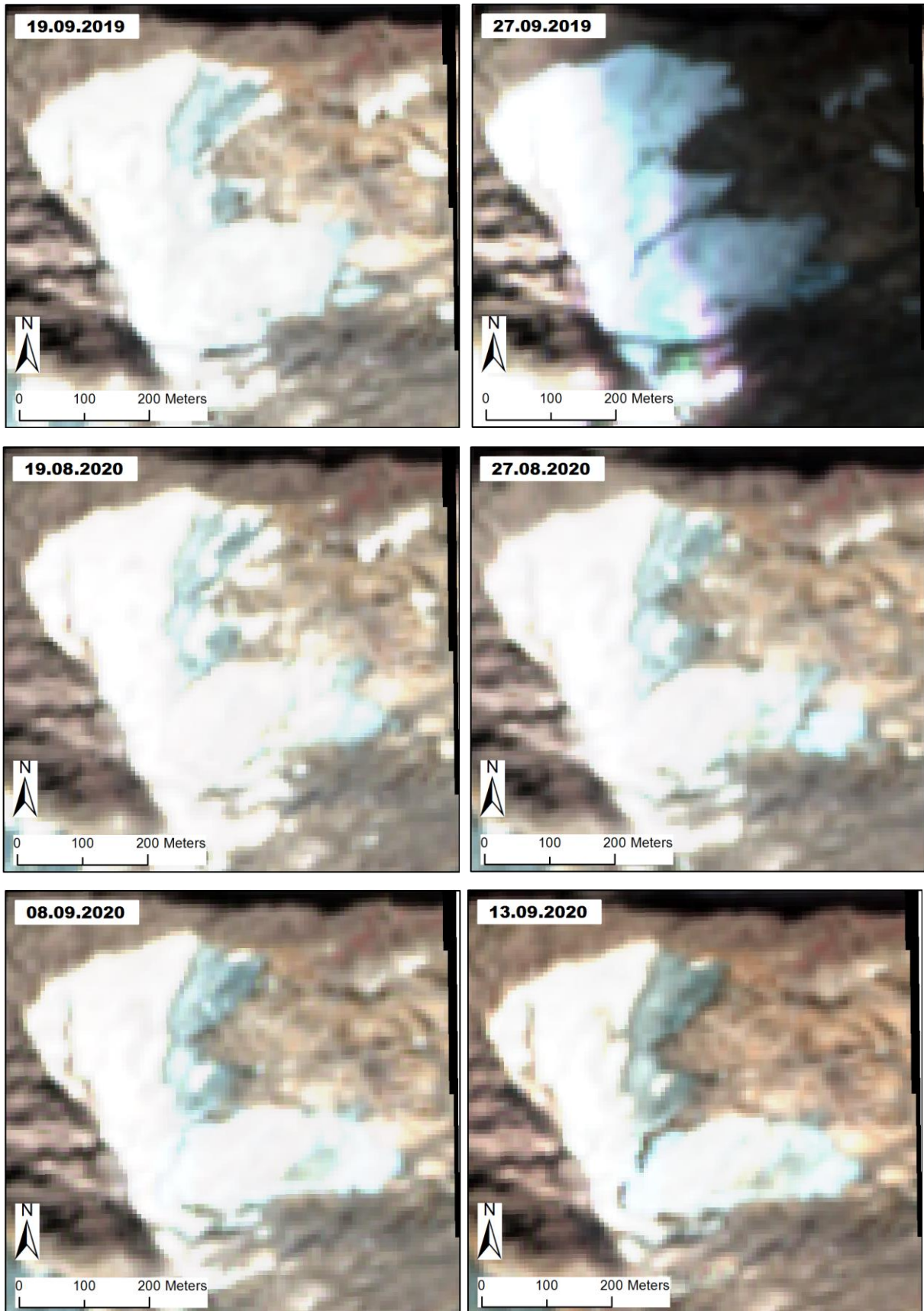
Figure A64: Sentinel-2 images available at (ESA, 2021) with no cloud cover, showing the events for Ärlen Glacier which could not be seen with Swisstopo imagery.

VII. Flow Velocity during 2018 and Comparison to 2020

Table A10: Displacement distances [m] and average daily velocity [m/d] for 2018 from the 26th of September (SWISSIMAGE) to the 23rd of October (World Imagery).

2018							
Ground Control	Pt 2	Pt 3	Pt 4	Pt 5	Pt 6	mean	m/d
[m]	10,08	3,52	7,41	7,48	7,43	7,18	0,26
Glacier quiet part	Pt 1	Pt 12	Pt 13	Pt 14	Pt 15	Pt 16	mean
[m]	12,24	9,96	10,62	7,25	10,96	8,05	9,85
Glacier sliding part	Pt 7	Pt 8	Pt 9	Pt 10	Pt 11	Pt 17	Pt 18
[m]	44,70	51,65	52,54	49,40	49,70	56,71	59,77

2018		
Ground Control		
[m]		
Glacier quiet part	GC corrected mean	mean m/d
[m]	2,66	0,10
Glacier sliding part	Pt 19	Pt 20
[m]	31,92	60,64

Table A11: Sliding distances [m] and average daily velocity [m/d] from the 26th of September to the 23rd of October. With corrections for the contortions caused by the reprojection to the LV03 coordinate system. Stable Ground are point measurements where no changes are expected and are therefore taken as error estimations.

2018		
Ground Control	mean	m/d
[m]	0,17	0,01
Glacier quiet part	GC corrected mean	mean m/d
[m]	2,66	0,10
Glacier sliding part	GC corrected mean	mean m/d
[m]	43,60	1,56

Table A12: Cumulative water availability, melt and rain for each year since 1989. Water availability calculated by adding rain to the melt from the PDDM. Rain by addition of all rainfall events at Grimsel Hospitz weather station while temperature over 0°C extrapolated for Ärlenglacier.

	Cum. summer water availability [mm w.e.]	Cum. Melt rate [mm w.e.]	Cumm. Rain [mm]
1989	1123	814	309
1990	1209	886	322
1991	1262	926	335
1992	1366	967	399
1993	1311	808	503
1994	1545	1075	470
1995	1117	839	278
1996	972	679	294
1997	1369	939	430
1998	1380	930	450
1999	1287	924	363
2000	1436	954	482
2001	1366	951	414
2002	1288	838	450
2003	1610	1316	294
2004	1375	1016	359
2005	1528	1041	487
2006	1547	1182	365
2007	1370	994	376
2008	1343	924	419
2009	1345	1097	248
2010	1222	866	356
2011	1424	1100	325
2012	1513	1077	436
2013	1347	989	358
2014	1408	884	524
2015	1522	1183	339
2016	1366	962	405
2017	1490	1169	322
2018	1532	1246	286
2019	1633	1197	436
2020	1514	1120	394
mean	1379	997	382

Table A13: Positive degree month model for the years 2010 - 2020. Calculated with the monthly mean temperature and the same method as the PDDM.

Positive Degree/Month Melt Model Ägl.	Mai	Jun	Jul	Aug	Sep	Okt	Tot [cm/summer]:
2010 [cm/month]	0,00	18,51	36,83	22,97	8,61	0,00	86,92
2011 [cm/month]	11,58	19,50	18,02	37,32	27,42	1,19	115,04
2012 [cm/month]	3,17	25,44	27,92	39,30	18,02	3,17	117,02
2013 [cm/month]	0,00	13,07	38,81	31,88	17,52	6,14	107,42
2014 [cm/month]	0,00	22,97	25,44	20,00	19,50	10,59	98,51
2015 [cm/month]	2,67	25,44	45,74	38,31	6,14	0,00	118,31
2016 [cm/month]	0,00	17,52	33,86	33,36	24,45	0,00	109,20
2017 [cm/month]	6,14	33,86	32,87	38,31	3,66	5,15	119,99
2018 [cm/month]	9,60	24,95	37,82	37,32	24,95	7,62	142,26
2019 [cm/month]	0,00	36,83	38,81	37,82	20,49	10,10	144,05
2020 [cm/month]	8,12	17,03	34,85	35,34	22,47	0,00	117,81
Mean/month	3,75	23,19	33,72	33,81	17,57	4,00	1276,51

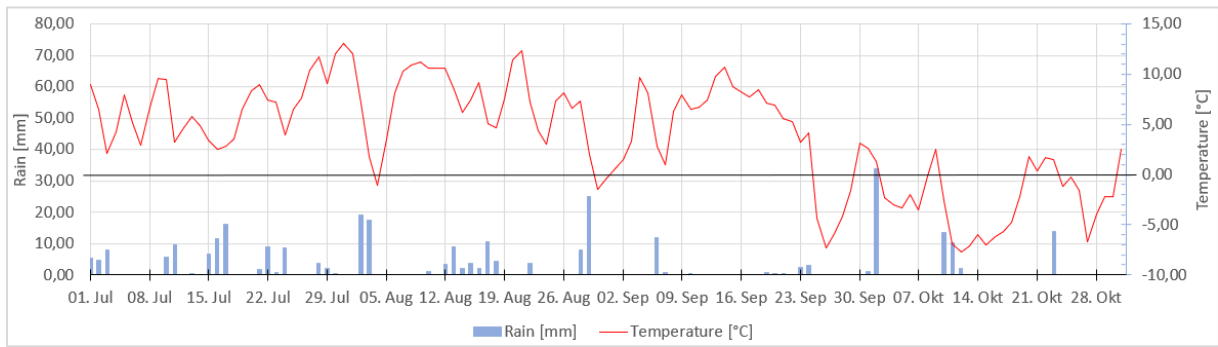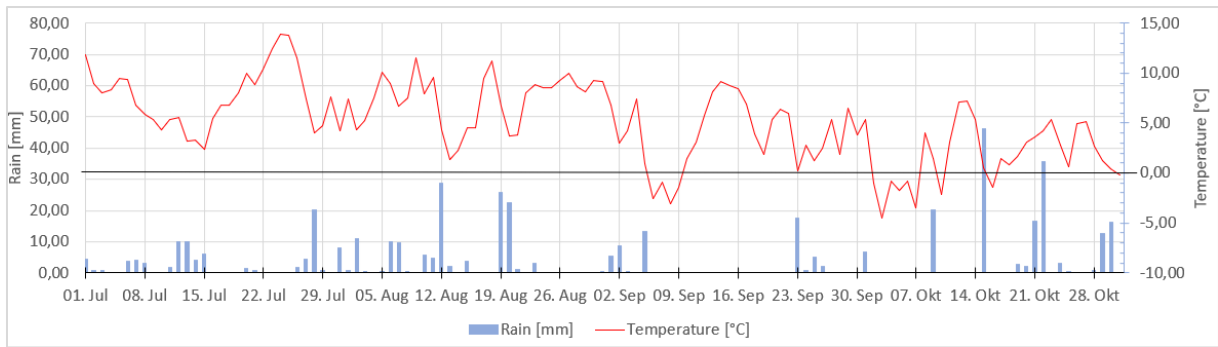## IX. Temperature and Rain (Juli – October) (2014-2020)
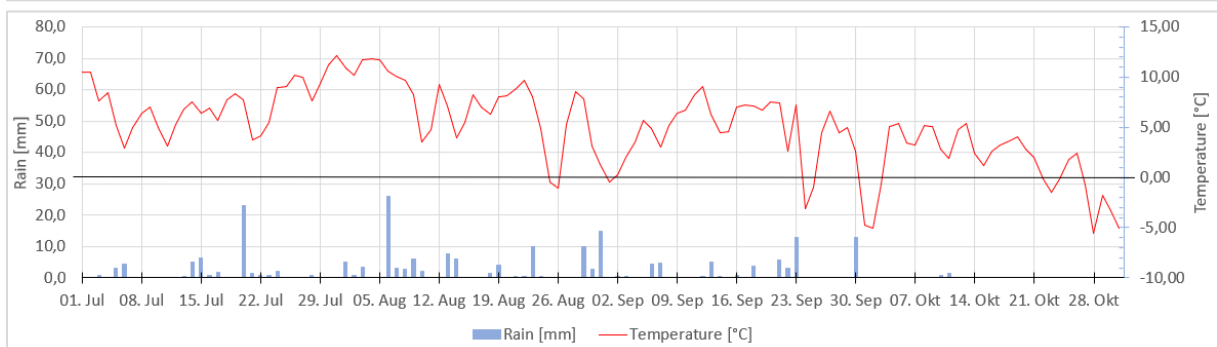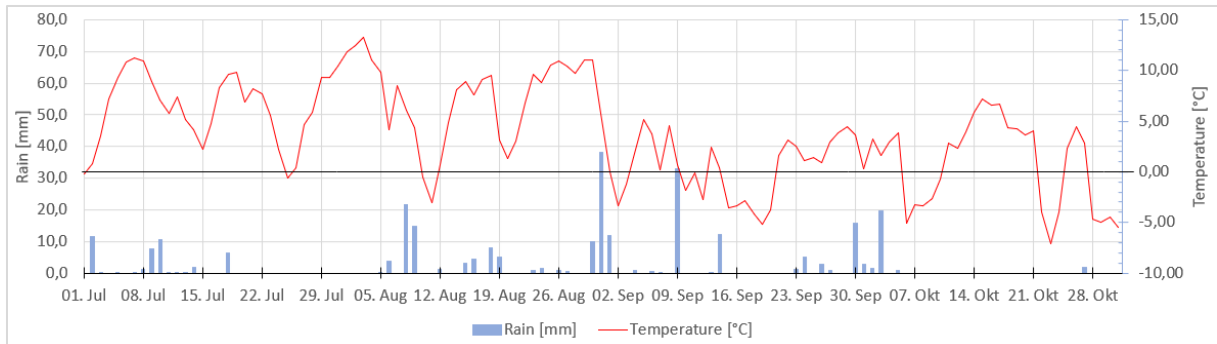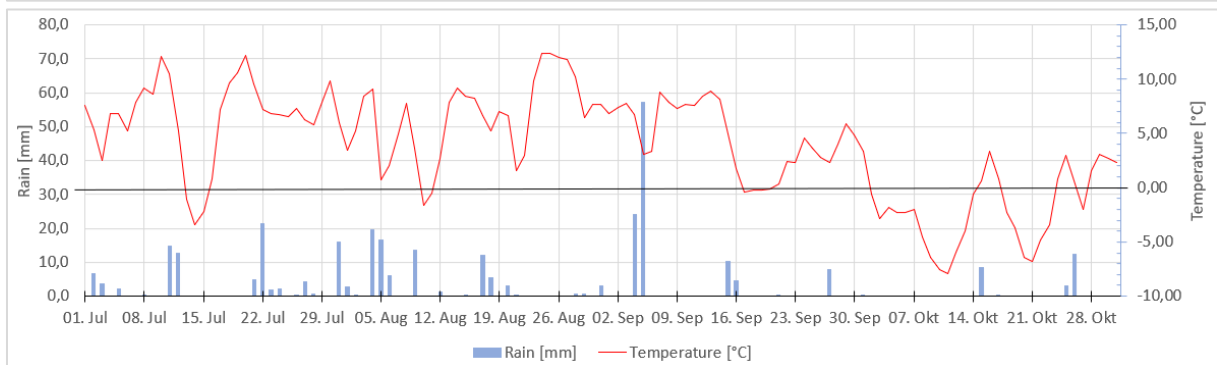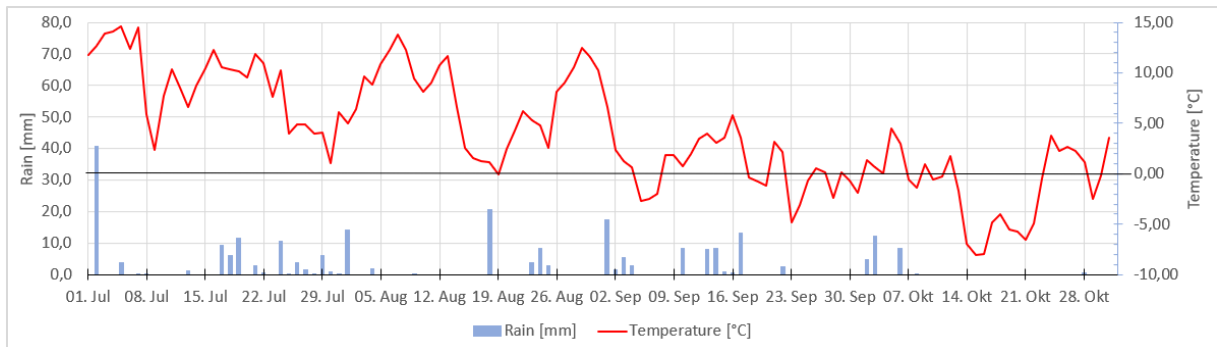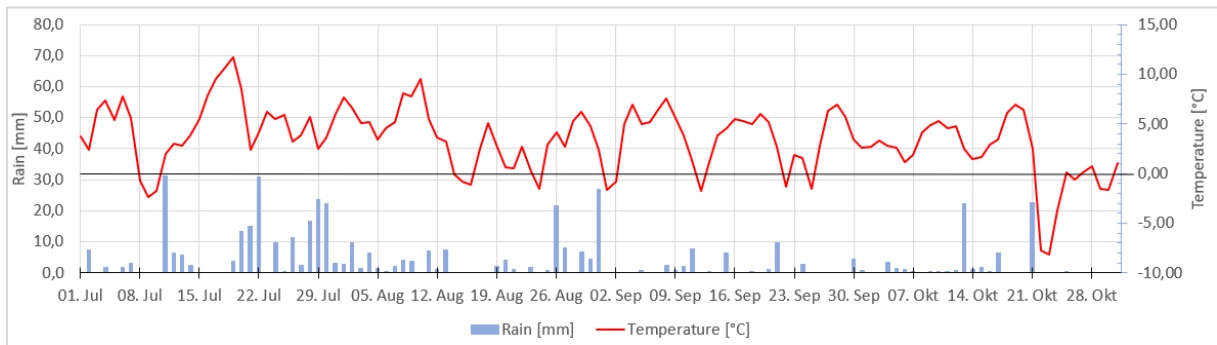
Figure A65: Temperature and Rain variations during July to October from 2014 to 2020. Snow is excluded due to the focus on melt for this study. Temperature drops beyond 0° are interesting due to their implications on glacier stability. Rain events could, combined with increasing melt, be a trigger for glacier sliding instabilities.

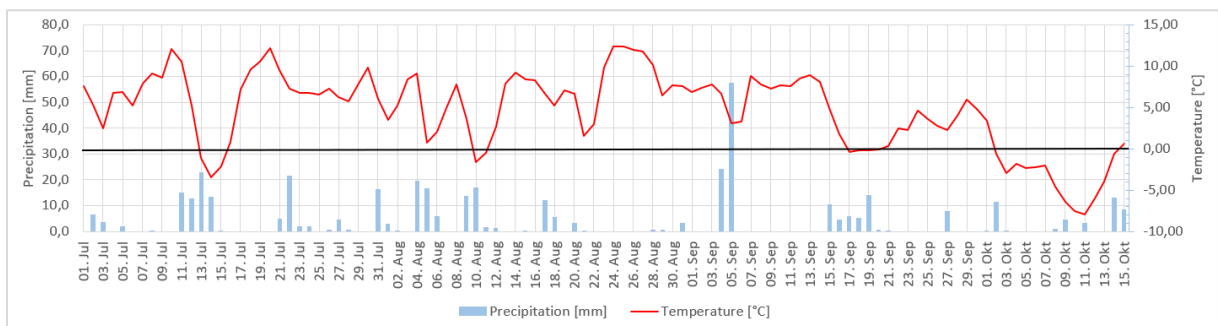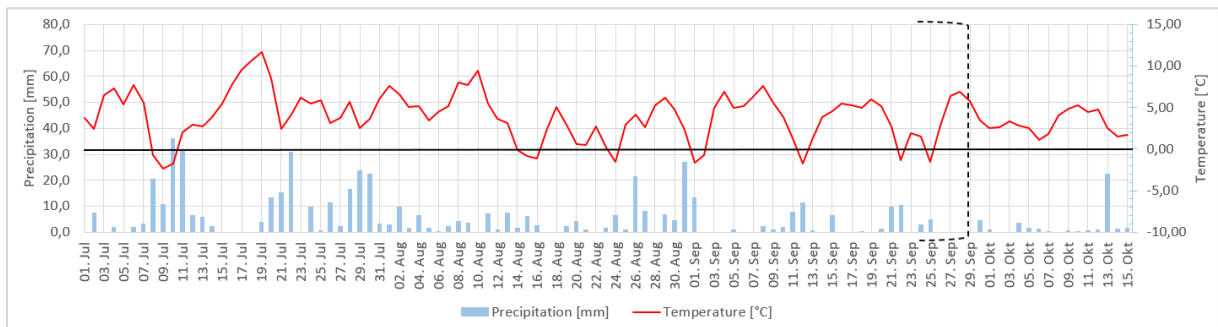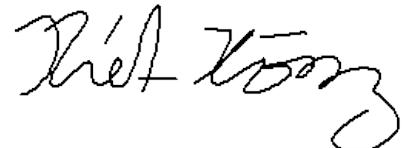## X. Timing of Events Compared to Climate Data (2014/15 and 2017-2020)

Figure A66: Precipitation events at Grimsel Hospitz weather station and temperature extrapolated for Ärlen Glacier. Combined with the observations of lacier instabilities made with the different data described in chapter 3. For the years 2014/15 and 2017 – 2020. Dashed lines are observed time periods where the whole glacier is sliding. Dotted lines stand for observations of small glacier avalanches at the glaciers tongue. Dashed and dotted lines show when the glacier melted back and reached the critical state of 2013 again.

Personal Declaration

I hereby declare that the submitted thesis is the result of my own, independent work. All external sources are explicitly acknowledged in the thesis.

Riet Armon Konz

Zurich, September 21, 2021